Title
Soft Spherical Tensegrity Robot Design Using Rod-Centered Actuation and Control

Author
CHEN, LEE-HUANG

Publication Date
2016

Peer reviewed|Thesis/dissertation

Soft Spherical Tensegrity Robot Design
Using Rod-Centered Actuation and Control

by

Lee-Huang Chen

A dissertation submitted in partial satisfaction of the

requirements for the degree of

Doctor of Philosophy

in

Engineering - Mechanical Engineering

in the

Graduate Division

of the

University of California, Berkeley

Committee in charge:

Professor Alice M. Agogino, Chair
Professor Dennis K. Lieu
Professor Ronald S. Fearing

Fall 2016

Soft Spherical Tensegrity Robot Design
Using Rod-Centered Actuation and Control

Abstract

Soft Spherical Tensegrity Robot Design
Using Rod-Centered Actuation and Control

by

Lee-Huang Chen

Doctor of Philosophy in Engineering - Mechanical Engineering

University of California, Berkeley

Professor Alice M. Agogino, Chair

This dissertation presents the design, analysis and testing of various actuated modular spherical tensegrity robots for co-robotic and space exploration applications. Tensegrity structures are of interest in the field of soft robotics due to their flexible and robust nature. They have the ability to passively distribute forces globally providing shock protection from unexpected impact forces. This feature makes them a robust mobile platform suitable for uneven terrain and unpredictable environments in which traditional robots struggle. Robots built from tensegrity structures, which are composed of pure tensile and compression elements, have many potential benefits including high robustness through redundancy, many degrees of freedom in movement and flexible design. However, to fully take advantage of these properties a significant fraction of the tensile elements should be actuated, leading to a potential increase in complexity, messy cable and power routing systems and increased design difficulty.

The first part of this dissertation presents an elegant solution to a fully actuated tensegrity robot: the TT-3 (version three) tensegrity robot was developed at University of California Berkeley, in collaboration with NASA Ames. The TT-3 is a lightweight, low cost, modular, and rapidly prototyped spherical tensegrity robot. This dissertation describes in detail the novel design mechanisms, architecture and simulations of TT-3, the first untethered, fully

actuated cable-driven six-bar tensegrity spherical robot ever built and tested for mobility. Furthermore, this dissertation discusses the controls and preliminary testing performed to observe TT-3's system behavior and performance and was evaluated against previous models of tensegrity robots developed at University of California at Berkeley and elsewhere.

The second part of this dissertation will present a new platform for prototyping spherical tensegrity robots that significantly reduces the time required for manufacturing and assembly. This simplified tensegrity system design allows for more scientific experiments to be performed in less time. This work describes the design architecture of the TT-4_{mini}, an example of a robot that uses this prototyping platform. In order to demonstrate the platform's use for scientific experiments, the TT-4_{mini} was shown to achieve uphill climbing, which has not been performed by any other spherical tensegrity robot in hardware. This dissertation discusses preliminary observations on the system's performance in uphill climbing from simulations and testing, including evidence of climbing surfaces with an incline up to 13 degrees. Furthermore, this new prototyping platform demonstrated the ability to create three complex 12-bar tensegrity structures with simplified procedures.

Lastly, the dissertation presents the improved tensegrity robot using the rod-centered architecture: the TT-4 (version four). It is a larger robot; its rod length is 1 meter compared to the 0.65 meter rod length of TT-3. The goal of the TT-4 robot prototype is twofold: to evaluate both the design improvements and the interaction of the robot with a center payload. Because the size of the robot has increased, the volume at the center of the robot available to hold payload has also increased. This allows researchers to further study the configuration, method of attachment, and the dynamics of a payload.

These robots are based on a ball-shaped six-bar tensegrity structure and features a unique modular rod-centered distributed actuation and control architecture. This revolutionary new architecture has been demonstrated in both software and hardware testing to increase the performance of tensegrity robots and has the potential to be extensible to a wide range of tensegrity configurations.

To My Family

Thank you for supporting me on my journey of learning.

Contents

List of Figures

List of Tables

Acknowledgments

The pursuit of a doctorate degree is a long and rigorous journey; it is impossible to achieve without the help and support of family, friends and colleagues. First and foremost, I would like to thank professor Alice Agogino. You inspire me everyday with your dedication and passion in teaching and research. With your mentorship, I have gained experience not only in research but also in education and outreach. These valuable opportunities have broadened my vision as an engineer. You have provided me a wonderful graduate school experience that I will never forget.

In addition, I want to thank professor Lisa Pruitt, professor David Dornfeld, professor Dennis Lieu and professor David Rempel. Thank you for your guidance and support for making my graduate career a smoother journey. And thank you for being on my qualifying exam committee. You showed me it was more than just an exam.

Professor Alice Agogino, professor Dennis Lieu, and professor Ronald Fearing, thank you for being on my dissertation committee. Your feedback and guidance helped me to achieve the highest quality in my research and dissertation.

I want to thank my co-authors for permission to use reference [6] [7] in Chapter 3. Kyunam Kim, your work on dynamics and controls helped characterize the performance of the TT-3 robot. Ellande Tang and Richard House, thank you for the study on the endcap design and friction characteristics. Kevin Li and Kimberley Fountain, thank you for your assistance on the study of the tensegrity structure's ability to absorb impact. Edward Zhu and Erik Jung, thank you for assisting with the simulations of the TT-3 robot. Professor Agogino, Dr. Adrian Agogino, and Vytas SunSpiral, thank you for guiding the research on the TT-3 robot.

I want to thank my co-authors for permission to use reference [10] in Chapter 4. Osvaldo Romero, Faraz Ghahani, Saunon Malekshahi, Grant Emmendorfer, and Yuen Wun Chau, thank you for your assistance on developing the hardware and software for the TT-4_{mini} robot. Carielle Spangenberg and Ellande Tang, thank you for your help on developing various elastic lattice structures. Mallory Daly, thank you for showing the extensibility of this novel prototyping platform. Professor Agogino and Dr. Adrian Agogino, thank you for guiding the development of the TT-4_{mini} robot.

To my colleagues in BEST lab, it has been my pleasure to share the creative space with you. Andrew Sabelhaus and Kyunam Kim, thank you for welcoming me to the BEST lab.

Many of the hardware parts in the prototypes described in my dissertation were made with the help of the mechanical engineering department machine shop. Thank you to Gordon Long, Mick Franssen, Dennis Lee, Jacob Gallego, Scott McCormick, Jesus Lopez, and Brien Angelo.

Thomas Clark, thank you for all electronic support, and your honest criticisms.

To my family: my mother, my father, my brother, and Hannah, thank you for all of your support. I would not be able to accomplish this without you.

Lastly, friends, there are many of you, thank you for enriching my life with your joy.

Chapter 1

Introduction

1.1 Background

Buckminster Fuller coined the term "tensegrity" in 1962 as a portmanteau of "tensile integrity" [11]. Tensegrity structures consist primarily of compression elements (rods) and tension elements (cables). The rods/cables of the structure experience pure compression/tension under equilibrium conditions. Tensegrity structures do not experience bending moments, which give them the unique and beneficial characteristic of simplifying the design process and reducing the number of failure modes. The rods and cables are only required to withstand single axis loading [12].

Tensegrity structures exhibit compliant behavior from their ability to distribute external forces globally. With this compliant characteristic, tensegrities can be used as a platform for soft robotic designs. Tensegrity soft robots have the ability to ensure that they will not injure humans during co-robotic applications, a critical trait behind the increased popularity in soft robots [13].

Tensegrity structures are currently an interest in the field of soft robotics due to their flexible and robust nature [14]. They have the ability to passively distribute forces globally providing shock protection from unexpected impact forces. This feature makes them a robust mobile platform suitable for uneven and unpredictable environments in which traditional robots struggle.

The unique properties of tensegrity robots make them well-suited for a new generation of robotic landers/rovers for space exploration. Tensegrity structures are considered to be: [15] [12] [16] [17] [13]:

- Light weight.
- Energy efficient.
- Highly deformable.
- Capable of a wide range of motion.
- Easily Tunable.
- Robust.

The ability to land an inexpensive rover without damage and traverse uncertain territory is highly desirable for successful space exploration. In addition, the robot's intrinsic structural robustness allows it to handle or recover from unexpected and undesirable interactions with the environment (e.g., collision with obstacles) while moving. This could allow significantly faster science return as compared to current rover concepts that must meticulously plan every operation to provide adequate safety.

The Berkeley Emergent Space Tensegrities (BEST) Laboratory at University of California, Berkeley has been collaborating with the National Aeronautics and Space Administration's (NASA) Ames Research Center on using tensegrity structures as the basis for next generation space exploration systems. Traditionally, rigid wheeled robots, like the Mars Curiosity rover, have been the primary space exploration platform. Heavy rigid robots require detailed sensing during operation, while robust compliant robots like the ones prototyped at BEST lab can operate with minimal sensing at a fraction of the weight.

In addition to less sensing required, the tensegrity robots have the ability to simplify the equipment required during entry, descent, and landing phase (EDL) of a mission. During the Mars Science Laboratory (MSL) mission which started its journey in November 2011, one of the main goal of the mission is to deliver the Mars Curiosity Rover onto the surface of Mars. The EDL phase of the mission was considered one of the most challenging tasks [18]. During the EDL phase of the mission, the system was fully autonomous due to the communication delay from Mars to Earth, so the scientists and engineers did not have any control of the system. If anything went wrong, even at the last second of landing, the complete mission would be compromised. Figure 1.1 generated by NASA shows the complexity of the EDL phase of the mission. Therefore, one of the goals with the use of tensegrity robots is to increase the chance of survival even if some parts of the EDL phase had failures. Tensegrity structures have the potential to increase the survival rate with its tolerance to errors.

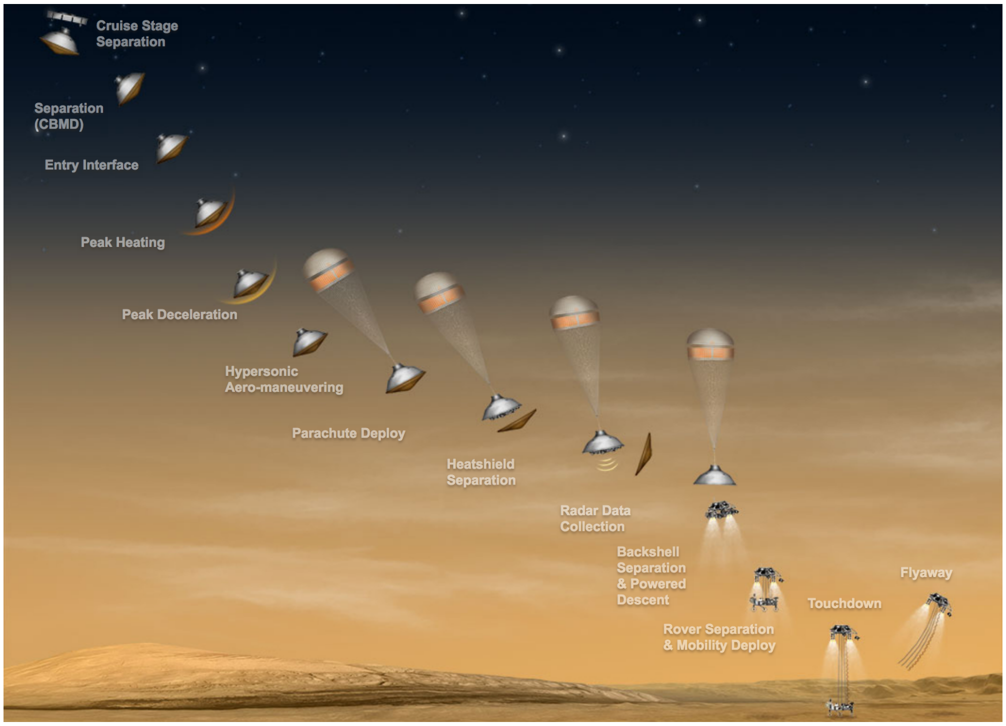

Figure 1.1: Graphic generated by NASA of the Entry, Descent, and Landing phase of the Mars Science Laboratory mission. Image is from NASA's website. [1]

1.2 Tensegrity Robot Design Requirements

The BEST lab has been awarded the Early Stage Innovation (ESI) grant by NASA with the goal of creating a 10 kg tensegrity ball robot that can deliver a 1 kg payload over 1 km distance on the Moon in a short time and with high precision. The robot would have to survive and traverse through various terrains on the Moon, which includes craters, caves, and lava tubes. Our proposed method of completing the mission is to attach a tensegrity robot, which has the ability of performing cable-driven rolling (high precision but slow), with a thruster system that allows the robot to fly (low precision but fast). Figure 1.2 demonstrates the concept of a flying tensgrity robot with a thruster system at the center.

This mission requires the tensegrity robots to be able to effectively perform cable-actuated rolling for short distance travel and precisely navigate through rough terrain. The robot will be able to travel large distances using thruster-based hopping, which will be less precise. These goals require the tensegrity robot to be:

- Light weight.

- Highly deformable for transportation.
- Energy efficient in rolling.
- Able to carry a 1 kg payload.
- Able withstand high impact forces during long distance hopping.
- Able to traverse through rough terrain.
- Robust.

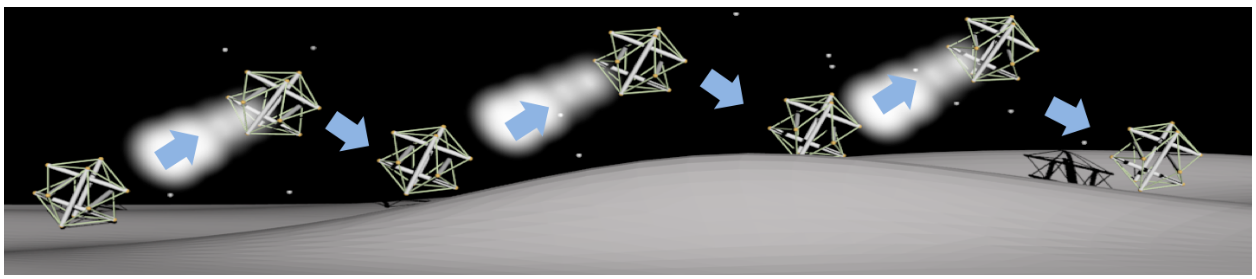

Figure 1.2: Graphic generated by NASA researcher Adrian K. Agogino demonstrates the concept of a flying tensegrity robot with a thruster system. Image used with permission [2].

1.3 Motivation of New Design

Tensegrity structures are ideal candidates for space missions as robustness is a critical component required in all space missions and robustness is one of the key characteristics of tensegrity structures. However, after evaluating the NASA's SUPERball robot (Figure 1.3) and BEST lab's TT-2 robot (Figure 1.4), I noticed the location of the actuators for these two robots were vulnerable to high impact force. In addition, the location of the actuators would result in ground contact during rolling.

It came to my attention that the mechanical design of the tensegrity robots needed to undergo fundamental design changes in order to improve its robustness. The center of the sphere is the point furthest from the surface of the sphere and therefore a good location for the payload. For six-bar tensegrity spheres, the center of the rods is the location furthest from the outer surface of the sphere. With this concept, new design ideas began to sprout.

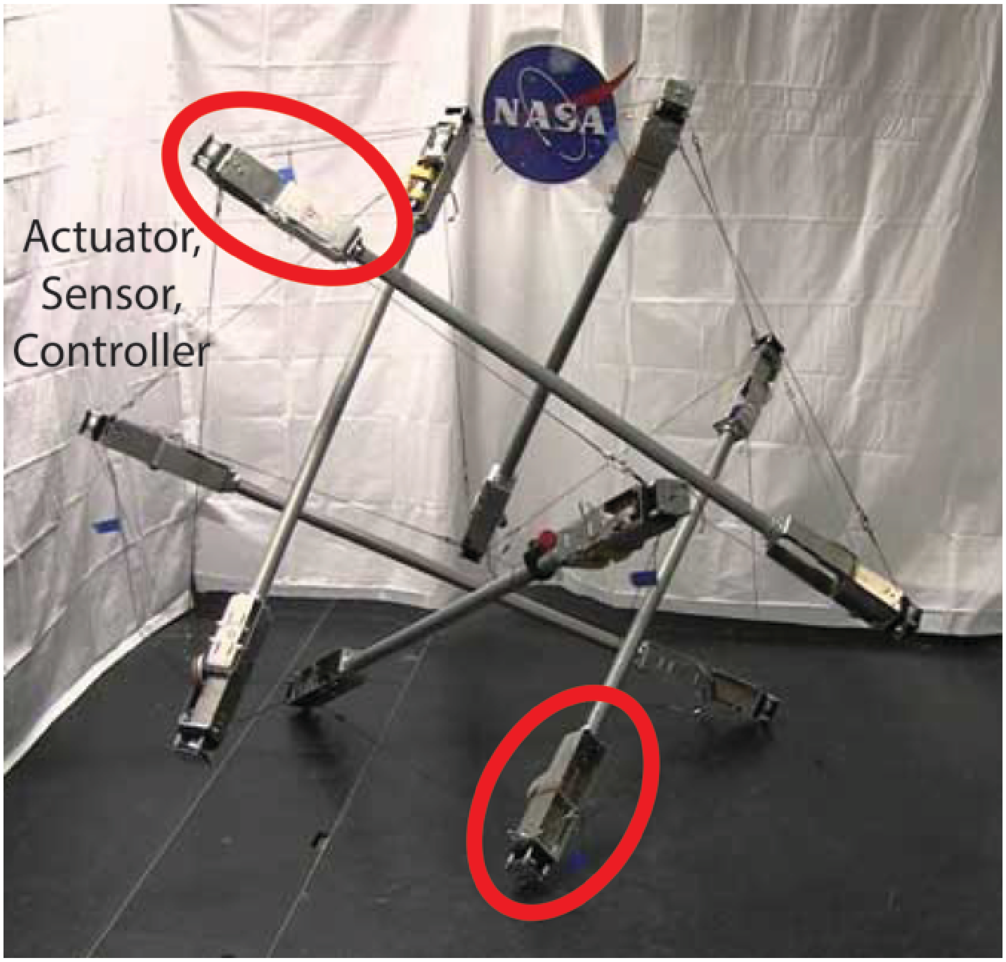

Figure 1.3: NASA's SUPERball spherical tensegrity robot has its controllers and actuators on the end of the rods.

1.4 Roadmap for the Dissertation

This dissertation describes in detail research on modular, rod-centered actuation systems for tensegrity robotics. The TT-3, TT-4, and TT-4_{mini} were created based on the concept of a rod-centered actuation architecture. The architecture uses novel methods to position all the required components for the tensegrity robot to the center of the rods. This dissertation will explain how this method will protect the critical functioning components during impact and landing.

The TT-3, TT-4, and TT-4_{mini} robots were created, in that order, to further study the modular, rod-centered architecture and the performance of tensegrity robots. This dissertation will discuss the design, simulation and experiments of each of these robots. It will

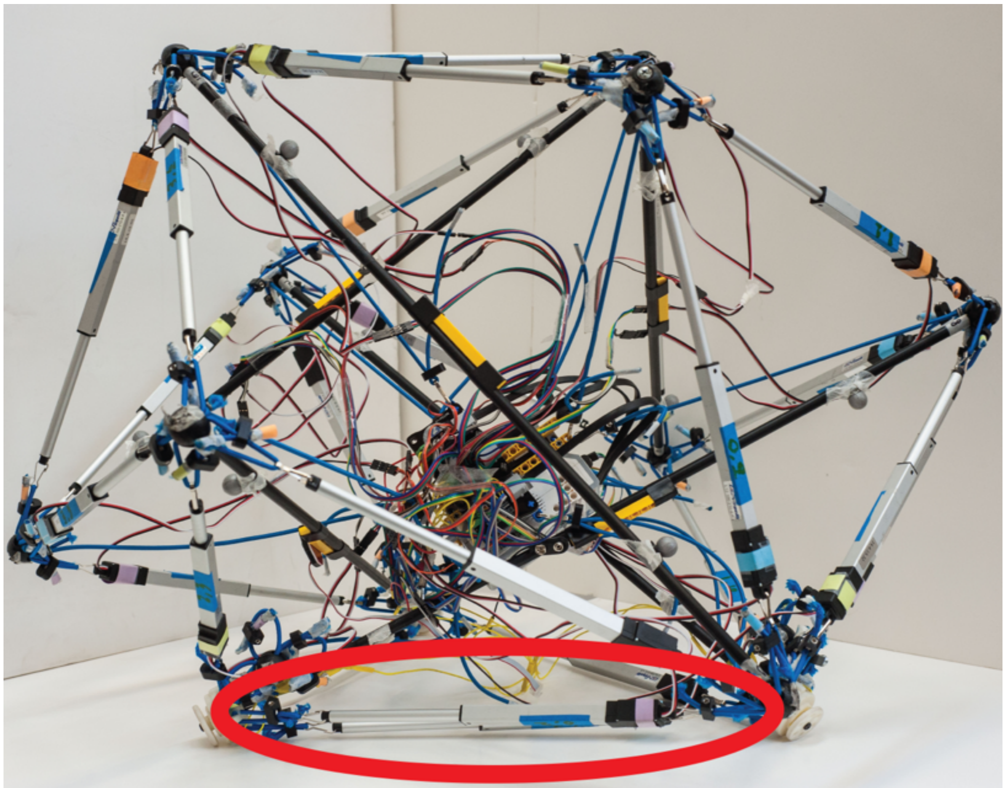

Figure 1.4: The Berkeley's TT-2 tensegrity robot prototype has its linear actuators located outer surface of the tensegrity sphere in between the ends of the rods.

further discuss the impact of these robots on the tensegrity robotics community.

Chapter 2 provides a summary of past work on tensegrity structures and tensegrity robots focusing on spherical tensegrity robots. Chapters 3 and 4, respectively describe the design, implementation and testing of the TT-3 and TT-4_{mini} robots. Chapter 5 provides a summary of related outreach activities. Chapter 6 ends with a summary of conclusions along with my recommendations for future directions of the research.

Chapter 2

Prior Work

This chapter is an overview of tensegrity systems that have been explored by other scientists, engineers, and artists.

2.1 Tensegrities

Tensegrity structures were first introduced in the mid-1960's by the three scientists: Richard Buckminster Fuller [19], David George Emmerich [20], and Kenneth D. Snelson [21]. The structures' passive combination of cables-in-tension and bars-in-compression became a significant design feature in several architectural and sculptural structures [17, 22, 23, 24, 25, 26, 27, 3]. Unique structures can be created because none of the elements in the structure are experiencing bending moments [12]. Some prior work with tensegrity structures has focused on robust static structures in modern architecture, art and structural applications. Examples include Snelson's unique, stable biotensegrity art pieces [3], Tibert's deployable tensegrity space structures [28] and Fu's work on designing large-scale tensegrity domes [29]. Snelson has been continuing to push the boundary of tensegrity structures in both architecture and art. He has creations from small indoor art displays to large-scale outdoor structures. His famous art works can be seen all around the world. Figure 2.1, 2.2, 2.3 are several examples of the beautiful tensegrity artworks created by Kenneth D. Snelson [3].

2.2 Tensegrity Robots

Only recently, in parallel with the rise of soft robotics, have tensegrities come to the forefront of robotic design. There are fewer examples of work on active tensegrity structures. Of note are the National Aeronautics and Space Administration (NASA) Ames Re-

Figure 2.1: Easy Landing, a 10 x 25 x 20m tensegrity art, created by Kenneth D. Snelson, in City of Baltomore, MD. Image from Kenneth Snelson's book, Kenneth Snelson; Art and Ideas [3].

search Center's work on the Spherical Underactuated Planetary Exploration Robot ball (SUPERball) and its predecessor, the Reservoir Compliant Tensegrity Robot (ReCTeR) [14, 30, 31, 32, 33, 34, 35, 36, 37, 38]. Both SUPERball and ReCTeR are untethered, six-bar spherical tensegrity robots capable of cable-actuated deformation and motion. Unlike the BEST lab's TT-3 robot, both SUPERball and ReCTeR are under-actuated systems with 12 and six actuators, respectively. The NASA's SUPERball has a rod length of 1.5 meters, which is the largest spherical tensegrity robot ever built shown in Figure 2.4. The NASA SUPERball robot team worked on modeling the landing of a tensegrity robot on Titan without additional entry, descent, and landing (EDL) landing gear [39, 40].

Apart from spherical tensegrity robots, spine-like tensegrity structures have also been explored as a locomotion strategy. Work has been done on cable-connected and cable-actuated spine vertebrate as well as on a duct exploring robot with two tetrahedral frames linked by hinge joints and controlled with linear actuators [41, 42, 9]. NASA's TetraSpine spine shape tensegrity robot was able to move in a snake-like motion [43, 9]. École Polytechnique Fédérale de Lausanne's (EPFL) Applied Computing and Mechanics Laboratory IMAC Labo-

Figure 2.2: B-Tree II, a 10.6 x 11.6 x 12.8m tensegrity art, created by Kenneth D. Snelson, in Frederik Meijer Gardens and Sculpture Park, MI. Image from Kenneth Snelson's book, Kenneth Snelson; Art and Ideas [3].

ratory has expandable tensegrities for dynamic use in rescue situations [44]. Paul, Lipson, et al. have demonstrated gait production in a three-strut, nine-cable arrangement [45, 46, 47].

2.3 Previous BEST Lab Tensegrity Robots

The dynamic, highly-specialized and non-standardized nature of tensegrity robotics has motivated the development of a rapid prototyping tensegrity system at the Berkeley Emergent Space Tensegrities (BEST) lab at the University of California at Berkeley. The BEST lab has been collaborating with the NASA Ames Research Center to design, simulate, and prototype tensegrity robots. The TT-1 (version 1) robot shown in Figure 2.5 was the first generation of a six-bar spherical tensegrity robot designed and prototyped by researchers in the BEST lab. The robot consists of 24 linear actuators and six balsa wood rods. The

Figure 2.3: Double City Boots, a 2.75 x 2.75 x 3.65m tensegrity art, created by Kenneth D. Snelson, in City of Miami-Dade Art in Public Places, FL. Image from Kenneth Snelson's book, Kenneth Snelson; Art and Ideas [3].

balsa wood rods were the compressive elements, and the the linear actuators in series with an elastic bungee cord combination were the tensile elements in the tensegrity structure. In addition, there was a LEGO Mindstorm EV3 controller at the center of the structure as the master controller for all of the linear actuators. The LEGO Mindstorm EV3 controller was used to simulate the ability of a tensegrity robot to carry a large payload. The elastic bungee cord on the ends of the linear actuator were the "springs" of a tensegrity system. The "spring" constant could be adjusted by changing the type of bungee cord. The pretension could be adjusted by changing the length of the bungee cord. The TT-1 tensegrity robot was very successful in demonstrating tensegrity mobility based on a fully actuated six-bar tensegrity robot. TT-1 robot was the first un-tethered fully actuated tensegrity robot ever built [13].

With the success of the TT-1 robot, the design foundation for the newer generations of

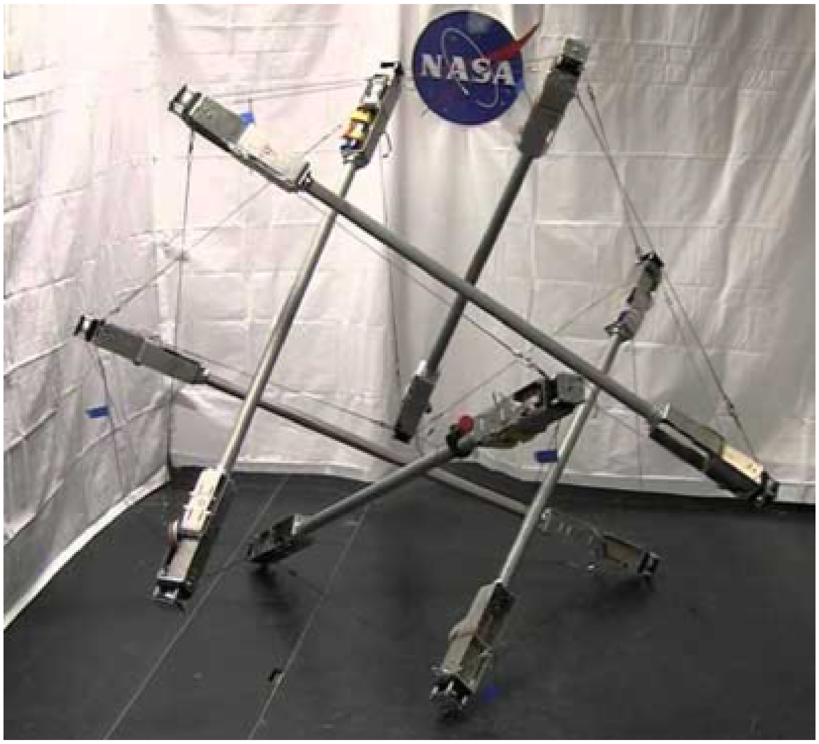

Figure 2.4: NASA's SUPERball tensegrity robot with rod length of 1.5 meters. Images taken from NASA.gov[4]

tensegrity robots was set. The next-generation robot, the TT-2 shown in Figure 2.6, was the improved robot based on the TT-1 architecture. The main difference between the TT-2 robot and the TT-1 robot is the material used as the compressive element. The balsa wood rods used in TT-1 were replaced with fiberglass struts. In addition to hardware upgrades, the software was improved with enhanced algorithms using a dynamic relaxation technique, which polished the locomotion of TT-2 robot [8].

In additional to spherical tensegrity robots, members of the BEST lab have been developing various tensegrity spine robots. The Underactuated Lightweight Tensegrity Robotic Assistive Spine (ULTRA Spine) is an actuated spine-shaped tensegrity robot [5, 48, 49]. The prototype has demonstrated the ability to shift its weight distribution between legs [5, 49].

The following chapter will discuss the development of the TT-3 (version 3) tensegrity robot in detail. The TT-3 robot uses a modular hardware and controls framework for tensegrity-based robotic structures that will accelerate the research in this emerging field.

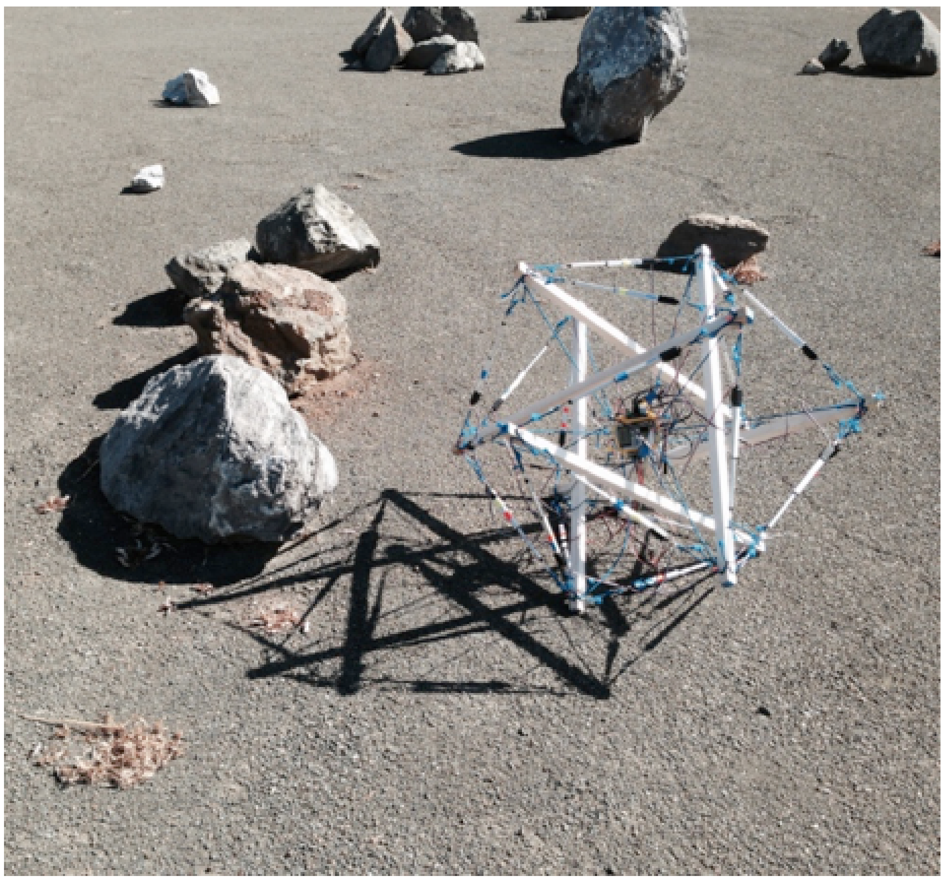

Figure 2.5: TT-1 tensegrity robot prototype, first six-bar tensegrity robot built by the BEST lab.

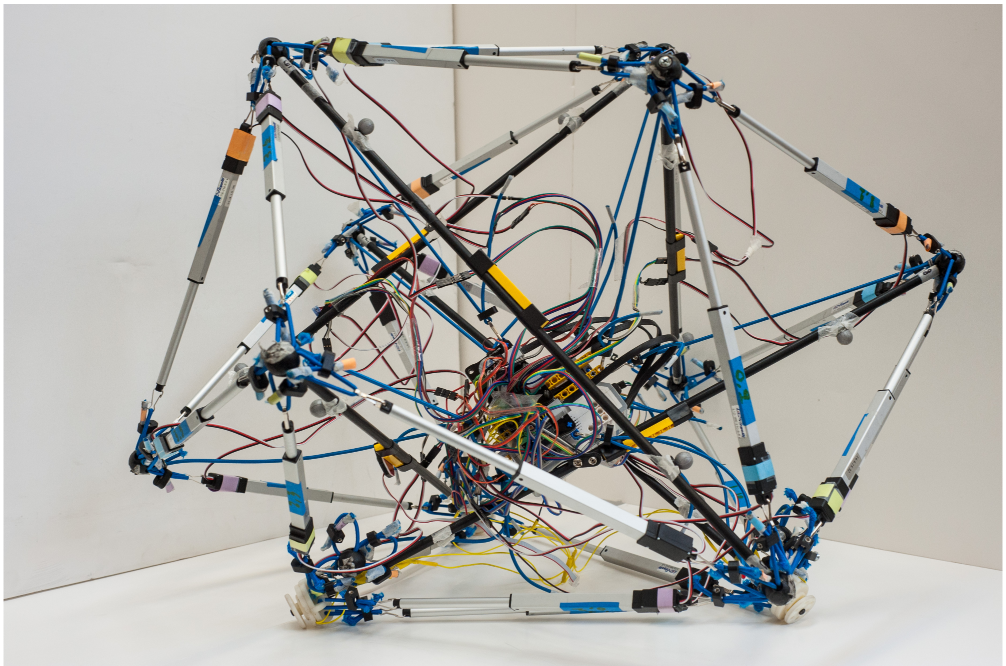

Figure 2.6: TT-2 tensegrity robot prototype.

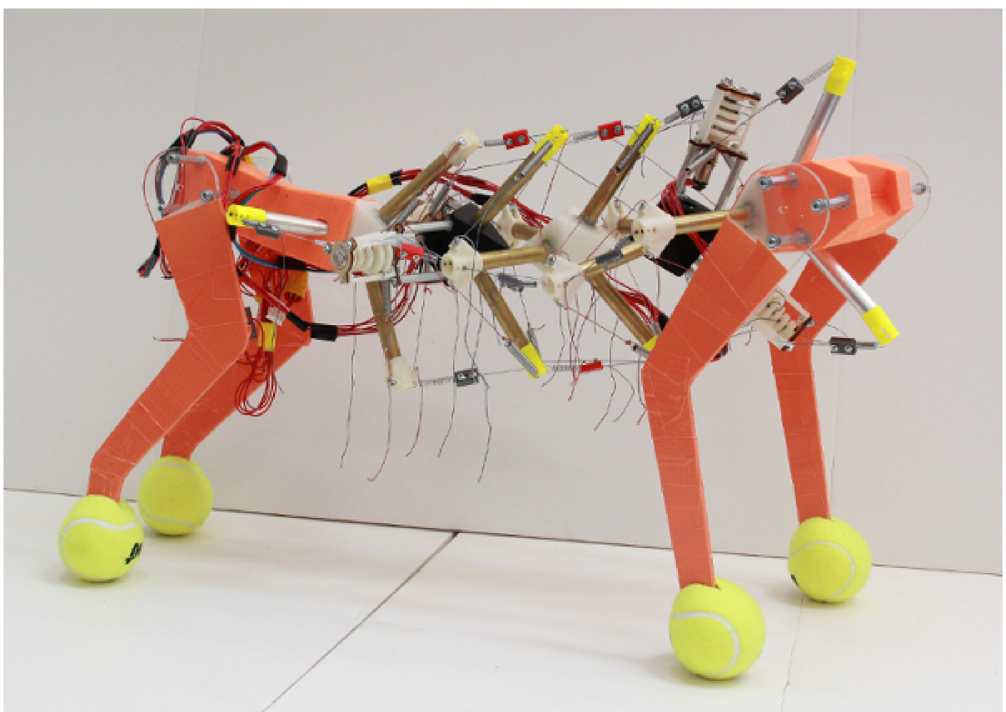

Figure 2.7: BEST lab's ULTRA Spine robot prototype [5].

Chapter 3

Berkeley TT-3 Robot

3.1 Motivation - Rod-Centered Actuation Concept

The original National Aeronautics and Space Administration (NASA) target mission was the development of a lander/rover system that could explore Titan, the largest moon of Saturn. Some of the main design challenges are:

- A robot system that can sustain high-speed impact.
- A robot that can maneuver around the surface of the planet after landing.
- A robot that can carry scientific payload.
- A robot that can transfer or absorb unexpected forces.
- A low-cost, lightweight system.

With these abilities, possible missions were expanded to include exploring the craters of Earth's Moon through a new grant from NASA in their Early Stage Innovation program.

With these target goals, tensegrity structures are predicted to be a good basis for a design platform as they have the ability to

- Distribute external forces globally.
- High strength to weight ratio.

- Adjustable structure stiffness.

The ability to distribute external forces throughout the structure means that the structure has the potential to absorb large impact forces during different forms of landing phases in the mission. The high strength to weight ratio allows for the development of a lightweight system. Combining the ability to distribute forces globally with stiffness adjustments, it is possible for the structure to change its shape by changing the tension levels at different segments of the structure. With proper control of this "shape-shifting" characteristic, the structure can perform punctuated rolling, which will be discussed in more detail in later sections.

The middle point of the rod is the furthest location from the surface of the six-bar tensegrity. It is the location to best protect the critical components during rolling and dropping. Therefore, placement of all the critical components (e.g., controllers and actuators) at the center of the rods can potentially improve the reliability and functionality of the system.

3.2 Simulation Modeling

For simulation, the NASA's Tensegrity Robotics Toolkit (NTRT) was used [50], an open-source tensegrity-specific simulator built to run on top of the Bullet Physics Engine (version 2.82). The NTRT data structure represents rods and strings as a tree of substructures that can be rotated and moved. Strings are represented in a two-point linear model using Hooke's law forces with linear damping. In simulation, the dynamics and kinematics of different designs can be explored, and inherent advantages and disadvantages of adjustments in parameters can be compared. The NTRT simulator has the ability to have rapid design iteration of structures in this physics-based environment. Since tensegrity structures have complex internal force distributions at different states, NTRT can be used as a tool to assist with designing tensegrity robots. With NTRT, a six-bar structure with known parameters, such as rod length, rod diameter, rod mass, and spring constant, can be modeled and its behavior simulated. With the modeled tensegrity, different pre-tension values can be applied to graphically visualize the appearance of the tensegrity structure.

Shown in Figure 3.1, a model of TT-3 is applied with three different pre-tension values. With a small tension value, TT-3 appears to be flat on the ground. With increasing tension, the structure will gradually stand up to be more sphere-like. NTRT can estimate the required

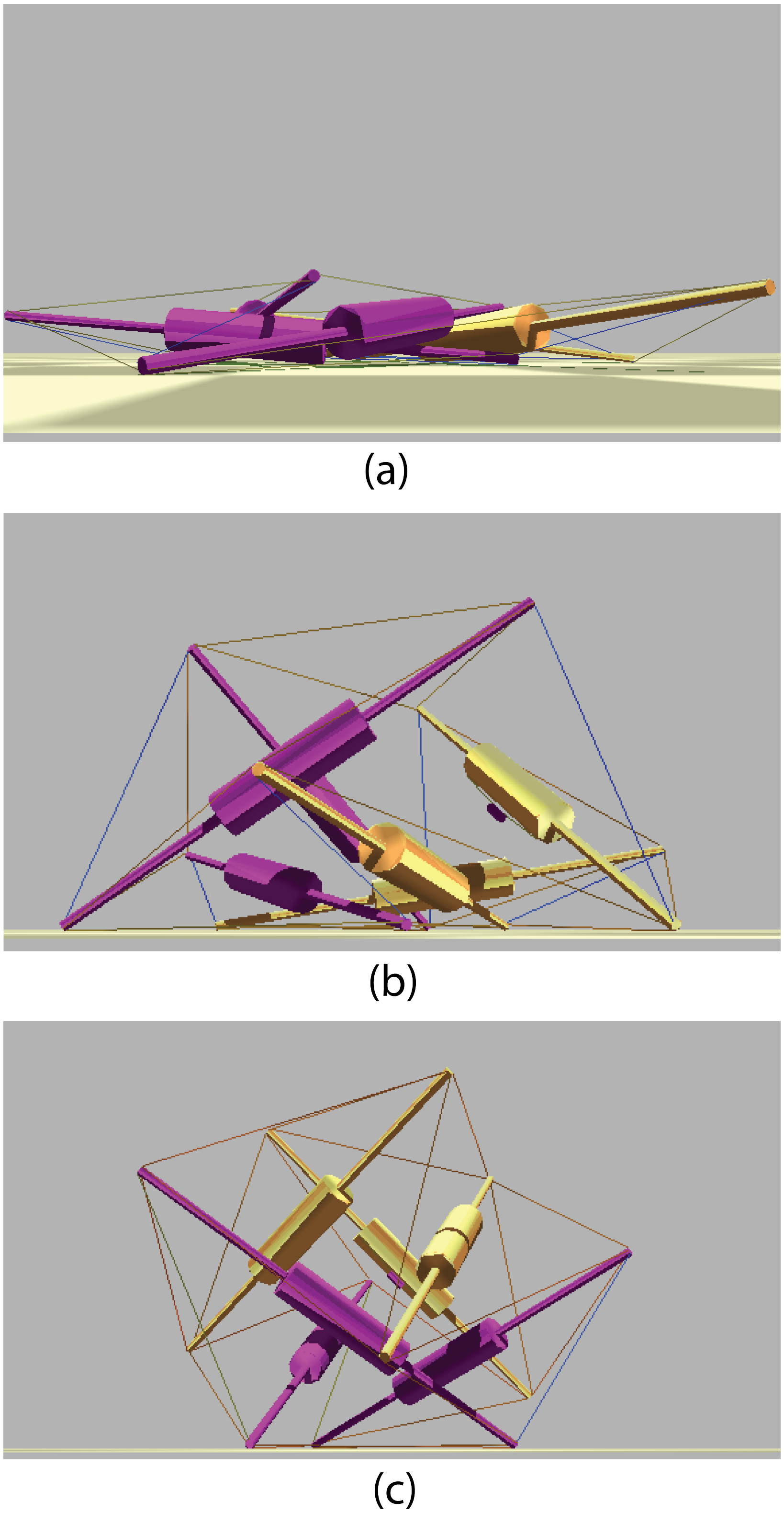

Figure 3.1: NTRT simulations of TT-3 with different pre-tensions. (a)(b)(c) is the sequence of increasing pre-tension.

tension force for modeled structures. In the case of TT-3, the initial modeling of TT-3 with close estimation of system parameters shows the minimum tension required for the structure to be 17.5N to be sphere-like. Knowing the potential tension requirement can help the designer better select critical components, such as the actuators, needed for the robot. This feature can greatly improve the efficiency of the design process and reduce the need for constant trial-and-error with designing physical prototypes.

3.3 Tensegrity Rod Dynamics

The compliant tensegrity structure has the ability to absorb forces during impact. This ability is due to the transfer of the energy throughout the system. During impact, the structure will deform; the deformation in the structure is the transfer of kinetic energy to the potential energy in the elastic element. For example, when a tensegrity structure uses extension springs as its elastic elements, the springs will stretch to a higher potential state during impact. This is the transfer of the impact energy to strain energy in the springs. Therefore, it is potentially more valuable to have a structure that can be deformed more during impact.

In a tensegrity system, rods are the main components that contribute to the mass distribution and inertia of the system and the contribution of cables is often neglected. As the rods do not touch each other and are only connected by the strings, each rod can be modeled as an individual subsystem of the structure subject to external forces such as the gravity and cable forces. As a result, dynamic behavior of individual rods, which is affected by the rod mass distribution, collectively can be used as a simple model of the response of the overall structure. A different rod design will result in different mass distributions across the rod, which in turn will affect the behavior of the rod upon impact. In order to see the differences two simple cases are presented in Figure 3.2. In the first rod design, the rod mass is concentrated at its center (Figure 3.2(a)). The second rod design divided the rod mass evenly on the two ends (Figure 3.2(b)). With the same mass of the rods and same coefficient of friction at the point of contact, Eqn. (3.1) and Eqn. (3.2) can be assumed.

$$F_{x1} = F_{x2} = F_x \tag{3.1}$$

$$F_{y1} = F_{y2} = F_y \tag{3.2}$$

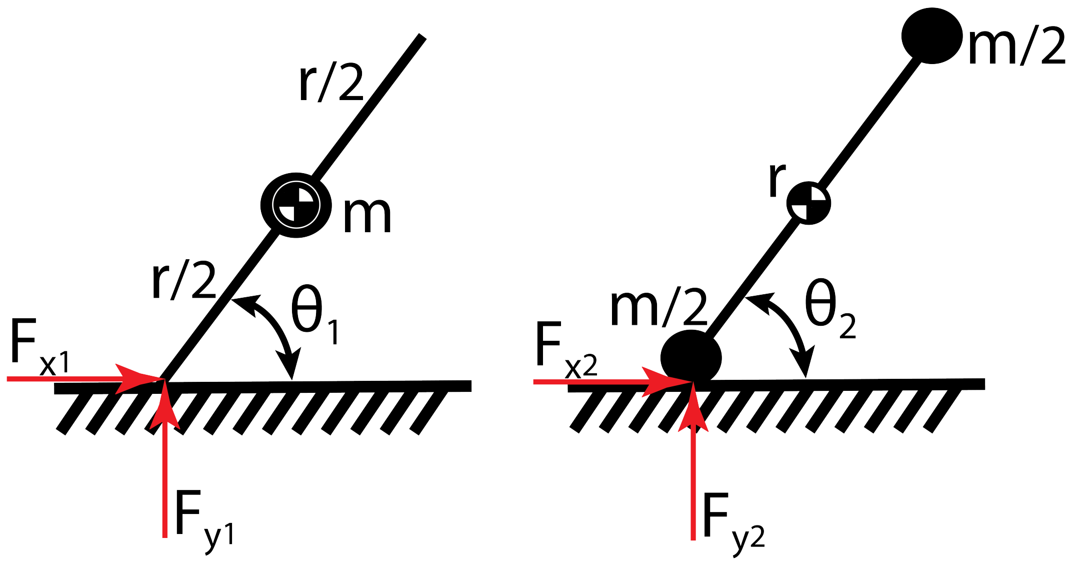

Figure 3.2: (a) A single rod of the tensegrity structure is modeled with a mass at the center of the rod (Berkeley TT-3). (b) A single rod of the tensegrity structure is model with two half masses on two ends of the rod (NASA's SUPERball). In the figures, m is the rod mass, r is the rod length and F_x and F_y are the ground reaction forces [6].

The moment generated at the center of mass from the ground contact can be calculated with Eqn. (3.3).

$$\tau = F_x \cdot \left(\frac{r}{2}\right) \cdot \sin(\theta) - F_y \cdot \left(\frac{r}{2}\right) \cdot \cos(\theta) \tag{3.3}$$

If each rod receives the same moment while the ground contact end is the pivot point, the different mass distribution will result in different angular acceleration. The relationship between the moment generated from ground contact and the angular acceleration can be expressed with Eqn. (3.4) and Eqn. (3.5) .

$$\tau = J \cdot \ddot{\theta} \tag{3.4}$$

$$\ddot{\theta} = \frac{\tau}{J} \tag{3.5}$$

$$J_{TT-3} < J_{SUPERball} \tag{3.6}$$

$$\ddot{\theta}_{TT-3} > \ddot{\theta}_{SUPERball} \tag{3.7}$$

According to Eqn. (3.5), the angular acceleration $\ddot{\theta}$ at the center of mass depends on the mass moment of inertia J if the moment generated on the rods τ are the same. Based on the rotation at the center of the mass, the rod in Figure 3.2(a) will have lower mass moment of inertia than Figure 3.2(b) configuration shown in Eqn. (3.6). With the lower mass moment of inertia J of the Figure 3.2(a) configuration, the angular acceleration of the rod will be greater than the rod configuration in Figure 3.2(b) shown in Eqn. (3.7). The higher angular acceleration of the rod is one of the main benefits of the rod-centered design because it implies the structure will deform more when the same moment is applied. The larger deformation in the structure means the displacement of the springs or the elastic elements in the structure will be larger, increasing the shape shifting capabilities and the transfer of energy.

3.4 Impact Simulation

NTRT simulations were performed to confirm the difference in behavior of the rods presented in Figure 3.2 at the structural level during impact. From the previous section, the structure with mass at the center of the rod should be more compliant than the structure with its mass evenly divided at the two ends of the rod. This means that the former should deform more than the latter structure.

Figure 3.3 shows the sequence of both tensegrity structures with different mass distributions impacting the ground from the same height. All parameters of the two structures are the same except the location of the mass. The structure on the left in Figure 3.3 has a large mass at the center of the rod, and the structure on the right has the same large mass but

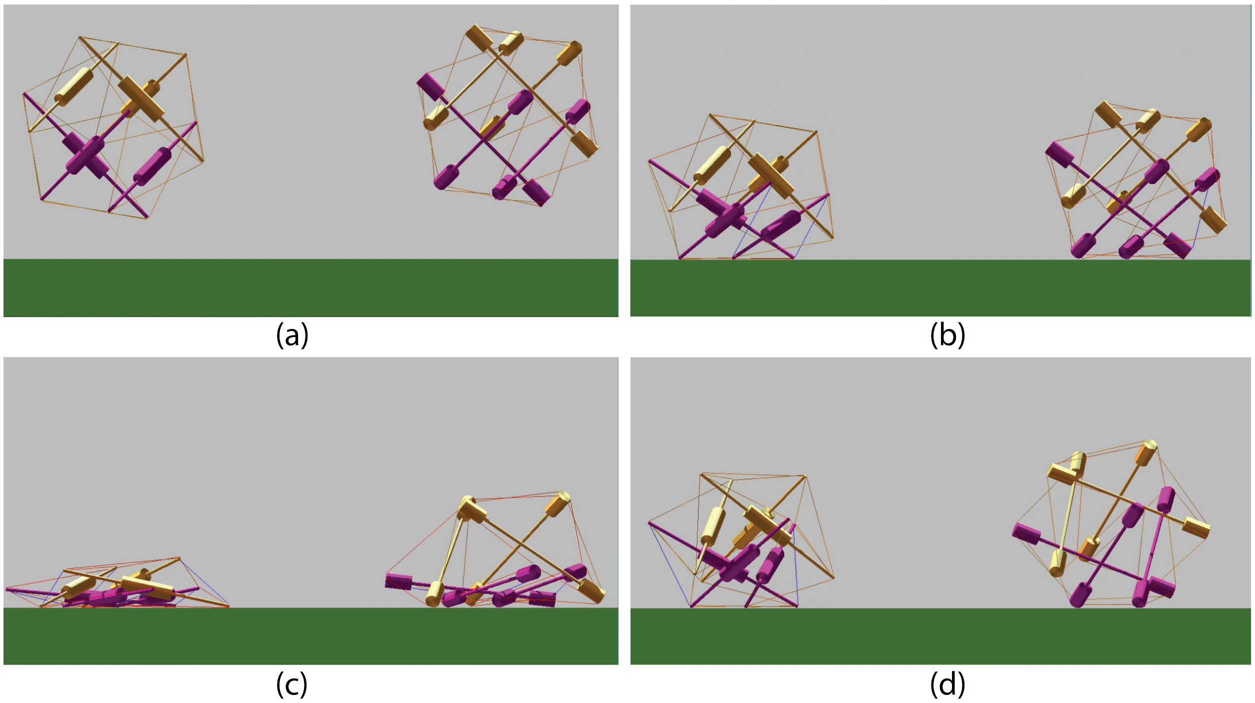

Figure 3.3: (a)(b)(c)(d) Is the sequence of impact from the same height of two tensegrity structures with different mass distribution (left tensegrity has mass at center and right tensegrity has mass on the ends) [6].

it is divided to the two ends of the rod. This simulation and resulting images (Figure 3.3) confirm the structure on the left is able to deform more during impact.

During the simulations, rod acceleration was recorded at the location where critical components are housed (the center capsule for TT-3 and the end modules used in previous prototypes). Data, showing the initial impact in Figure 3.4, illustrate the impact intensity experienced by critical components during landing. From the graph, it can be seen that the TT-3 architecture can better protect the critical components as they do not come in direct contact with the ground and thus experience a lower magnitude of acceleration (high g forces) during impact.

3.5 Impact Experiment

To further study the impact absorption properties of the TT-3 robot, a TT-3 robot replica was developed (Figure. 3.5). Since theTT-3 robot was the only functioning robot of its kind, we did not want to perform the impact testing on it as we did not want to risk

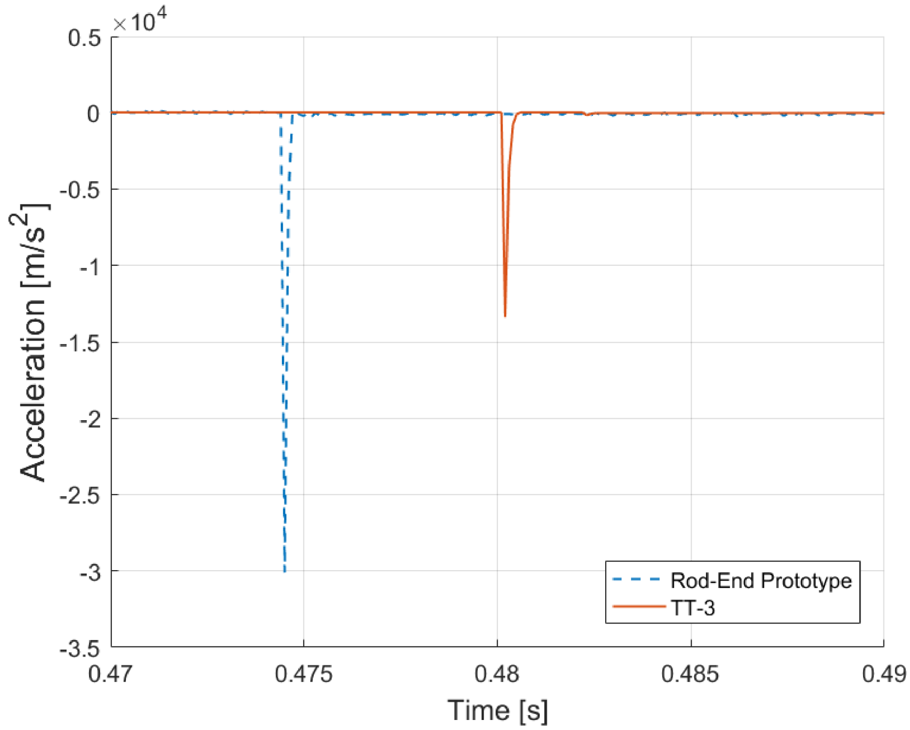

Figure 3.4: Acceleration data of rod-centered TT-3 versus Rod-End prototypes during impact in simulation [7].

damaging it. Therefore, a TT-3 robot replica was constructed to study the behavior of the TT-3 robot under various impact heights. The TT-3 replica was named the TT-3_{IMPACT}. The TT-3_{IMPACT} was an exact replica of the TT-3 robot except that the actuation system was replaced with weights of the exact mass, so the robot had the same weight distribution as the TT-3 robot. In order to study the impact behavior from various heights on tensegrity structures or robots, an adjustable drop test system was developed to consistently observe the robot during impact at various heights shown in Figure 3.6.

The TT-3_{IMPACT} structure was dropped from five different heights. During each drop, a high speed camera was used to record the deformation (top to bottom) from rest (25 in.) of the tensegrity structure during impact (Figure 3.7). Figure 3.8 is a plot of the deformation of TT-3_{IMPACT} structure from each height drop.

Figure 3.5: A replica of the TT-3 robot was developed to test the impact behavior of the TT-3 robot.

3.6 Hardware Design

The previous sections have shown the benefits of locating the majority of the mass of the system at the center of the rod; therefore, the rod-centered design will be the base architecture of the TT-3 robot design.

The goal of the research is to create a robot that can absorb the energy from landing and be actuated to perform locomotion. It is also important to design a robot that can maneuver around various terrains. It is shown in the later sections that one mode of locomotion for tensegrity robots is to shift its center of mass outside of the base triangle to perform a punctuated roll.

An actuated cable in series with a spring is the chosen method for changing the shape of the structure to adjust the location of the projected center of mass. Cable actuation is chosen due to its ability to have long displacements between the nodes of the tensegrity robot. The range of displacement between the nodes of the structure can greatly determine the potential of shape shifting.

A simple motor and spool design is the selected method to change the length of cable

Figure 3.6: An adjustable drop test system was developed to consistently drop tensegrity robots/structures from different heights.

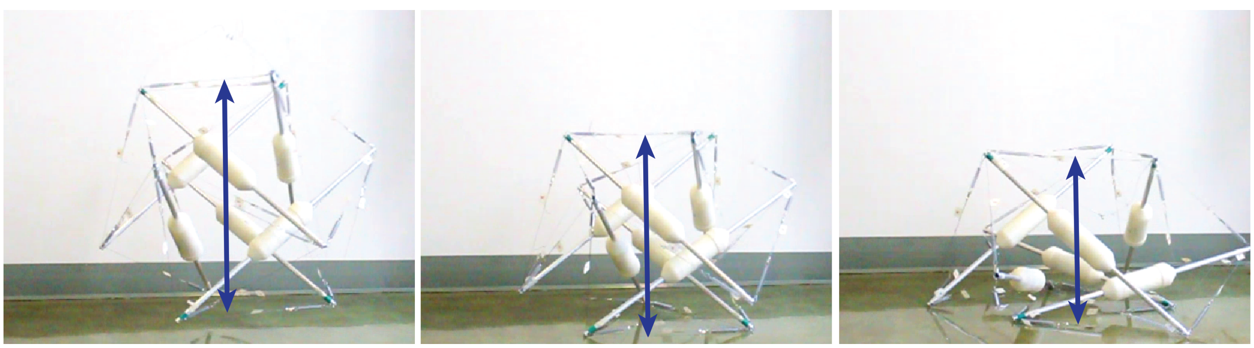

Figure 3.7: High speed video footage showing the deformation of the TT-3 structure during impact [7].

between the nodes of the structure. This method allows for the ease of placement of the motor at a desired location, which is the center of the rod for TT-3.

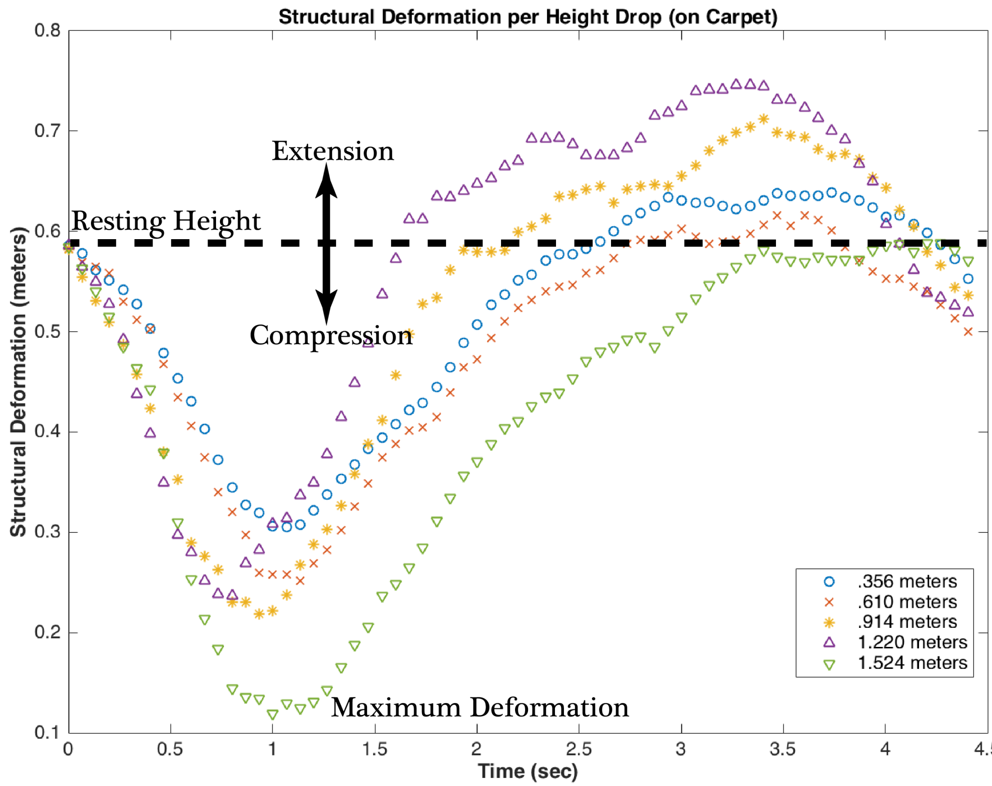

Figure 3.8: TT-3 structure deformation from different heights [7].

3.6.1 Actuator Selection

After performing the required force simulation from NTRT, a few motors were selected for potential actuators for the robot. One key criterion during actuator selection was the high torque to weight ratio. High torque to weight ratio creates the possibility to develop a lightweight tensegrity robot with a large range of tension adjustments and stiffness.

Three motors were selected: Pololu model 1595, Pololu model 2275, and Pololu 2218. They are all brushed DC motors because low cost is a goal for the overall system. The Pololu motor model 1595 weights 10.5g. The Pololu motor model 2275 weights 103g. And the Pololu motor model 2218 weights 9.5g. Pololu 2218 and 1595 are both very lightweight, making them highly useful as there will be 24 motors needed to construct a fully actuated robot.

3.6.2 Actuator Testing

The selected motors were tested with the EXTECH heavy-duty digital torque meter to measure the stall. The motors were secured on a fixer, and voltage was supplied to the motors individually. The supply voltage was started with one volt, and then increased with the increment of one up to 9 volts. At each voltage, the stall torque value was recorded. This process was used to observe the behavior of the motors at different voltages, and was used to compare with the manufacturer specification. Pololu 2218 was the chosen actuator through this process as the other two actuators did not perform reliably under high voltage.

3.6.3 Endcap Design

Due to the relatively low power of the driving motors, any means of reducing cable friction in the robot will improve its functionality. For a cable driven robot, the cables might experience high friction while in contact with material with different velocities or routings through corners. In the TT-3 system, one of the main locations of high friction force is the point of contact where the cable is routed out of the rod to connect with the neighboring rod. To address this issue, several "endcaps" were designed to fit on the end of the compression members, which will provide various routing methods for the cables. In addition to friction force reduction, these endcaps also need to provide non-permanent connection points for the other two tension members that connect to the end of a compression member.

Direct Routing through Polished Aluminum Tubes

Shown in Figure 3.9(a), the aluminum tubes have four holes drilled and polished on each end of the compression member. Two of the holes are used as the routing path for the cables inside of the rod to come out and connect to the neighboring rods. The two other holes are used for the neighboring cables to connect to.

3D-printed ABS+ Plastic End Caps

One method for reducing friction is to guide the cables out of the hollow aluminum tubes that form the compression members by introducing a smooth contoured surface rather than having the cable travel over the edge of the tube.

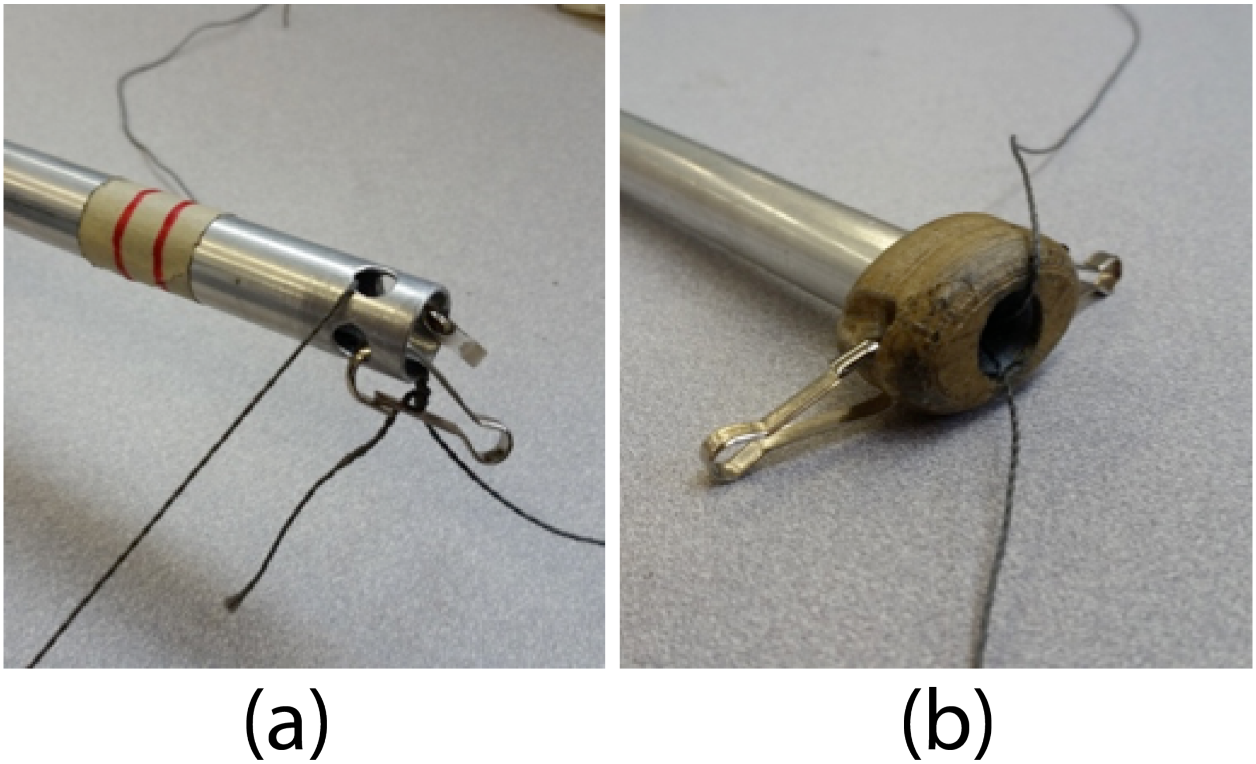

Figure 3.9: (a)Cable routed directly through polished aluminum tube. (b) Cable routed through 3D-printed endcap [6].

The first iteration was made of 3D-printed ABS+ plastic and was modeled relatively simply shown in Figure 3.9(b).

Although it served its basic purpose, several flaws existed in the design. The cable still traveled over a relatively sharp angle while exiting the tube. Even though the design had an exterior fillet that reduced friction effectively, the ABS+ plastic was not resistant to wear which led to the cable wearing channels into the endcaps. These channels increased the cable wear, friction, and prevented the cables from sliding along the circumference of the tube during shape shifting. The off-the-shelf clips used as attachment points for the springs would also frequently tangle with the cables and were inconvenient to attach and detach from the endcap. Also, during punctuated rolling, wear was shown on the endcaps after hours of testing. Lastly, with the elliptical outer geometry, the endcaps seemed to have unpredictable behavior on dirt, sand and other types of rough terrain.

Machined Aluminum Endcap

A new set of aluminum endcaps were designed to address the shortcomings of the 3D-printed plastic endcaps. Machining the next design out of aluminum instead of 3D printing the design addressed the wear problems and reduced the friction by having the cables move on a polished machined surface instead of rougher, 3D printed surfaces. The redesign could be prototyped quickly using standard machine shop tools to maintain the goal of rapid prototyped robot. Due to the unreliability of the off-the-shelf clips for connecting and disconnecting the cables, an inset spring pin was designed as the new attachment system. However, the spring pins did not function as well as intended. They were meant to be inserted and removed by hand, but due to inconsistencies between pins as well as difficulty creating a hole of the required size for the desired fit, the attempted fits resulted in the pins being too difficult to insert or falling out when tension was released. In addition, a minor sharp edge from one of the milling operation was observed on all endcaps after detailed inspection.

To address the issue of minor sharp edge on the inner wall, the machining method and sequence were adjusted to produce a polished inner wall without defects from machining. In addition, the new design removed the spring pin system and replaced it with two easily machined vertical holes for tying a cable loop for attaching the springs shown in Figure 3.10(a). The vertical hole size was adjusted to try different methods of spring attachment shown in Figure 3.10(b).

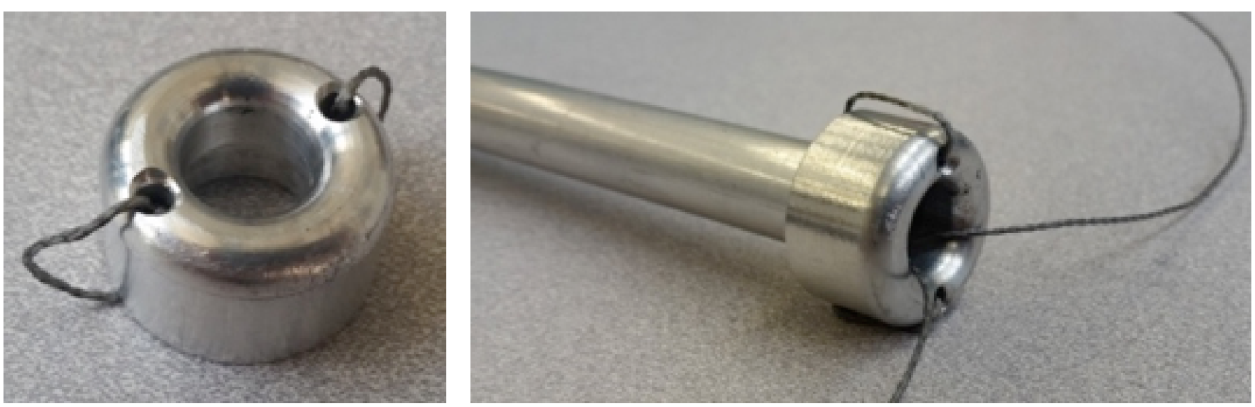

(a) (b)

Figure 3.10: (a)The machined aluminum endcap. (b) Cable routed through the machined endcap installed on the aluminum tube [6].

3.6.4 Endcap Evaluation

The endcaps were redesigned with the goal of lowering the friction force between the endcap and the cable. This friction delivers a large load on the motors causing them to stall if not handled properly.

An endcap testing platform was developed to quantify the static friction experienced on the cable from the endcap. This testing tool was able to repeatedly test various endcap designs to provide insights on the performance of the designs. With the endcap tester, the baseline performance for the current endcap was established and used to compare with future iterations.

The endcap was first installed on the tester shown in Figure 3.11, then a cable was connected to both scales through the endcap and rod assembly. The turnbuckle was tightened until scale 1 read between 0.5 kg and 1 kg. The cable was pulled away from the endcap and towards scale 2 and then released. This was to ensure there was not a false binding force associated with tensioning the cable. After the readings on each scale were recorded, the turnbuckle was then tightened to a higher tension force, and a new reading was recorded. This process was repeated until nine different tension readings were recorded. When the data collection was finished, the turnbuckle was loosened until the scales again read between 0.5 kg and 1 kg. The process was repeated until there were a total of four sets of data per endcap design.

As seen in Figure 3.12, the data revealed an expected linear relationship between the reading on scale 1 and scale 2. The friction force between the cable and the endcap was determined by subtracting the two scale readings. A frictionless endcap would result in no difference between the two readings due to no external forces, so the ideal slope of the data would be 1 with a y-intercept of 0. Therefore, the slope of the line can determine the performance of different endcap designs regarding the friction force between the cable and endcap. The endcaps with high friction forces will have a line with low slope. With this information, the performance of different endcap designs can be ranked.

Shown in Figure 3.12, the machined aluminum endcap had the least amount of friction between the cable and the endcap, followed by the 3D-printed ABS+ plastic endcaps. The cable routed through the aluminum rod without an endcap generated the most friction force.

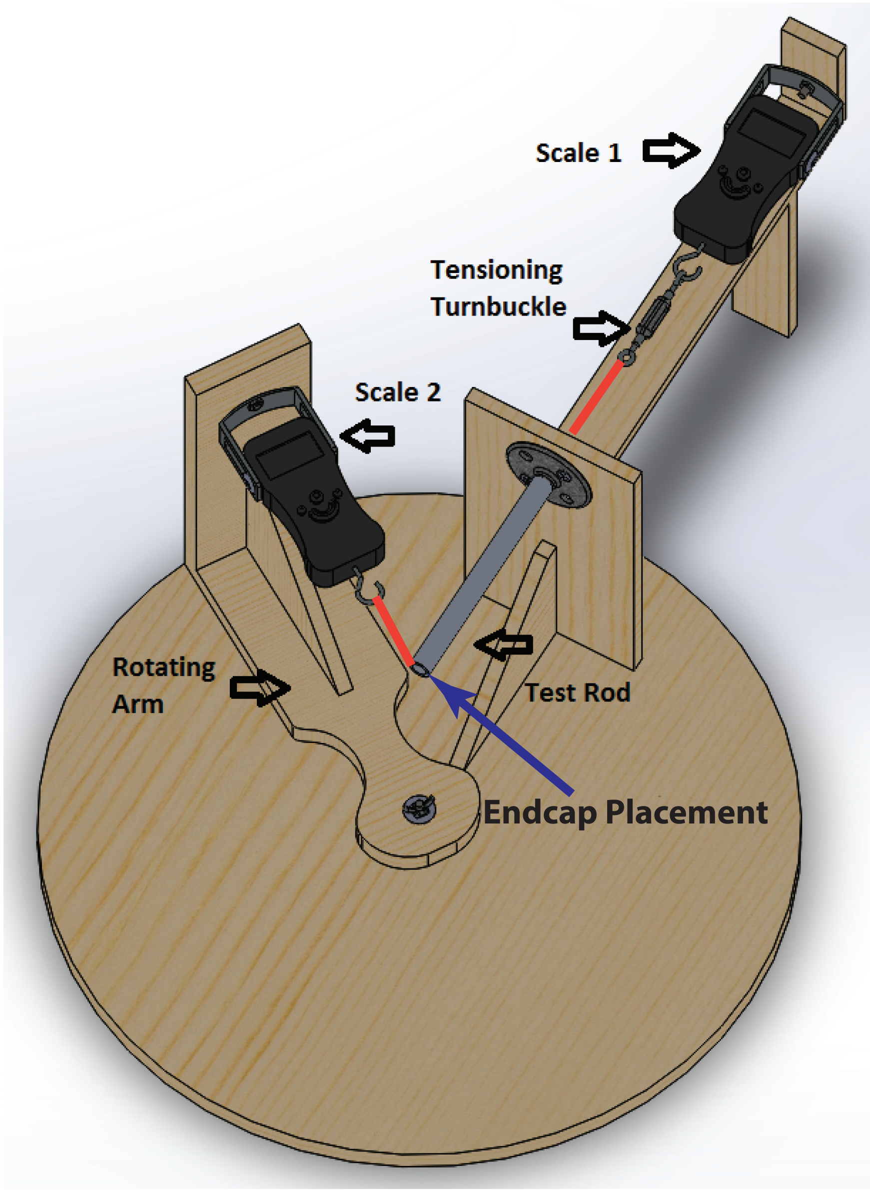

Figure 3.11: 3D model of the endcap testing platform [6].

3.7 Hardware Prototype

3.7.1 Actuation Module using Acrylic Platform

The new design strategy was to design a modular actuation module that is located at the center of the rod. There are a total of 24 motors; six rods and 4 motors in each module. It is important to have a reliable and robust system for space exploration. Therefore,

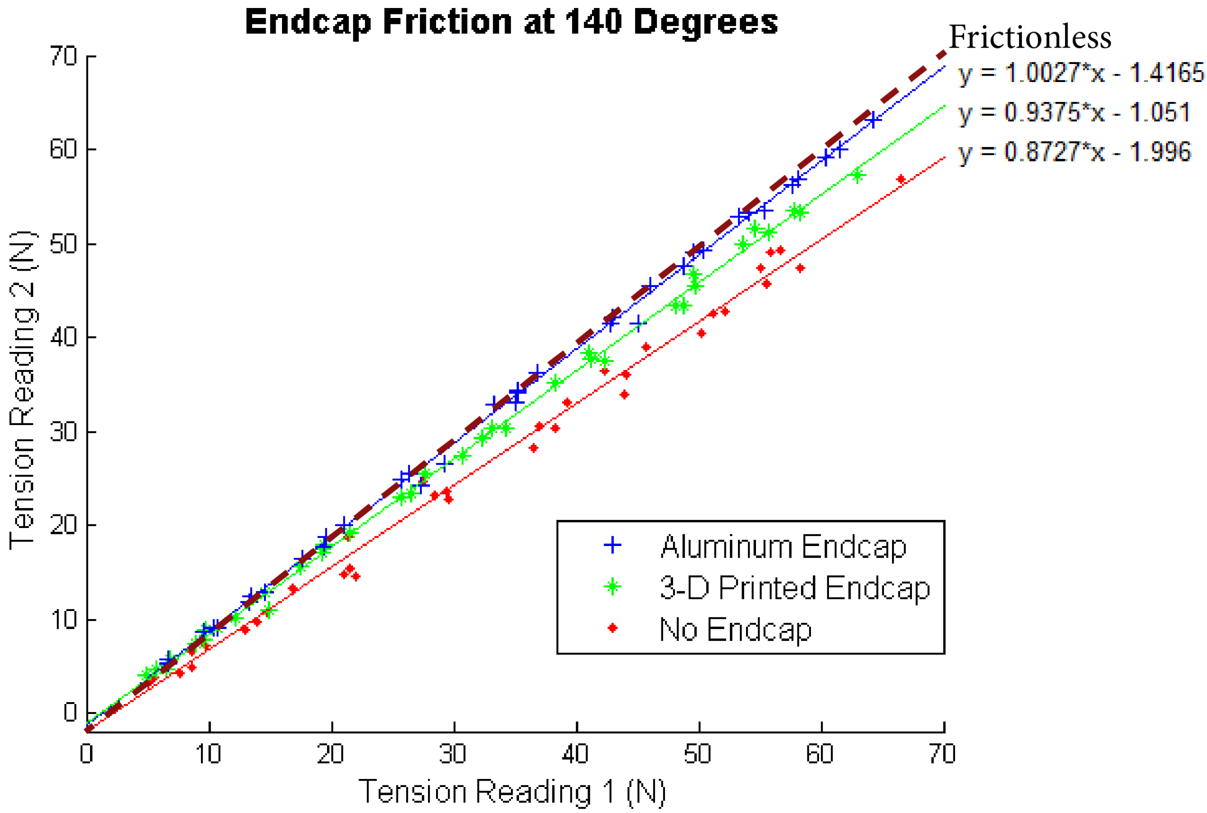

Figure 3.12: Plot displaying the relation of tension force on scale 1 and scale 2 [6].

redundancy should be a key design feature. Therefore, TT-3 is designed with an individual microcontroller in its actuation module.

Wireless communication is used as the main method for command signals and data transfer. The use of wireless units greatly simplifies the wiring, and no wires are required between the rods.

For the first prototype, an acrylic sheet was used as the platform for mounting all the components for the actuation module. Most of components used were off-the-shelf, including a microcontroller, a wireless unit, a voltage regulator, two motor drivers, four motors and a battery pack. The hole patterns on the acrylic board were first modeled on a computer-aided design (CAD) program, then the pattern was exported to a laser cutter for manufacturing. Shown in Figure 3.13 is the top and bottom of the assembled acrylic actuation module.

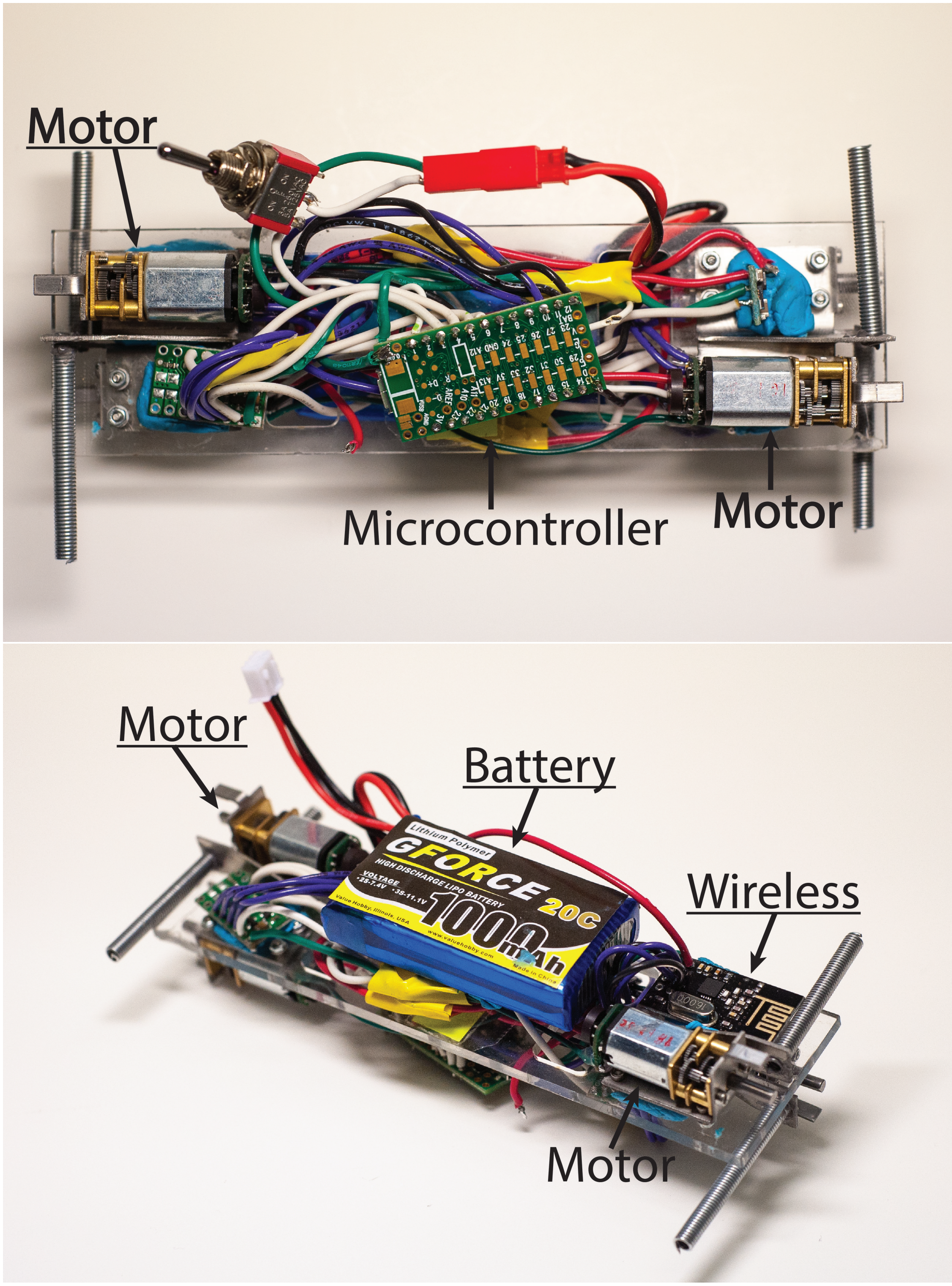

Figure 3.13: Top and bottom of the actuation module with four motors, a microcontroller, a wireless unit, two motor driver, a voltage regulator, and a battery pack [6].

An enclosure was designed to house the actuation module. The enclosure has an internal rail for the acrylic plate to slide into with a cap placed over the open end to fully enclose the actuation module. Currently, the gold colored enclosure shown in Figure 3.14 and Figure 3.15, is manufactured with a fused deposition modeling (FDM) machine. Two 0.5 inch diameter aluminum tubes are connected to both ends of the 3D-printed enclosure. One of the design features allows for the quick removal of the tubes, and the tube length can be adjusted for modularity. With different tube lengths, different sizes of tensegrity robots can be built, making the TT-3 platform modular and adjustable.

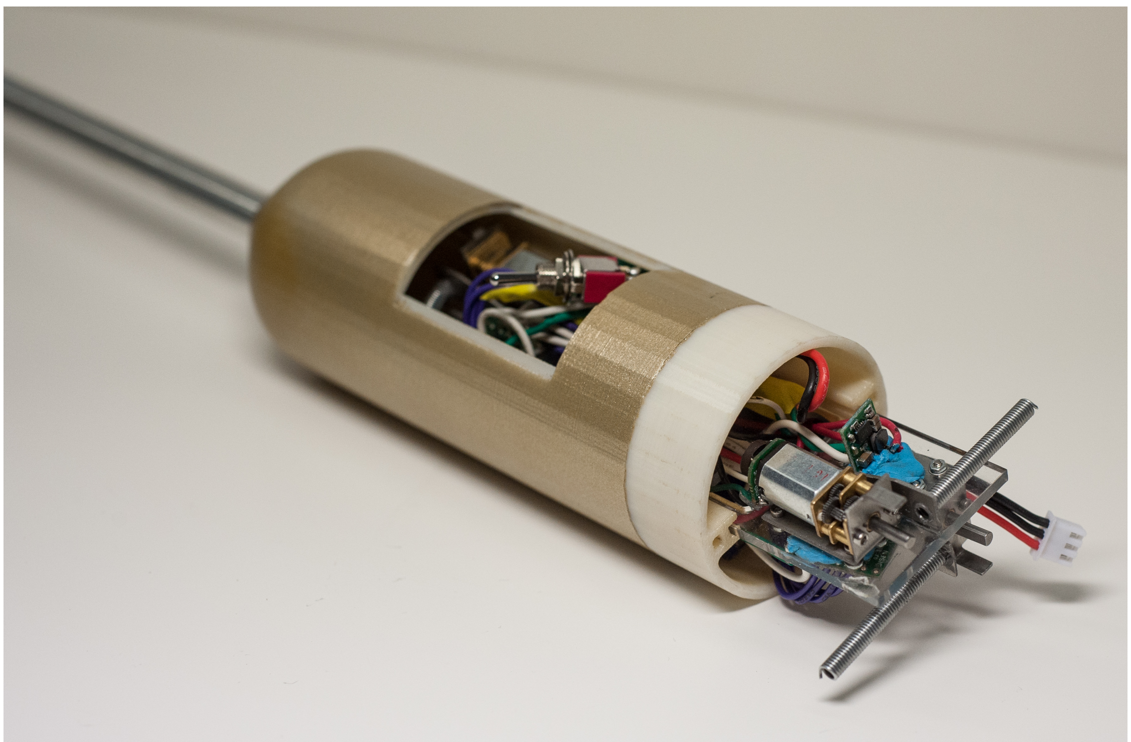

Figure 3.14: Actuation module slides into the plastic enclosure.

3.7.2 Printed Circuit Board Actuation Module Design

The acrylic plastic prototyped actuation module design described previously was able to provide promising results during preliminary testing. The TT-3 built with this actuation module was able to perform punctuated rolling with only a single motor actuated. However, the robot experienced unreliability during testing of long durations. Sometimes, the slave module would power off during rolling. After performing a failure mode analysis, it was discovered that the complex wiring on the actuation module was causing the inconsistent

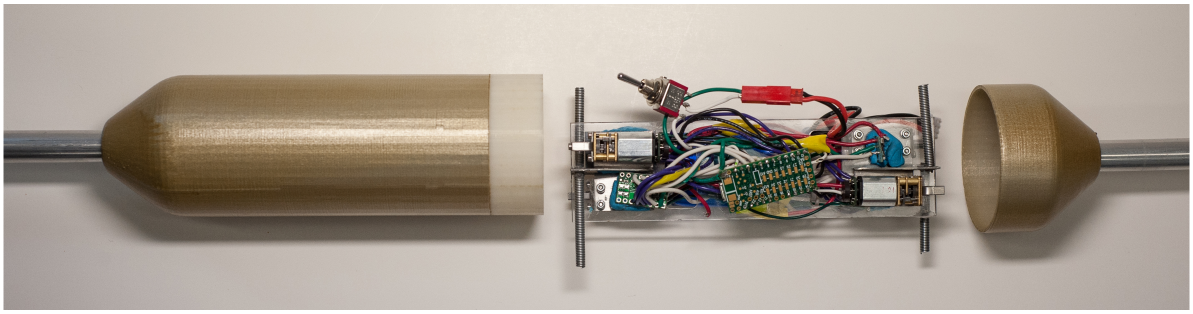

Figure 3.15: Aluminum tubes, plastic enclosure, actuation module, and enclosure cap, which constructs a rod of TT-3 robot [6].

connection. One of the main causes of the inconsistent connection was the quality of the solder of the wire to wire connection. In addition to the unreliability of the wire connections, this actuation modules were difficult to reproduce, which make it less ideal as a rapid prototyped robot.

The solution for this issue was the use of a custom printed circuit boards as the replacement of the wires and acrylic support structure show in Figure 3.16. The custom printed circuit board (PCB) as the base structure for building the actuation modules not only increased reliability, but also reduced the time and complexity of the prototyping process. The assembly time was reduced from 24 person-hours to eight person-hours for the full assembly of the six actuation modules.

Figure 3.17 shows how the printed circuit board actuation module is placed on TT-3, and how the cables are routed from the motors out to the neighboring rod to form the six bar tensegrity structure.

3.8 Control and actuation strategy

The TT-3 robot is based on a six-bar tensegrity structure, which is similar to an icosahedron, a spherical polyhedron. Unlike an icosahedron, the structure is missing six edges on its outer surface, resulting in a total of 24 cables, which form eight equilateral and twelve isosceles triangles. The most natural choice of locomotion for this robot is rolling based on its ball-shaped structure. However, the motion is discontinuous because the robot's outer surface is not perfectly smooth, and therefore this motion is refer to as "punctuated rolling motion." The basic building block of this motion is a "step" which refers to a rotation of the body from one base triangle to another (Figure 3.18). The TT-3 robot realizes this step by

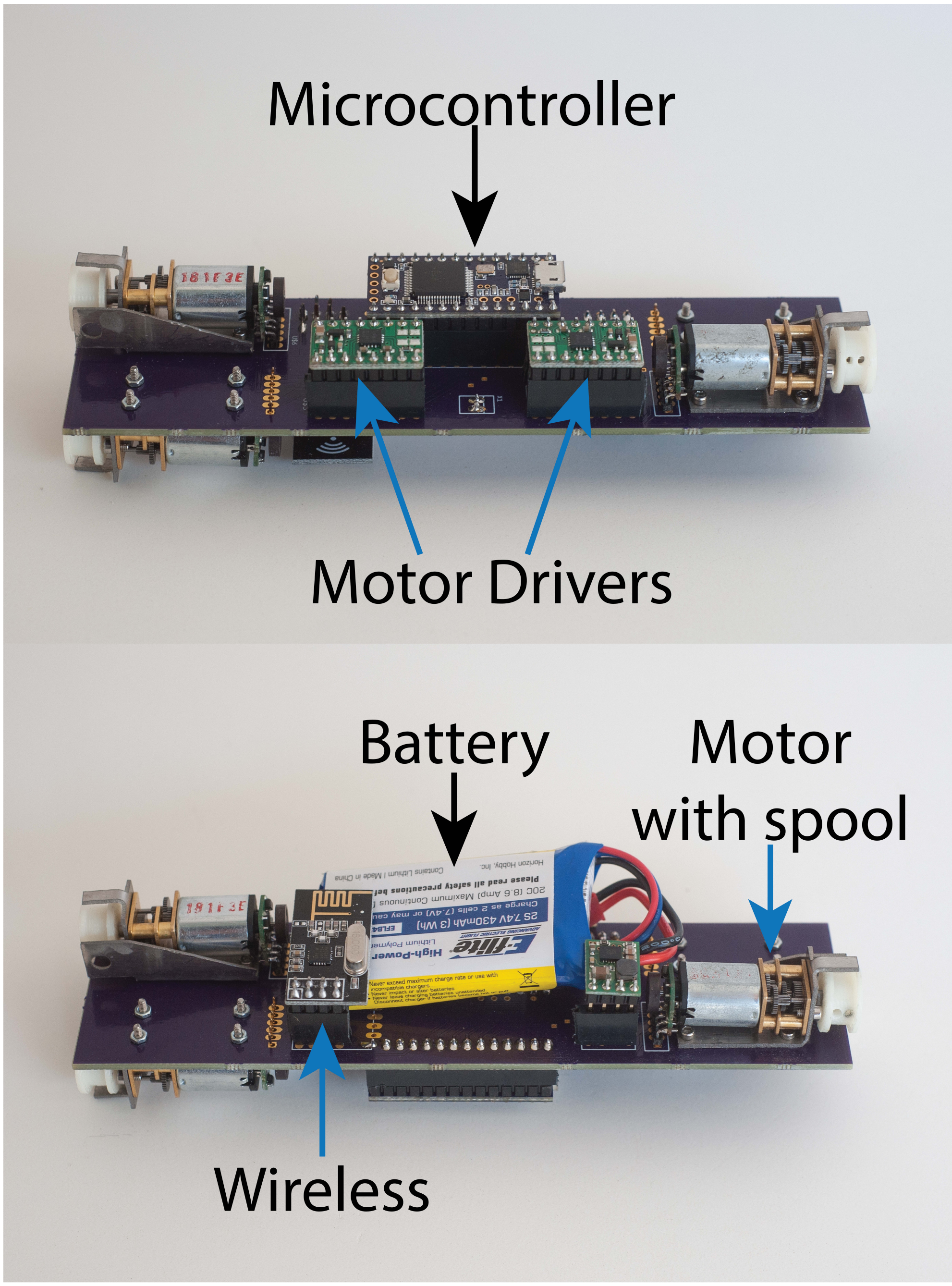

Figure 3.16: This image displays the top and bottom of the actuation module using printed circuit board as its base platform [6].

deforming its body shape by changing the lengths of its member cables in a shape-shifting manner. Not all deformations lead to a step; in order to make a successful step, the defor-

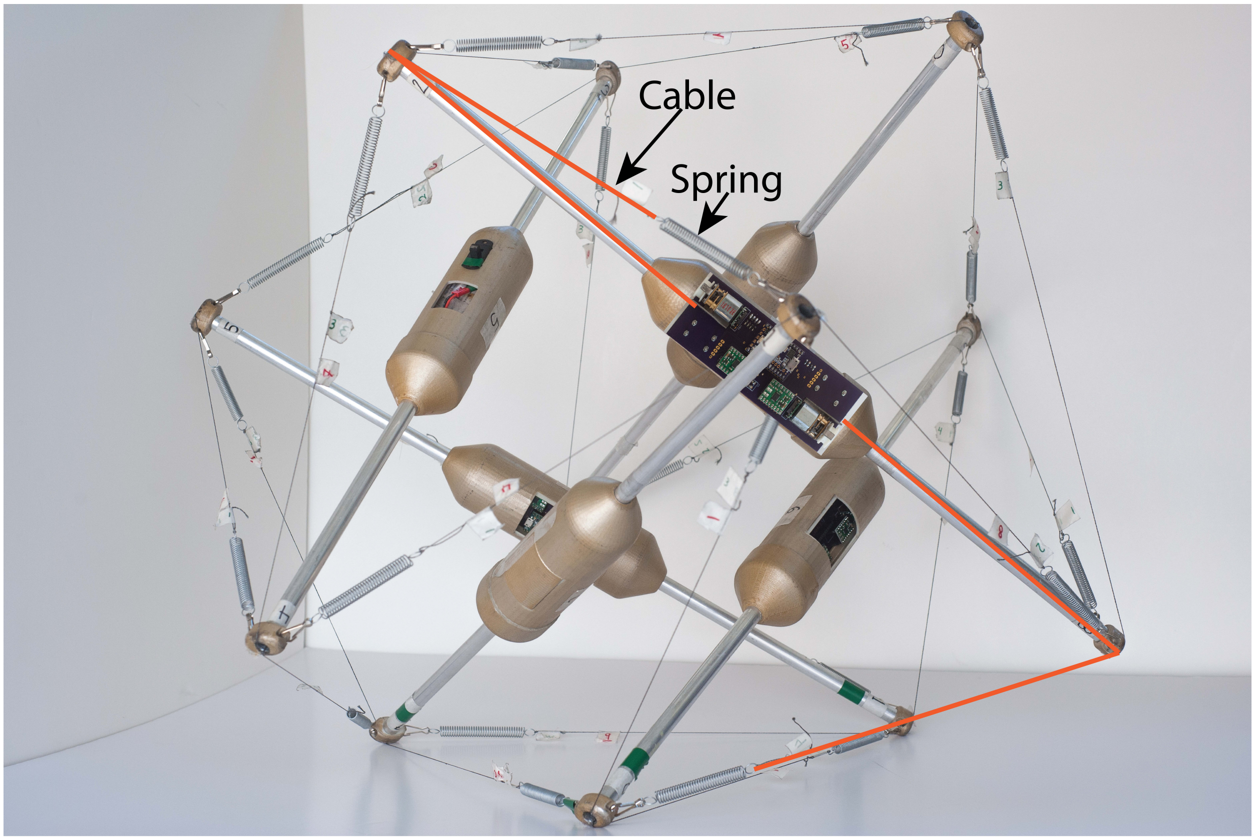

Figure 3.17: Image displaying how the cables are routed from the center module [6].

mation should take the ground projection of the center of mass (GCoM) outside of the base triangle.

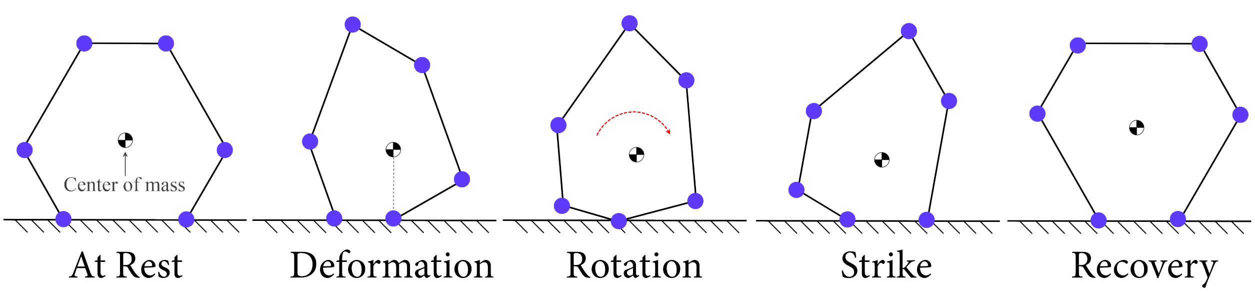

Figure 3.18: A conceptual diagram that represent the different stages of shape-shifting performed by TT-3 to complete punctuated rolling [6].

In previous research, the actuation policies developed actuation resulted in successful performance of punctuated rolling motion for a fully-actuated and cable-driven six-bar tensegrity robot. The search method [13] and multi-generation learning algorithm [8] were used to efficiently handle high dimensional control inputs. The symmetry of the structure was exploited when developing the actuation policies. The policies attempt to achieve two goals with the structure deformation: a) reduce the area of the base triangle, and b) shift the position of GCoM as far as possible from the base triangle to make the structure unstable, thus leading to a step. Depending on the design of the tensegrity robot, multiple cables could be actuated simultaneously to make a step. For example, the TT-2 robot had a rigid linear actuator at the center of each cable edge, and this poses a limitation on the range of cable lengths that could be controlled [13]. As a result, the robot had a limitation on the maximum deformation it could achieve per cable actuation. For this reason, in order to achieve a step, at least three cables required actuation at the same time with the TT-2 robot.

The new design of the TT-3 robot can overcome this barrier. The edges of the TT-3 robot consist of cables and springs without any rigid body components; therefore, there is no mechanical restriction on how much a cable can be retracted, resulting in a greater deformation per actuation when compared to TT-2. In fact, a single cable actuation is sufficient to realize a step with the TT-3 robot. If one of the base triangle cables is fully retracted, the area of the base triangle becomes very small and the structure goes unstable. Hence, no additional actuation is required to shift the position of GCoM away from the base triangle because this will happen as a natural consequence of having a small area base triangle. The direction of a step is determined by which edge of the base triangle is being actuated. There are a total of three edges in a triangle; therefore, at each face, there are three potential directions of travel shown in Figure 3.19. In this work, only the single actuation strategy is implemented on the TT-3 as this is sufficient for the robot to move around on a flat ground. However, when the robot is required to move on uneven terrain (e.g., inclines), greater deformation may be favorable. In this case, the actuation policies developed by Kyunam Kim [8] [13] can potentially be useful. Currently, TT-3 uses wireless communication to signal the actuation commands. Each of the six actuation modules on the tensegrity robot has its own dedicated wireless communication unit. These wireless communication units act as slave units in the wireless network. The master wireless unit that is used to send commands to the slave unit is placed externally. However, there is no difference between the master and slave units, and any of the slave units can serve as a master, untethering the communication system from external devices. The current communication architecture is chosen for ease of debugging. With the current control, the desired motor encoder value is sent from the master module to the slave modules. The motor in the slave module will actuate the motor to the desired encoder count, and then send back the updated encoder value when the target is achieved. All 24 motors on TT-3 can be controlled through the method described above.

Currently, TT-3 uses wireless communication to signal the actuation commands. Each of the six actuation modules on the tensegrity robot has its own dedicated wireless communication unit. These wireless communication units act as slave units in the wireless network. The master wireless unit that is used to send commands to the slave unit is placed externally. However, there is no difference between the master and slave units, and any of the slave units can serve as a master, untethering the communication system from external devices. The current communication architecture is chosen for ease of debugging.

With the current control, the desired motor encoder value is sent from the master module to the slave modules. The motor in the slave module will actuate the motor to the desired encoder count, and then send back the updated encoder value when the target is achieved. All 24 motors on TT-3 can be controlled through the method described above.

3.9 Hardware Testing

Various locomotion experiments were performed to observe the behavior of the robot.

3.9.1 Single Punctuated Roll and Rolling in Circular Pattern

The first test for the robot was to test its ability to perform single step punctuated roll. If the robotic was not able to perform a single step rolling, then it signals some potential design flaws. The TT-3 robot was successful in shape-shifting its structure to achieve a single step punctuated roll. A six-bar tensegrity robot only required minimally four steps to complete a full circle rolling pattern. This rolling pattern can be achieved by a single actuation module since there are four actuators in a module. And the TT-3 robot was able to demonstrated successful rolling in a circular pattern continuously on flat ground.

3.9.2 Continuous Punctuated Rolling in Straight Line

The second test on the robot was to walk in a straight trajectory. It was able to accomplish the straight line-walk in a punctuated rolling style on a flat concrete floor shown in Figure 3.20. The measured rolling velocity was 5 cm/s for TT-3.

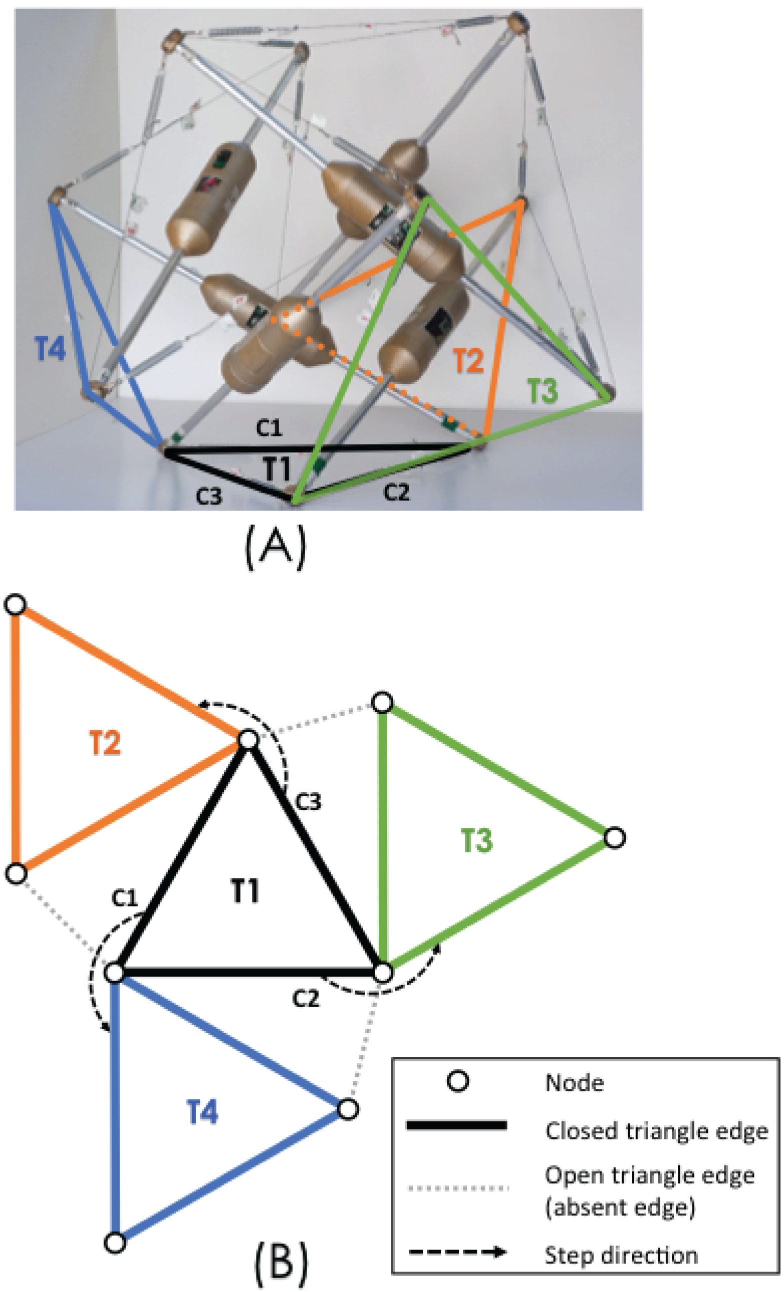

Figure 3.19: (a) A diagram of TT-3 with labeled based triangle T1 and three other neighbor triangles T2, T3 and T4. (b) the diagram displays the three cables C1, C2, C3 and its resulting triangle if actuated. [8] [9] [6]

Figure 3.20: TT-3 performing straight line walk [6].

3.9.3 Continuous Punctuated Rolling in Straight Line with Payload

The third experiment on the robot was to perform punctuated rolling in a straight line while carrying a simulated payload at the center of the robot. This experiment helped us to visualize the interaction between the payload and the robot during locomotion. Figure 3.22 shows the steps performed by TT-3 while carrying a payload at the center of the robot. The payload did not interfere with the shape shifting required for a step during the experiment.

Figure 3.21: TT-3 performs straight line walk while carrying a center payload [6].

3.9.4 Turning Capability

Since the TT-3 is a fully actuated six-bar tensegrity robot, it has three direction options at the start of each punctuated roll. During the turning experiment, the TT-3 was able to successfully demonstrate the during capability from resting shown in Figure 3.23.

3.9.5 Punctuated Roll on Outdoor Terrain

In addition to the indoor tests, TT-3 was tested to roll on an uneven outdoor terrain shown in Figure 3.22. Not surprisingly, it appeared to be more difficult for the robot to roll on loose dirt than flat concrete floor. The rods of the robot seem to dig into the dirt or drag along the dirt during punctuated rolling. However, the robot was successful in performing the straight line roll command.

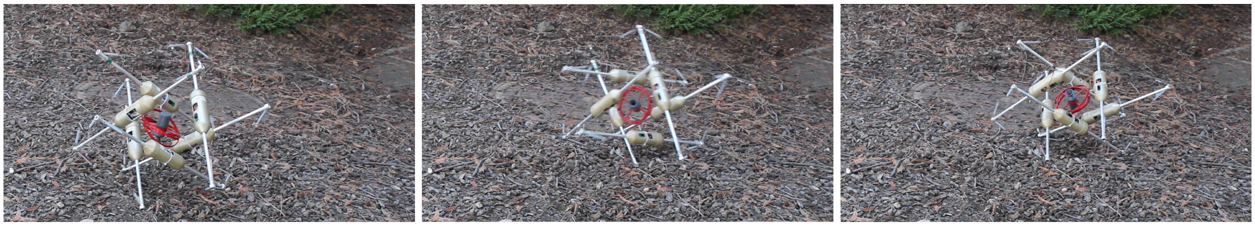

Figure 3.22: TT-3 performs straight line walk on an uneven outdoor terrain [6].

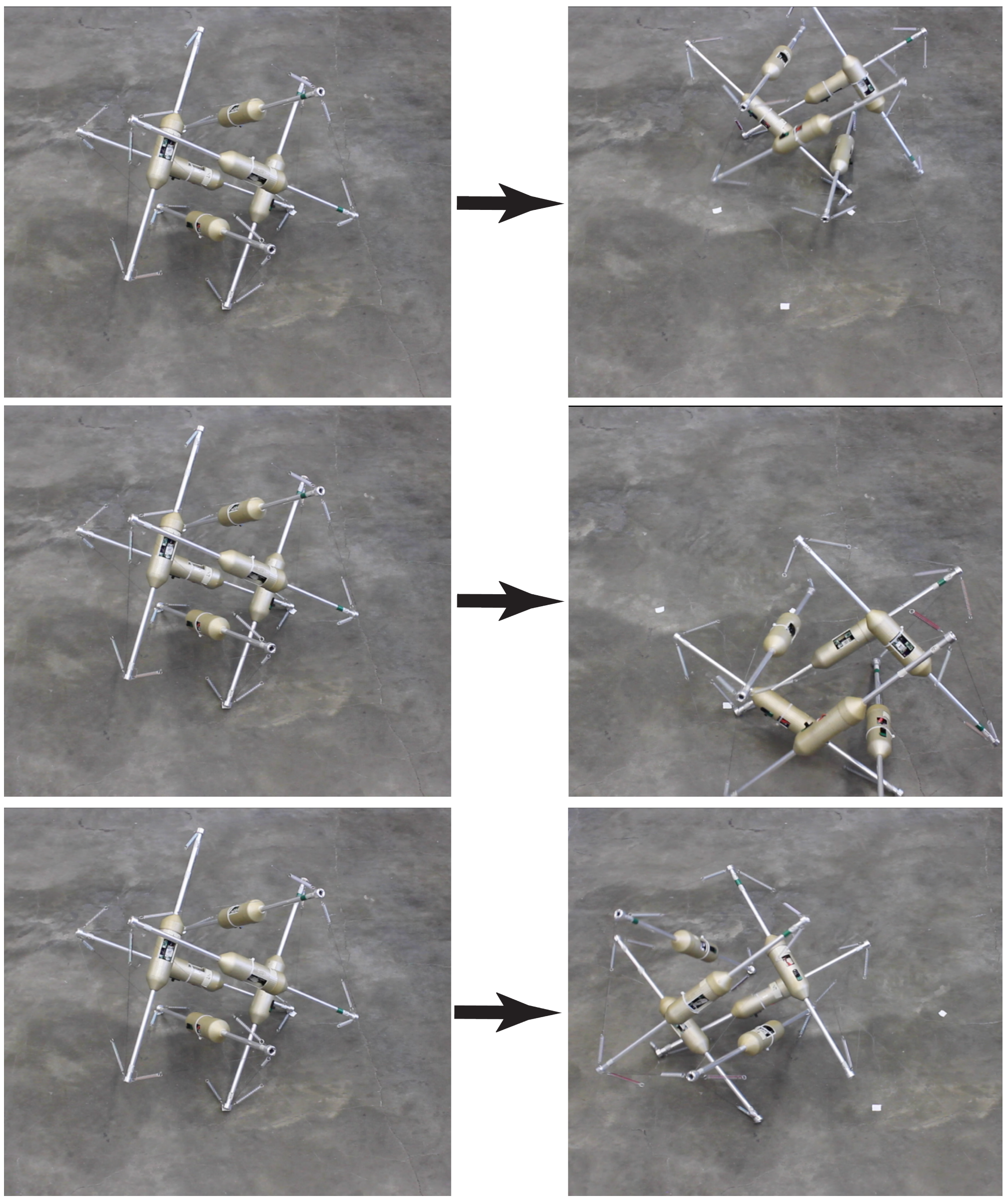

Figure 3.23: TT-3 was successful in demonstrating its ability to turn.

Chapter 4

Berkeley TT-4_{mini}

4.1 Motivation - Challenges in Tensegrity Prototyping

Tensegrity structures are notoriously difficult to assemble because the members are not in balanced compression and tension until the structure is fully assembled. In the intermediary steps of assembly, forces are unevenly distributed and the structure is difficult to constrain. It is easy to make mistakes in assembly, such as connecting the wrong tension and compression members. To illustrate the complexity of assembly, a low-fidelity prototype of a 6-bar tensegrity structure made with wooden dowels and springs can take as long as an hour for a team to assemble. Since the research team at the University of California at Berkeley has been simulating, designing, and prototyping various tensegrity systems, it is critical to develop an efficient prototyping platform for rapid creation of new tensegrity robots to experiment with novel concepts.

4.2 Development of the Modular, Elastic Lattice

The idea for an elastic lattice came from examining an assembled six-bar tensegrity structure and conceptualizing how the tension members (cables in series with springs) could be deconstructed from a 3D structure to the 2D plane. As I visualized this deconstruction, I had the idea that a new elastic medium, sheets of silicone rubber, could be used to construct the tension members. I observed that the tension members of the six-bar robot form an icosahedron. Thus I expected that a regular pattern of triangles would map the structure in the 2D plane. This was tested using a plastic sheet, which was cut to trace the tension members of an assembled six-bar tensegrity robot. The production of this low fidelity prototype made it evident that eight triangular units, such as the one in Figure 4.1, were needed to form the six-bar tensegrity structure.

The first elastic prototypes of the lattice for a six-bar spherical tensegrity were created using 0.02 in. thick, 20A durometer silicone rubber and cut with a single-beam Universal Systems laser cutter. The lightness of the silicone rubber caused challenges during the laser cutting process. Because it was so light, the venting system of the laser cutter caused the rubber to lift up and flap as it was being cut, risking the correct profile of the cut. This risk was averted by putting masking tape on both sides of the rubber sheet, thus making the sheet heavier so it did not lift up and flap. This ensured that the proper design could be created without impeding the cutting ability of the laser.

After we made a number of prototypes with this silicone lattice, it became clear that the 0.02 in. thick, 20A durometer silicone rubber did not have the correct material properties for our six-bar tensegrity application. The hardness and thickness of the silicone rubber did not provide enough tension to the system, even with different width profiles.

The prototypes in the next iteration were made with 0.0625 in. thick, 60A durometer silicone rubber. By experimenting with various widths of the rubber elastic lattice, the desired tension in the system was achieved using this material. These prototypes were produced using a double-beam Universal Systems laser cutter. The heavier silicone rubber did not face the same manufacturing issues as the 20A durometer silicone rubber but presented new difficulties in the laser cutting process. Initially the laser cutter was just etching the silicone rubber instead of cutting it. The optimal laser cutting setting was achieved on the cutter by using only the top laser beam instead of both laser beams.

The elastic prototypes made with 60A durometer silicone rubber (Figure 4.1) were much stiffer than the previous versions, and they could withstand higher tension. Thus these prototypes better demonstrated the unique characteristics of tensegrity structures.

4.3 Use of the Elastic Lattice to Assemble a six-bar Tensegrity Structure

The modular, elastic lattice enables rapid prototyping and testing of tensegrity structures. Production of the elastic lattice is efficient, as laser cutting is straightforward and fast. The timeline of assembly of any tensegrity structure is vastly accelerated by the use of an elastic lattice; assembly is on the order of a couple minutes rather than an hour. Many other

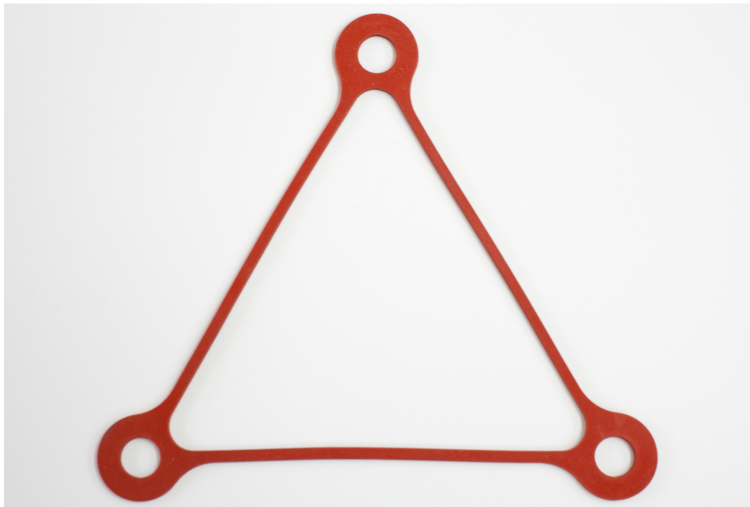

Figure 4.1: Modular elastic lattice prototype made with 60A durometer rubber [10].

tensegrity structures have tension members arranged with triangles as the basic unit, so this methodology can be used to prototype tensegrity structures other than the six-bar structure.

Modularity is a benefit for early-stage construction of more complex structures. For the six-bar tensegrity, it was found that combining the eight triangles into a single piece made assembly quicker and simpler. The single-piece lattice is shown in Figure 4.2. This lattice structure is then used in the demonstration assembly shown in Figure 4.3.

Figure 4.3 illustrates the step-by-step sequence required to assemble a six-bar tensegrity structure using this newly developed prototyping method. Since the main two elements of a tensegrity structure are tension and compression, it was decided to use thin-walled aluminum rods as the compression elements in our static tensegrity prototype. The 3D printed endcaps were used as the connection between the modular elastic lattice and the aluminum rods. A fully assembled six-bar tensegrity structure requires one of the one-piece lattices (or eight of the rubber elastic triangle lattices), twelve of the 3D printed endcaps, and six of the aluminum rods. The result is a tensegrity structure that can be built in a few minutes by a single person.

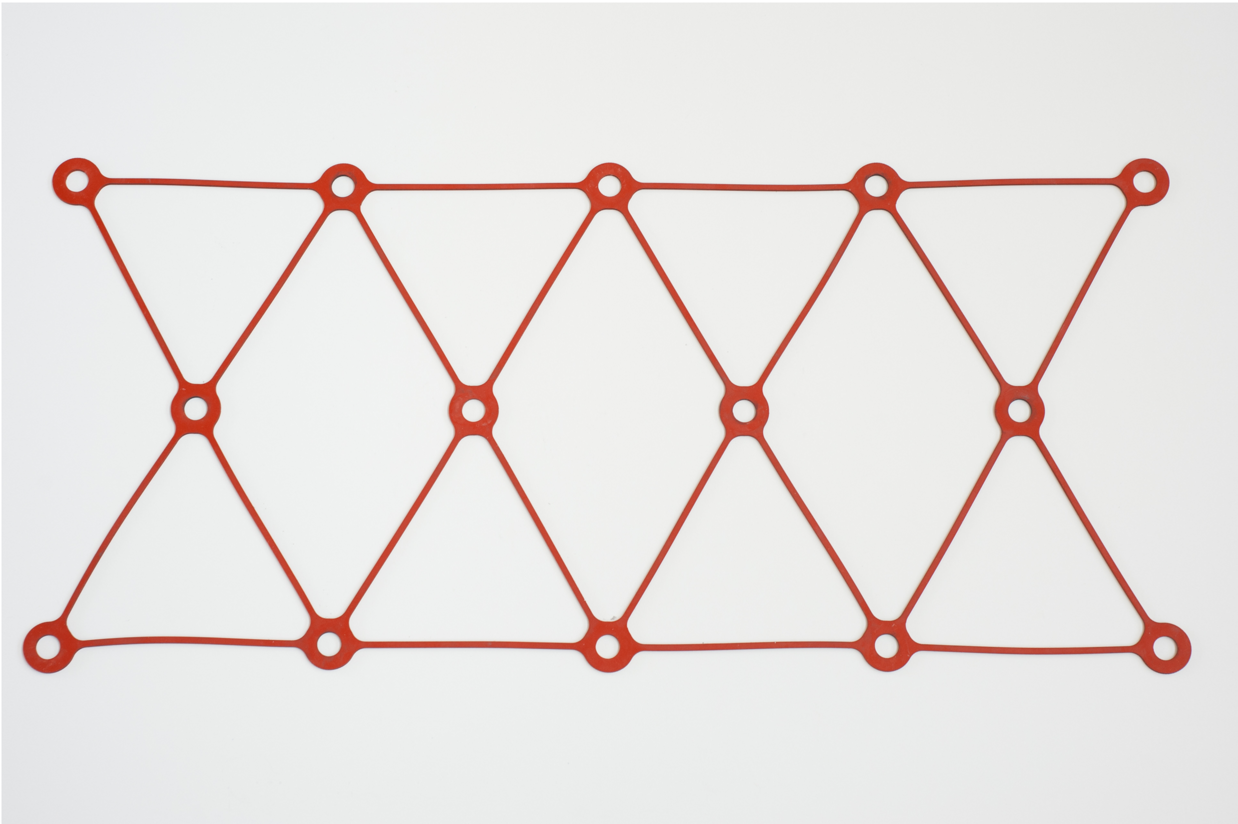

Figure 4.2: Single-piece elastic lattice for six-bar tensegrity structure [10].

4.4 Modular, Elastic Lattice Platform for an Actuated six-bar Tensegrity Robot

While a static model is used to demonstrate the basic concept of a tensegrity structure, an actuated tensegrity robot is required to gain scientific insight into its capabilities. To do so, a six-bar tensegrity robot with six actuators was constructed, which is referred to as the TT-4_{mini}, the 4th generation spherical tensegrity robot of miniature size (Figure 4.4). The TT-4_{mini} makes use of small components and the modular, elastic lattice to allow for rapid hardware iterations and performance testing. The design of the robot is described in order to illustrate the use of the prototyping platform.

4.4.1 Modular Actuation Unit

Actuators are required for rolling locomotion through shape-shifting in a tensegrity structure. Shape-shifting is used here to change the projected center of mass of the robot by

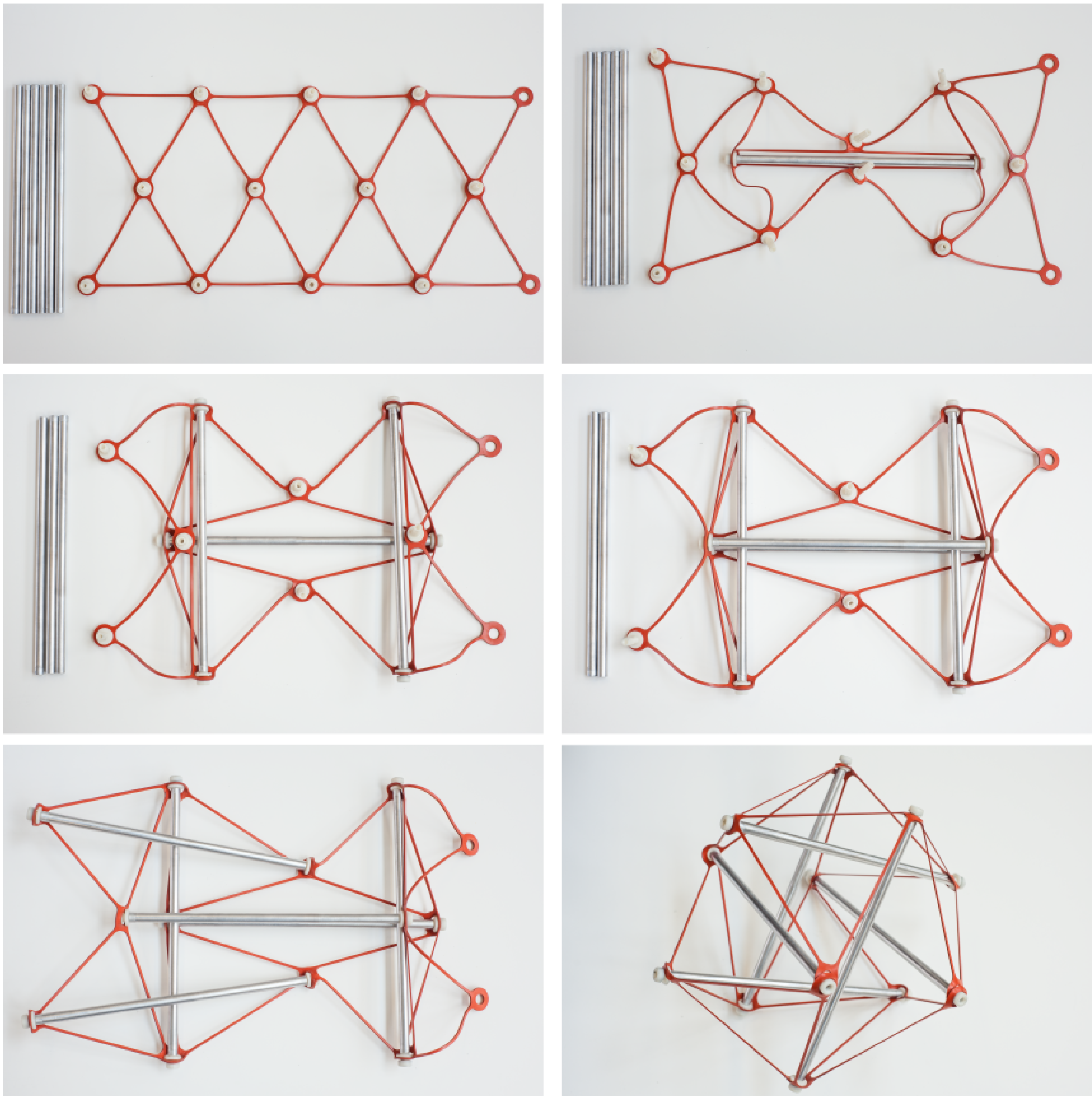

Figure 4.3: Step-by-step assembly sequence of a six-bar tensegrity static model [10].

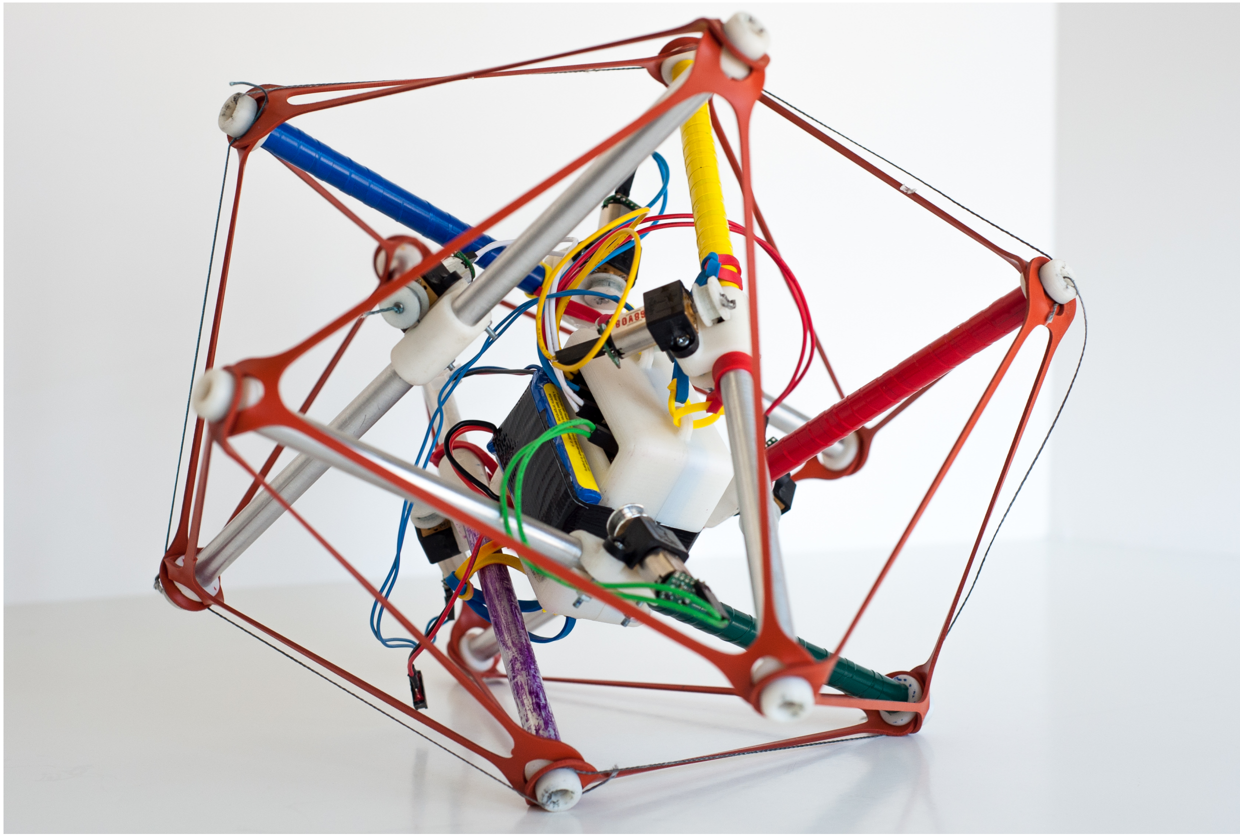

Figure 4.4: TT-4$_{\text{mini}}$ prototype [10].

adjusting tension within the elastic lattice network, which effectively causes the robot to perform a punctuated rolling motion [8]. Twenty-four actuators are needed to achieve full actuation of the system, but six actuators still allow for complete forward locomotion and are used for simplicity. The six-volt, 298:1 DC micro-gear motor from Pololu [51] was selected as the actuator. Each motor is positioned on the center of a rod, and adjust the shape of the system by spooling in cables to change the distance between endcaps.

The actuation unit conducting this line of motion is entirely modular and comprised of four principal components: an ABS plastic motor mount that attaches to the structural aluminum rods, the motor, an aluminum spool, and a plastic motor cover. An assembly of the unit is shown in Figure 4.5.

The aluminum spool is secured to the motor's shaft with a set screw. The rod is slid through the motor mount, atop which the motor and its cover are fastened using two screws and bolts. The cable is slid from the spool through the central opening in the motor mount

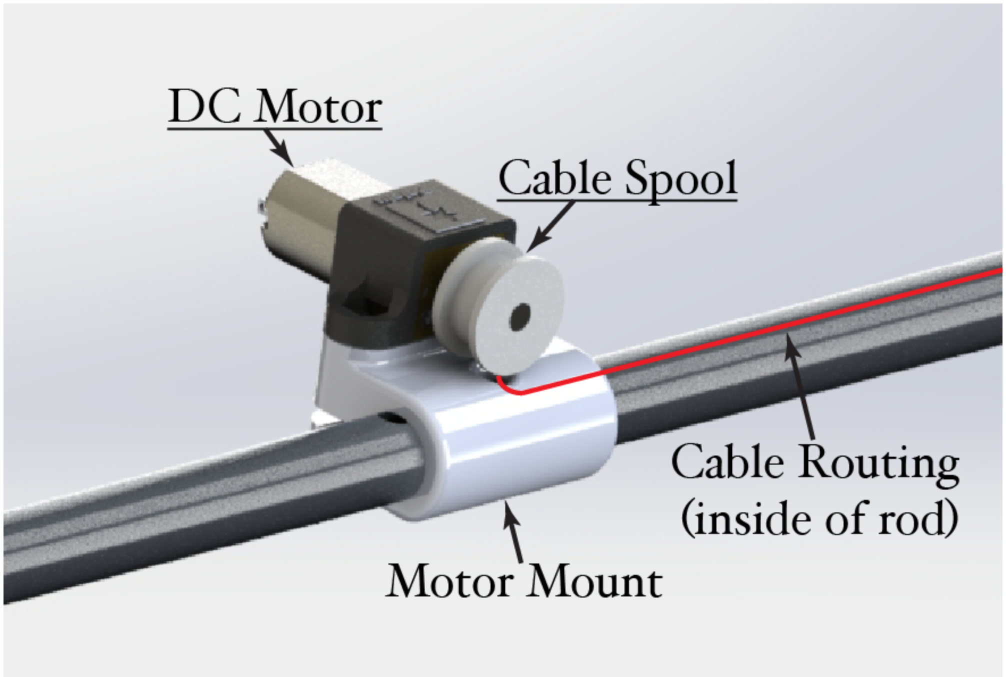

Figure 4.5: Modular actuation unit attached to the aluminum rod [10].

and directed outward to one of the rod's ends. It is then tied to the endpoint of another rod. During actuation, the motor's shaft rotates the spool which permits contraction and retraction.

The modularity and simple assembly process of the actuation unit greatly facilitate accessibility for a wide range of users, while remaining cost effective.

4.4.2 Central Electronic Controller

A central electronic controller was selected to control the actuators of the TT-4_{mini}. It is protected by a plastic case and suspended in the center of the robot. This unit contains the electrical and controller components (Table 4.1), which will be discussed in the following sections. The circuit diagram is given in Figure 4.6.

Microcontroller

The Arduino-based board Sparkfun Pro Micro [52] was the microcontroller selected for this project. It has 18 I/O pins, hardware serial connection, and internal voltage regulator,

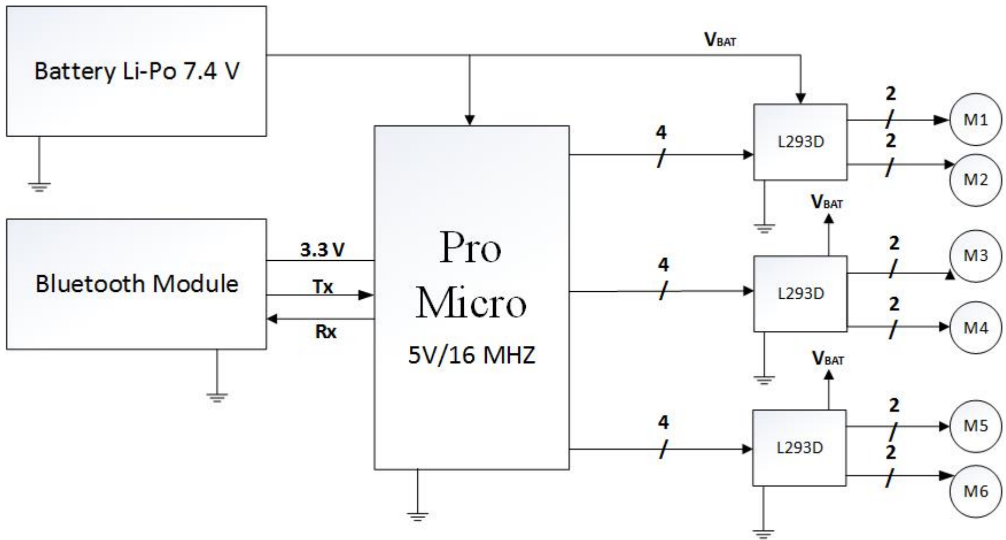

Figure 4.6: Circuit diagram of the central electronic controller [10].

Element	Type/Model	Quantity
Battery	E-Flite 430 mAh 2S 7.4V 20C LiPo	1
Microcontroller	Sparkfun Pro Micro -5V/16 MHz	1
Motor driver	L293D dual H motor driver	3
Bluetooth module	HC-06 Bluetooth module	1

Table 4.1: Elements of the Central Electronic Board [10].

among other features. Twelve digital output pins were connected to the motor drivers to control the direction of the motor's spin.

Three routines were created to receive character values associated with the list of digital output pins. The first routine allowed the user to move the motors by using delay functions, and calibration was done by testing. The second routine allowed for the possibility to store the times needed to move each motor forward and backwards in 12 different registers of the microprocessor. These times were calibrated by the user using an Android application that was developed in house. The third routine was similar to the second one but without delays and calibration. The application was also modified to allow the user to control forward and backwards motion of the motors.

Motor Drivers

Three dual H-bridge, model L293D motor drivers were used to power and control the six DC motors. Each motor driver allows currents up to 1 A per channel and a peak current of 1.2 A.

Wireless Communication

Bluetooth technology is used as the main means of communication between the tensegrity robots and the corresponding Android mobile application that serves as a remote control. Two Bluetooth modules, HC-05 and HC-06 Bluetooth-to-UART Serial Wireless Adaptor, were considered. Both of these met our requirements for signal coverage and were relatively low cost. The difference between them is that the former can act as both a master and slave device whereas the latter can only operate as a slave device. Since for the present application, only a slave device is required, the Bluetooth module chosen for the robot microcontroller was the HC-06. It creates a wireless serial data bridge between the connected microcontroller and smart devices that have installed the remote-control Android application.

4.4.3 User Controller

An Android application was developed as the user controller to allow for accessibility in the user interface. The remote controller is part of a master-slave communication system, where the tensegrity robot contains the slave device and the Android device is the master.

4.5 Robot Behavior in Level Ground Rolling and Uphill Climbing

4.5.1 Simulation of Actuation Policies

One of the unique challenges that is encountered in tensegrity robotics is the development of policies for actuation. While most of the work in this area has been based on taking advantage of the deformability of the tensegrity structure, the methods that have been proposed vary in approach and complexity. These range from the relatively simple case of single-cable actuated mobility [53], to punctuated rolling through form-finding using dynamic relaxation [8], to complex dynamic gaits generated through evolutionary algorithms [54].

However, one unifying element exists throughout our past work on this topic, and that is the assumption of locomotion on a flat surface. The NASA Tensegrity Robotics Toolkit (NTRT) [50] allows us to develop simulations on both flat and hilly terrain in order to investigate the potential of uphill locomotion using a six-bar spherical tensegrity robot on varying degrees of incline using a simple single-cable actuated punctuated rolling locomotion scheme. Using the results from simulations on a flat surface as a baseline, uphill rolling behavior will be characterized to illustrate the capabilities and limitations of this locomotion scheme.

Level Ground Rolling

In order to provide context and baseline results for uphill rolling simulations, a simulation of punctuated rolling for a six-bar tensegrity robot with a centrally located payload was performed first. The following results were all acquired through simulations with the NTRT.

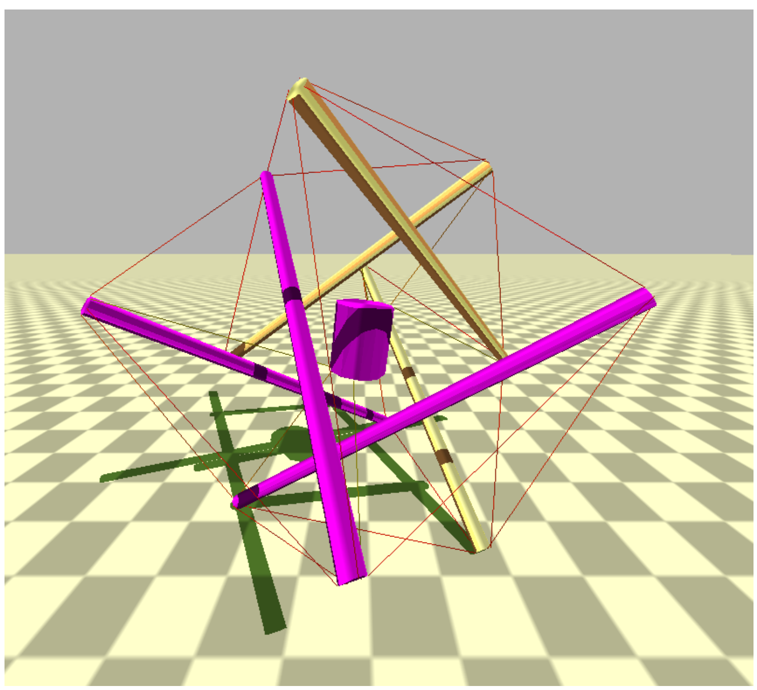

Figure 4.7: The model of a six-bar tensegrity robot with centrally located payload that is used in simulation [10].

As there had been no previous work done on uphill rolling, it was decided to implement a simple single-cable actuated punctuated rolling locomotion scheme. This means that during any forward locomotion phase, only one cable out of the 24 available is being retracted. This

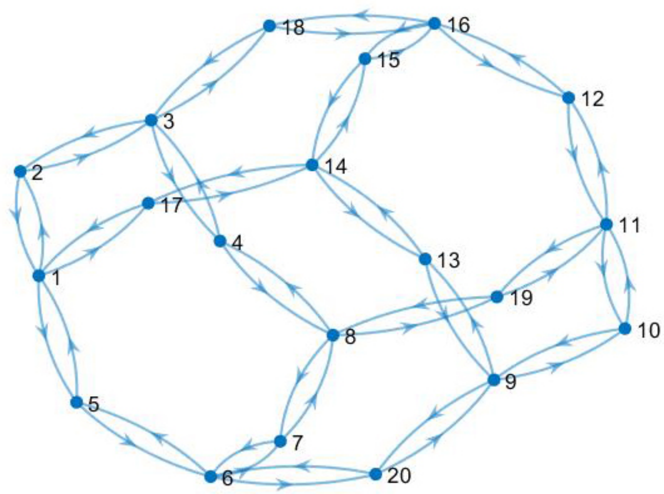

Figure 4.8: Digraph representing surface connectivity on a six-bar spherical tensegrity robot [10].

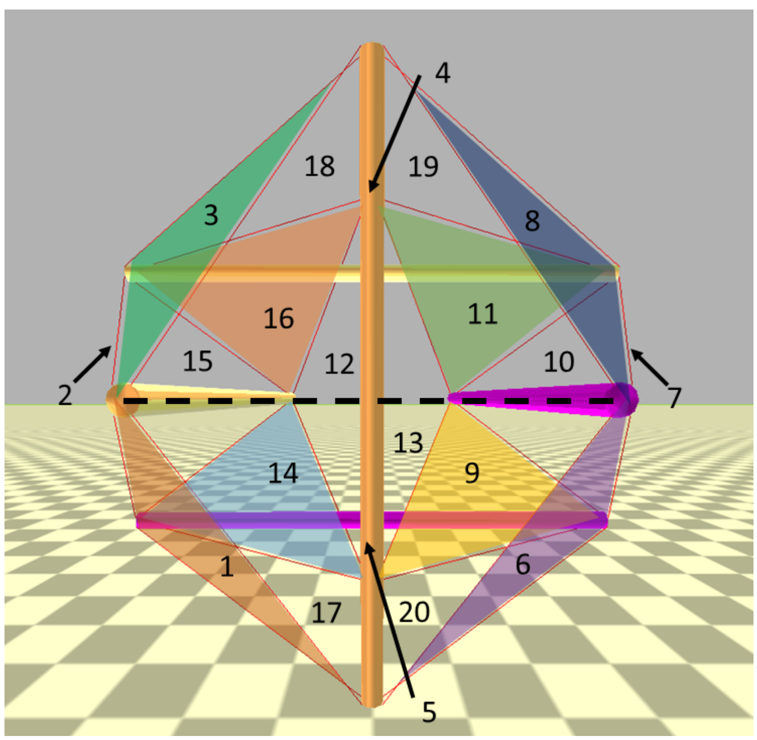

Figure 4.9: Surface number convention used in simulation and path generation [10].

serves to deform the robot and move its center of mass outside of its current base triangle and thus roll, in a punctuated manner, to the next base triangle. By specifying a series of steps from one base triangle to an adjacent one, the robot is able to move in a zig-zag pattern in a certain direction. For both the flat and uphill rolling simulations, the repeating unit of the path is 15 13 0 5 7 10 where the numbers correspond to the face numbering convention specified in Figure 4.9, and the model parameters for the robot correspond to those of the SUPERball robot [30], which is being developed by collaborators at the National Aeronautics and Space Administration (NASA).

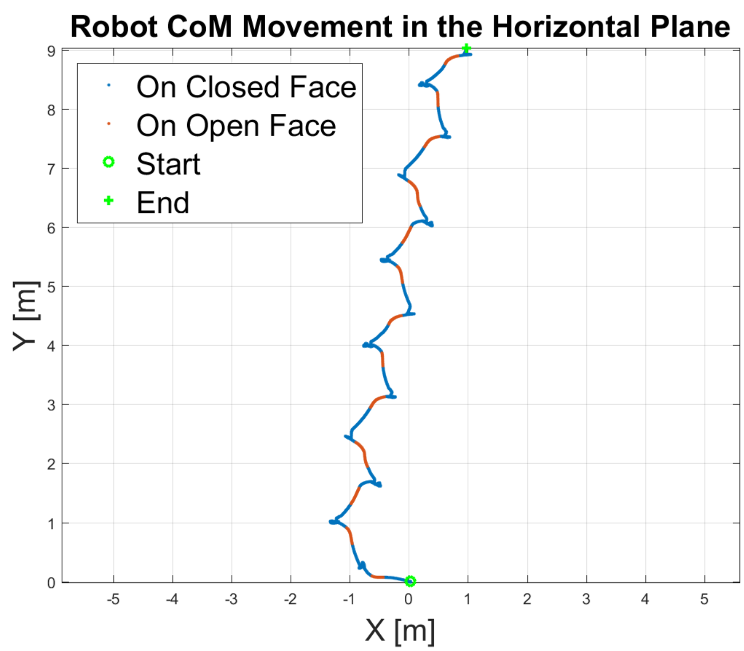

Figure 4.10: Robot center of mass position on the horizontal X-Y plane [10].

The movement pattern as seen in Figure 4.11 confirms the observations of single-cable actuated punctuated rolling on both the SUPERball and the TT-3 [6] robots and indicates that even with an open-loop path and simple locomotion scheme, the robot is capable of moving consistently in a desired direction. Furthermore, based on the cable retraction profile in Figure 4.9, it can be seen that the motions seem to occur in two sets of repeating triplets where two triplets make up one repetition of the path as specified earlier. While the symmetry of the spherical six-bar tensegrity structure suggests that each step during the punctuated rolling sequence should be identical, due to the inclusion of a cable-connected, centrally located payload to the external structure, variance is introduced into the rolling steps. This is because the connecting cables are compliant and thus allow for relative motion between the

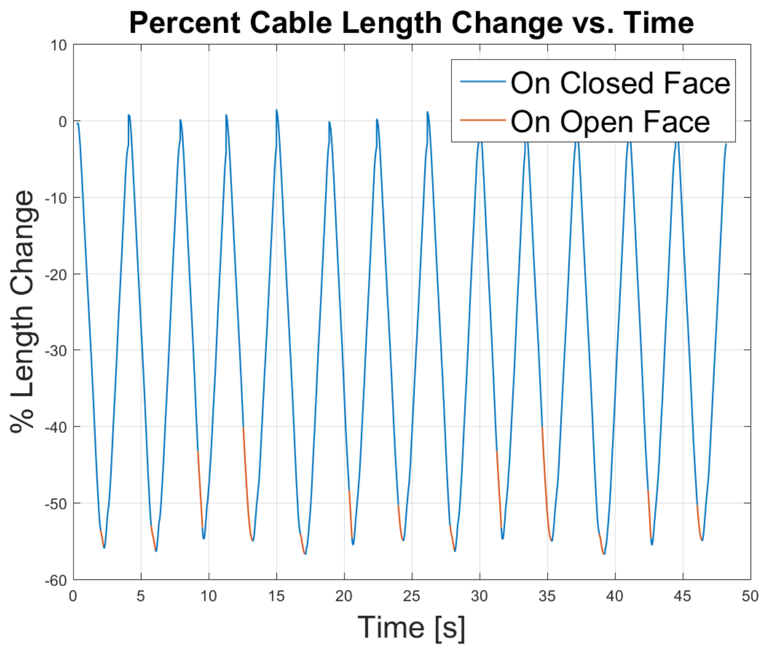

Figure 4.11: (Percent length change of the actuated cable during locomotion. (Note: closed faces correspond to triangular surfaces of the robot that are bound by cables on all three sides while open faces correspond to surfaces bound by cables on only two sides) [10].

payload and the external structure, thereby causing the overall robot center of mass to shift unpredictably during each step. This behavior, as will be seen in the next section, persists in uphill rolling and could potentially be used to augment current methods of contact surface detection.

Uphill Rolling on an Inclined Surface

In order to further evaluate the rolling performance of the six-bar tensegrity robot, the rolling controller implemented on flat ground was also repeated on various inclined planes, up to 10 degrees of incline shown in Figure 4.12. Simulated sensor data was then analyzed to ascertain any significant relationship between actuation efficiency versus inclined angle. The instant of initiation of rolling was observed for multiple steps for each angle of inclination by detecting when the central scientific payload of the robot recorded a projected velocity which exceeded a designated threshold. This threshold value was selected low enough to detect the initial moment of rolling as early as possible for each step but also greater than transient non-zero linear velocities from the central payload due to oscillations arising from natural compliance in the system, even when the robot is at rest. A relatively large velocity magnitude signified that the robot was in motion due to an unstable configuration and the cable actuation retraction length at each time of the initial rolling behavior was recorded.

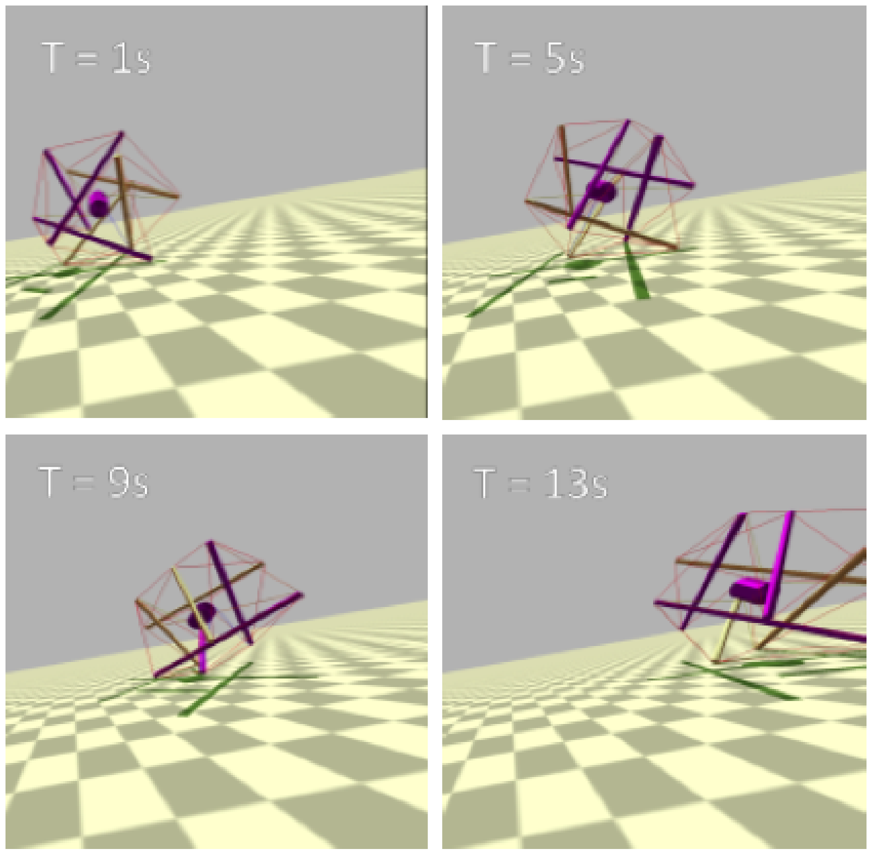

Figure 4.12: six-bar tensegrity robot rolling up a 10-degree incline with single-cable actuation [10].

From the analysis results shown in Figure 4.14, a clear relationship between necessary cable retraction for a single step versus incline angle is apparent, with greater angles of inclination correlating to larger necessary percent retraction of the initial cable length before rolling behavior begins. Interestingly, depending on the specific cable being actuated, the inclined angle has varying effect. The repeating unit of six steps in one direction can be separated into two groups of three "characteristic rolls" due to symmetry of the robot structure, with each group forming a repeated pattern of necessary cable retraction lengths before rolling. Although the extent to which the incline angle affects each cable varies from step to step, the average percent length change before rolling is initiated follows the same general linear trend. From this, it is clear that climbing steeper hills leads to greater power con-

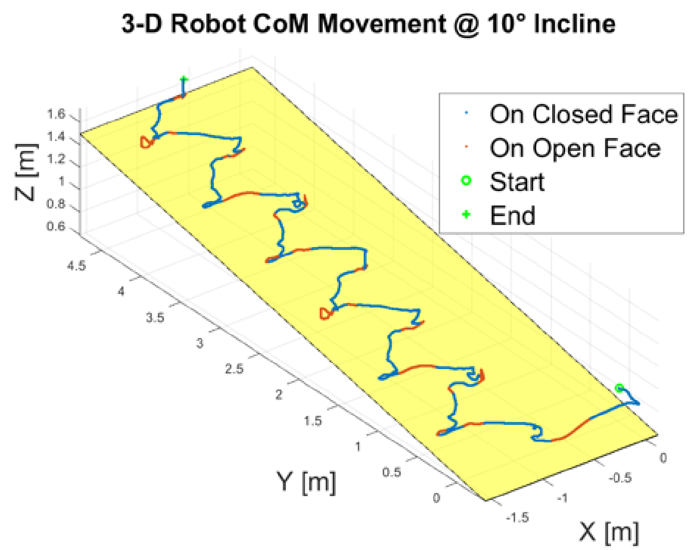

Figure 4.13: Trajectory of robot center of mass position [10].

sumption for the robot, motivating energy costs which are now more definitively quantifiable and clearly dependent on angle of inclination.

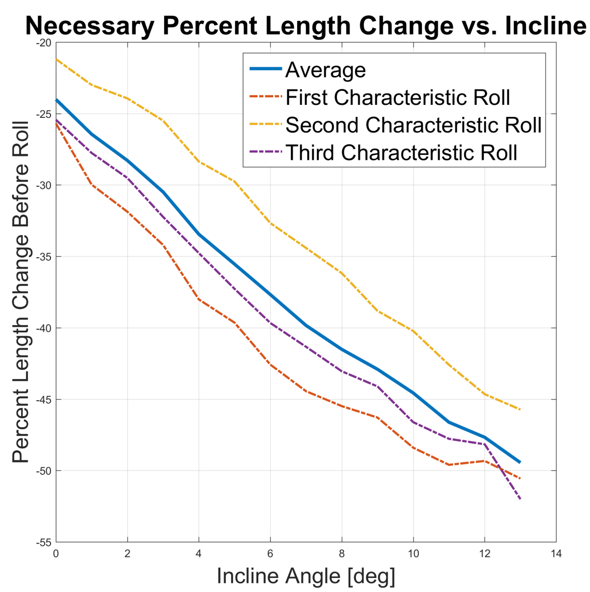

Figure 4.14: Percent cable length change required for tipping for the three characteristic rolls in each repeating triplet [10].

4.5.2 Hardware Experiments

Level ground rolling and uphill rolling on an incline were the two main experiments performed on the TT-4$_{\text{mini}}$ in order to observe the behavior of the robot. To better simulate tensegrity structures for space exploration applications, it is important to understand the tensegrity robot's ability to operate on various terrain through hardware prototype testing. First the TT-4$_{\text{mini}}$ was tested on level ground to verify the robot's basic functionality. To further confirm the simulation results, the TT-4$_{\text{mini}}$ was tested on various incline surfaces. Lastly, the TT-4$_{\text{mini}}$was tested on the lunar simulant to study the behavior of tensegrity robots on a simulated lunar environment.

Level Ground Rolling

The first experiment with the TT-4$_{\text{mini}}$ prototype was performed on a flat surface as a benchmark of its basic mobility. Punctuated rolling was accomplished through shifting its center of mass by deforming the base triangle with a single cable contraction. This method has been successfully demonstrated with the TT-3 robot [6], and with the single-cable actuation policy. The TT-4$_{\text{mini}}$ prototype reliably performed punctuated rolling in a straight line on a level ground, as shown in Figure 4.15 .

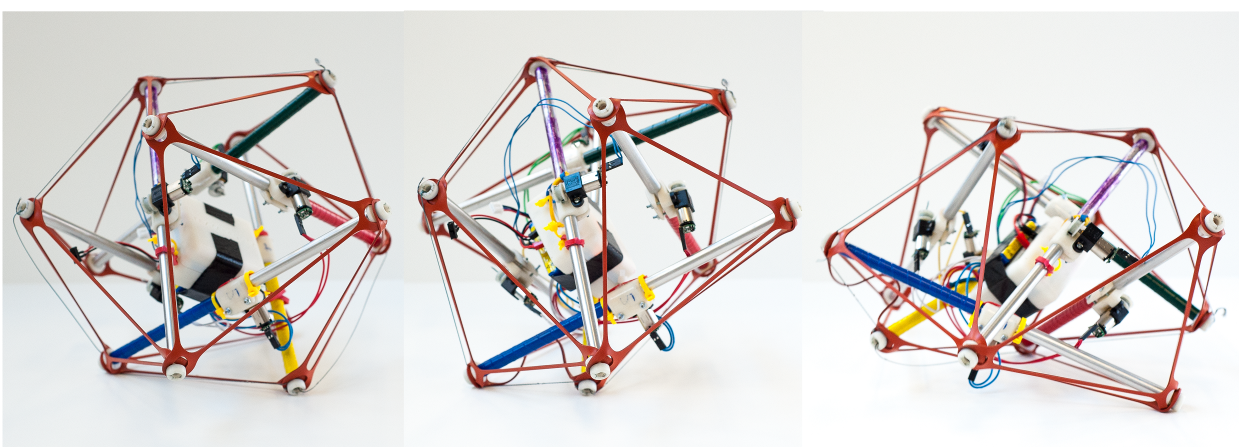

Figure 4.15: TT-4$_{\text{mini}}$ prototype rolling on a flat surface with single actuation [10].

Uphill Rolling on an Inclined Surface

In order to test punctuated rolling uphill, an adjustable testing platform was constructed that allows the incline surface to be changed to any desired angle between 0 and 25 degrees. Several trials were run in which the incline angle was incrementally increased after the TT-4_{mini} was able to perform a complete six-step rolling sequence at the set incline. The robot was successful in performing uphill climbing up to 13 degrees with a single actuation policy.

Figure 4.16 shows the TT-4_{mini} climbing uphill. This is the first time a tensegrity robot has shown the possibility of performing uphill climbing through hardware experiments.

Moon Regolith Rolling

NASA's mission goal is to land these tensegrity robots on the Moon. In order to perform realistic testing using the Moon conditions, the TT-4_{mini} robot was tested at NASA Ames' Moon regolith testing facility at building 503. Since the amount of lunar dust is very limited, it would be difficult for various scientists to perform their experiments with it. The solution to the problem of limited amount of lunar dust, scientists and engineers seek out to create replica material that best represent the lunar dust. The first simulant created by the NASA Johnson Space Center (JSC) that has the most similar material characteristic was the JSC-1. JSC-1 was made with basaltic volcanic cinder cone deposits from a quarry near Flagstaff, Arizona [55]. The total amount available from the quarry was about 25 tons [56]. The JSC-1 simulant's reserve was soon depleted, therefore, NASA had to manufacture more lunar simulant for researchers. One of the simulants released was JSC-1A, a similar characteristic lunar simulant to JSC-1 [57] [58] [59] [60] [61]. The simulant used at NASA Ames to simulate the Lunar regolith/soil is JSC-1A. The lunar testing facility consist of 10 tons of the JSC-1A simulant shown in Figure 4.17.

The goal of performing rolling experiments on the lunar simulant is to observe the behavior of the robot on super fine dust; no tensegrity robots had ever previously been tested in a lunar soil environment. The TT-4_{mini} robot was chosen for this experiment as it had successfully demonstrated punctuated rolling motion on both even and inclined terrain and was a convenient size for testing (Figure 4.18). It was observed, however, that the robot experienced more difficulty in performing rolling on the lunar simulant. Through close observation, it appears the method for shape shifting on a tensegrity robot would cause the robot to move

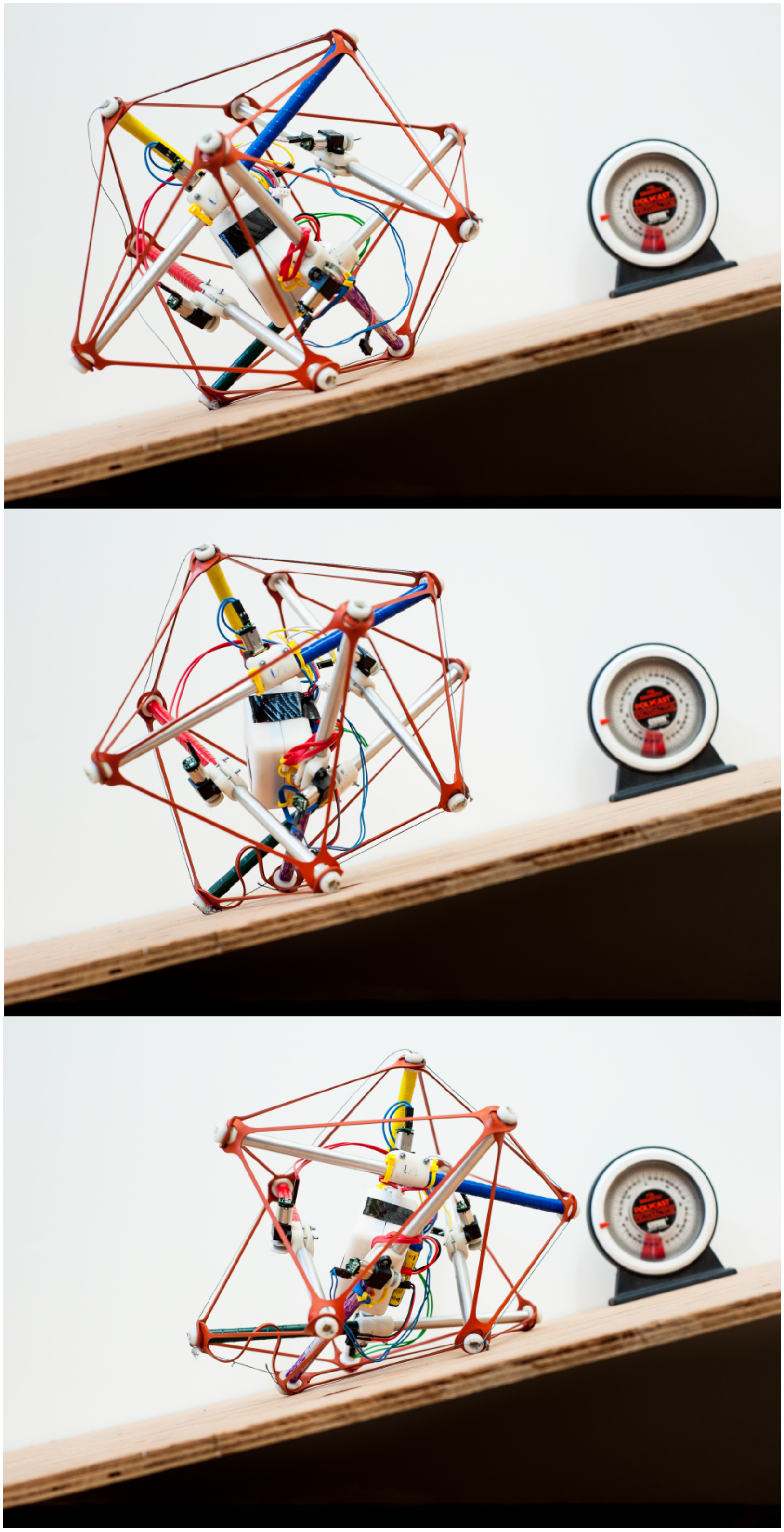

Figure 4.16: TT-4_{mini} prototype climbing up a 13-degree incline surface with single actuation [10].

Figure 4.17: NASA Lunar Facility which house 10 tons of JSC-1 lunar simulant for Moon terrain testing.

its rods through the dust having a similar effect of clawing through the sand. The motion of dragging the rods through the lunar simulant increases the friction force on the end of the rods, which would increase the torque required to perform shape shifting. This experiment reminded me of the importance of testing in a realistic mission environment. Many of the challenges faced during this experiment were not apparent during laboratory testing.

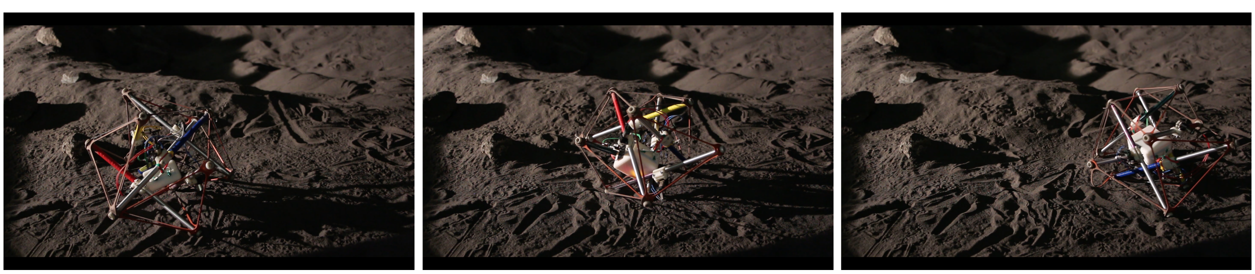

Figure 4.18: The TT-4_{mini} robot demonstrated successful punctuated rolling on slight incline and uneven lunar terrain consist of lunar simulant.

The following chapter will discuss my outreach experience using the various tensegrity prototypes created by the Berkeley Emergent Space Tensegrities (BEST) lab.

Chapter 5

Tensegrity for Outreach and Education

Sharing my knowledge of tensegrity robotics with various groups of children was one of the highlights of my graduate career. The following are a few of my most memorable outreach events.

5.1 Tensegrity for Outreach

5.1.1 Silicon Valley Robot Block Party

My first presentation of the Berkeley Emergent Space Tensegrities (BEST) lab's tensegrity robot was at the San Francisco Bay Area's Silicon Valley Robot Block Party in 2015. There were 400-500 children and parents at the event, and the age of the children ranged from K-12. Majority of the children at the event were on the younger side of K-12 as shown in Figure 5.1. Here are a few of the most important things I learned from the event:

- Many of the children at the event had tensegrity toys growing up.
- Children were not intimidated by tensegrity robots.
- Children liked to press or push on our tensegrity robots because they liked to see it deform.
- Children enjoyed their interaction with the robot and structures.
- For younger children, fewer visible actuators/complex components seemed to make the robots more approachable.

Figure 5.1: Children exploring various tensegrity toys and robots during our visit at Silicon Valley Robot Block Party.

- Tensegrities are gender neutral.

This event was inspiring for both me and my audience. I was able to share my research to a large audience, and I was able to receive feedback from people with different backgrounds. Another benefit of presenting robotic hardware to children was to record the various failure modes. I realized I am careful with the handling and testing of the robots because I understand the hours involved in the construction of the prototypes. However, the children would play with them like their own toys, which was some intense real world testing. I noted down a list of improvements throughout the day of real world testing.

5.1.2 Black Girls CODE

Another inspiring outreach event which I presented the BEST lab's robots was the Black Girls CODE. The goal of the Black Girls CODE was to inspire African-American girls from 7-17 in the fields of science, technology, engineering, and mathematics (STEM). The audience was excited to see robotic concepts that has the potential of performing space missions Figure 5.2.

Figure 5.2: Young female scientists and engineers were excited to see our presentation on the tensegrity robots. Image used with permission from Black Girls CODE.

5.1.3 Lawrence Hall of Science

The Lawrence Hall of Science had an exhibit on Space Exploration. The BEST lab was invited to demonstrate the various tensegrity prototypes used to study the use of tensegrity structures as robots for space exploration. It was well received by the crowd.

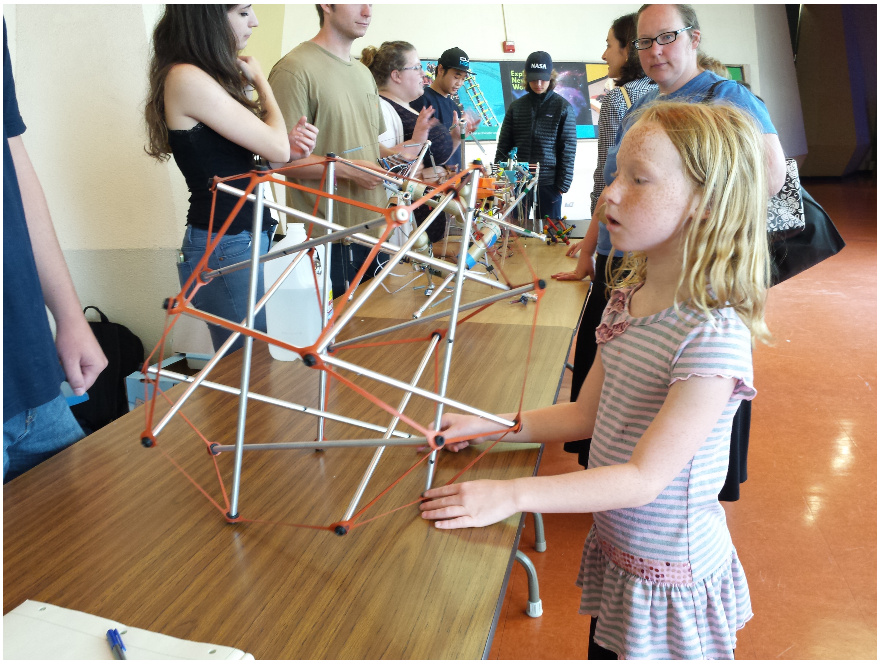

Figure 5.3: Young child playing with the 12-bar tensegrity prototype. Image used with permission from Lawrence Hall of Science, Copyright©2016 Regents of the University of California, Berkeley, All rights reserved.

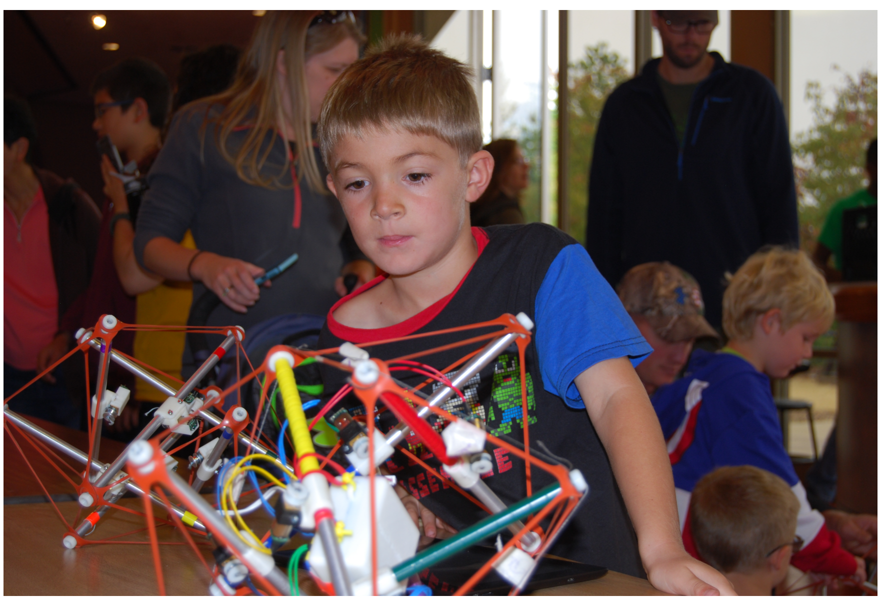

Figure 5.4: Young visitor of Lawrence Hall of Science observing the demonstration of the TT-4_{mini} robot. Image used with permission from Lawrence Hall of Science, Copyright©2016 Regents of the University of California, Berkeley, All rights reserved.

Chapter 6

Conclusions and Future Work

6.1 Conclusions

6.1.1 TT-3 Robot

TT-3, a six-bar tensegrity robot, has been demonstrated to be an effective mobile robot that can sustain impact. The robot was able to continuously roll in a circle with a single active actuation module and in a forward motion trajectory with three active actuation modules, with and without a payload at the center. A comparison of performance parameters of TT-3 with the rod-centered cable-driven design versus the previous TT-2 with linear actuators is provided in Table 6.1 below. For space missions, the payload may consist of sensors, spectrometers, cameras or other light-weight scientific equipment. Based on its compliant nature, there are other potential co-robotic applications for the TT-3. For instance, the TT-3 can be envisioned as a medicine transport robot in a hospital environment. Due to its intrinsic compliance, the robot is unlikely to injure humans.

Furthermore, the rod-centered design has been shown to improve the system's ability to absorb impact, and minimize the damage to critical components like actuators and controllers. It has been shown that the TT-3 robot can absorb and dissipate energy during impact by greatly deforming its shape.

Robot	Rod Length	Weight	Max Cable Displacement	Speed
TT-2	69 cm	2.7 kg	10 cm	1 cm/s
TT-3	65 cm	2.0 kg	20 cm	5 cm/s

Table 6.1: Comparison of TT-2 and TT-3 tensegrity robots.

A current challenge with the robot is the lack of feedback control as most of the work so far has used open-loop control.. The robot must be autonomous in order to successfully execute space missions where human support is limited. This requires a high-level feedback controller as well as sensors to gather information about surroundings. Sensors for tensegrity robots will be further discussed in the future work section.

6.1.2 TT-4_{mini} Robot

The newly developed rapid prototyping method using modular, elastic lattices has simplified the traditional methods of building tensegrity structures. The time for assembly of a static structure can be shortened from one hour to a few minutes. In addition, static structures can be modified into an actuated robot by attaching modular actuation units and a central controller; the total construction time of an actuated robot using this prototyping platform is less than one hour. The latest tensegrity prototype, TT-4_{mini}, was built using the modular elastic lattice prototyping system. TT-4_{mini} was used to test actuation policies by climbing on an inclined surface. This marked the first successful demonstration of an untethered spherical tensegrity robot climbing an incline.

For researchers, this rapid prototyping platform can significantly reduce the complexity of constructing tensegrity structures. Finally, the new tensegrity prototyping method illustrates the extensibility of the platform for related applications, such as the rapid prototyping of 12-bar tensegrity structures. This topic is further discussed in the future work section.

6.2 Future Work

6.2.1 TT-4 Robot

In parallel with the TT-4_{mini} prototyping, the TT-4 (version 4) tensegrity robot is under development. The TT-4 robot was designed to be a larger robot than the TT-3 robot with 1 meter rods to better study the effect of a larger and heavier payload on a tensegrity robot. The TT-4 robot design was inspired by the TT-3 robot. The TT-4 robot is also a fully actuated (24 actuators) six-bar spherical tensegrity robot like the TT-3. The TT-4 also uses the modular, rod-centered actuation architecture like the TT-3 robot. However, the TT-4 was an attempt as an improved TT-3 robot. For example, after many hours of testing with the TT-3 robot we found that actuator alignment generated a large friction force on the cable, leading to significant wear on the cable. This design mistake not only affected the reliability of the robot, but also affected the efficiency and performance of the robot. Here is a list of design improvements implemented on the TT-4 robot:

- Improved actuator alignment to minimize friction force.
- Modular, manufacturable enclosure to replace the 3D printed housing.
- A boost regulator to maintain the voltage level to the actuators.
- A battery protection circuit.
- A 9-axis IMU sensors on each actuation modular to perform contact surface detection.
- A power latch circuit to reduce the current level to the switch.

Figure 6.1 shows the rendered image of the TT-4 robot design generated from the 3D computer aid design (CAD) program. And Figure 6.2 is a rendered detail view of the actuation module with the manufacturable enclosure to replace the 3D printed FDM casing. Figure 6.3 shows the manufactured actuation module based on the 3D CAD design.

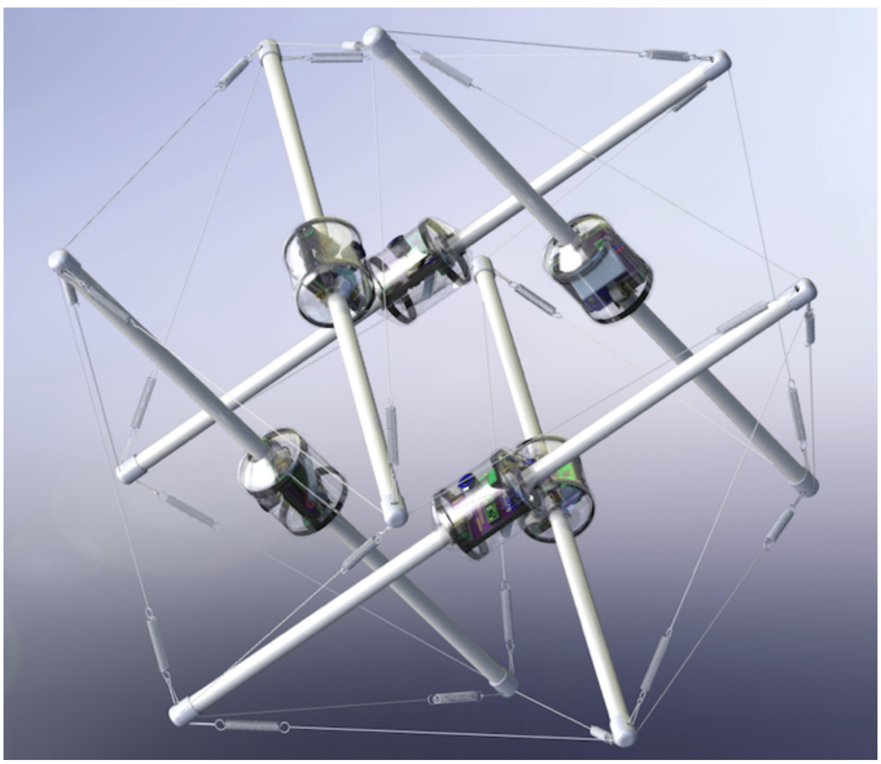

Figure 6.1: A 3D render of the TT-4 robot design [62].

It is expected that the TT-4 robot will be ready for testing in early Spring 2017.

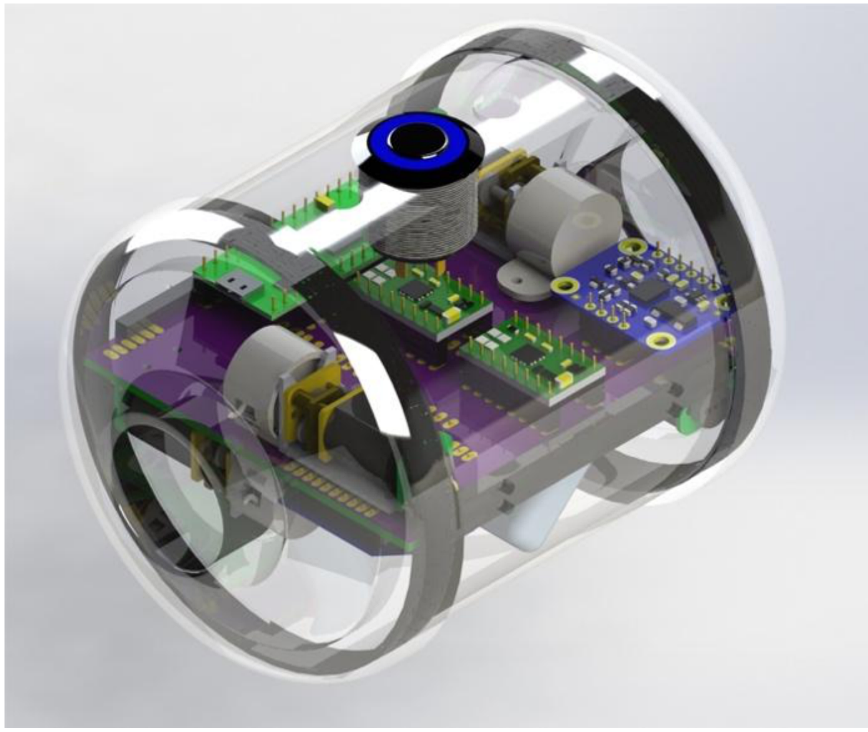

Figure 6.2: A closer look of a 3D rendered imaged of theTT-4 robot's actuation module [62].

6.2.2 TT-4$_{\text{IMPACT}}$ Structure

TT-4$_{\text{IMPACT}}$ is a replica of TT-4 constructed to perform impact analyses of tensegrity robots and its payload from higher heights shown in Figure 6.4. One of the goals of the TT-4$_{\text{IMPACT}}$ is to study the impact forces on the rods and payload. In order to measure the impact, a set of IMU sensor and wireless transmitters will be mounted on the center of each rods and payload. It is planned to drop the structure from up 10 meters height.

6.2.3 Sensors for Tensegrity Robots

Tensegrity structures, non-touching solid rods connected by tensile cables, are of interest in the field of soft robotics due to their flexible and robust nature. This makes them suitable for uneven and unpredictable environments in which traditional robots struggle. The compliant structure also ensures that the robot will not injure humans or delicate equipment in co-robotic applications [13]. Currently, most of the six-bar tensegrity robots developed in the Berkeley Emergent Space Tensegrities (BEST) lab at University of California at Berkeley utilize an open loop control method for actuation. Only the TT-2 robot has the capability to

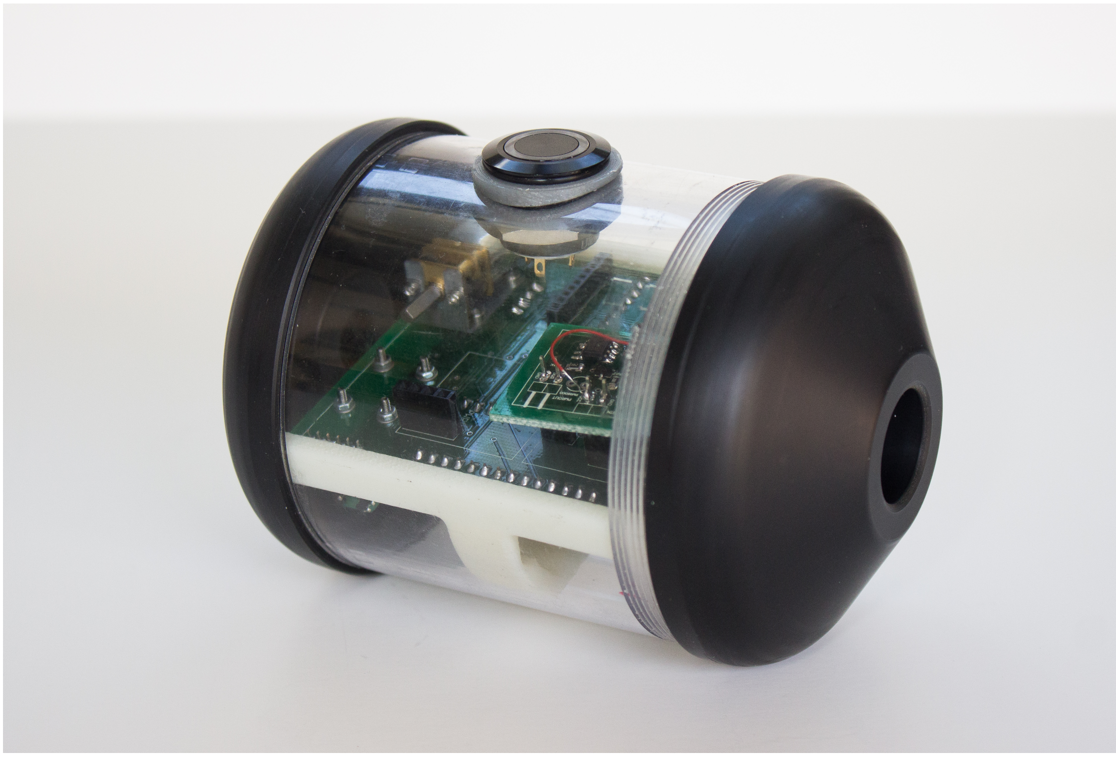

Figure 6.3: A prototype of the TT-4 actuation module.

perform limited closed-loop control. Due to limited sensors implemented on the robots, they cannot perform state estimation and localization of the system. This chapter will describe some of the sensors investigated as the potential solution for the robot to estimate its current state and surrounding to achieve closed loop control.

Using Contact Sensors for Contact Surface Detection

A six-bar tensegrity structure has 20 unique triangular faces. Currently, the robot is not aware of which of those surfaces it is resting on. The six-bar tensegrity structure chosen as the base architecture for the robots have eight "closed" triangles and 12 "open" triangles. The "closed" triangle is a region which the three end nodes of the rods are bounded by three tensile elements. The "open" triangle is a region where the three end nodes of the rods are only bound by two tensile elements. The particular triangle surface that supports the structure on the ground is referred as the "contact surface".

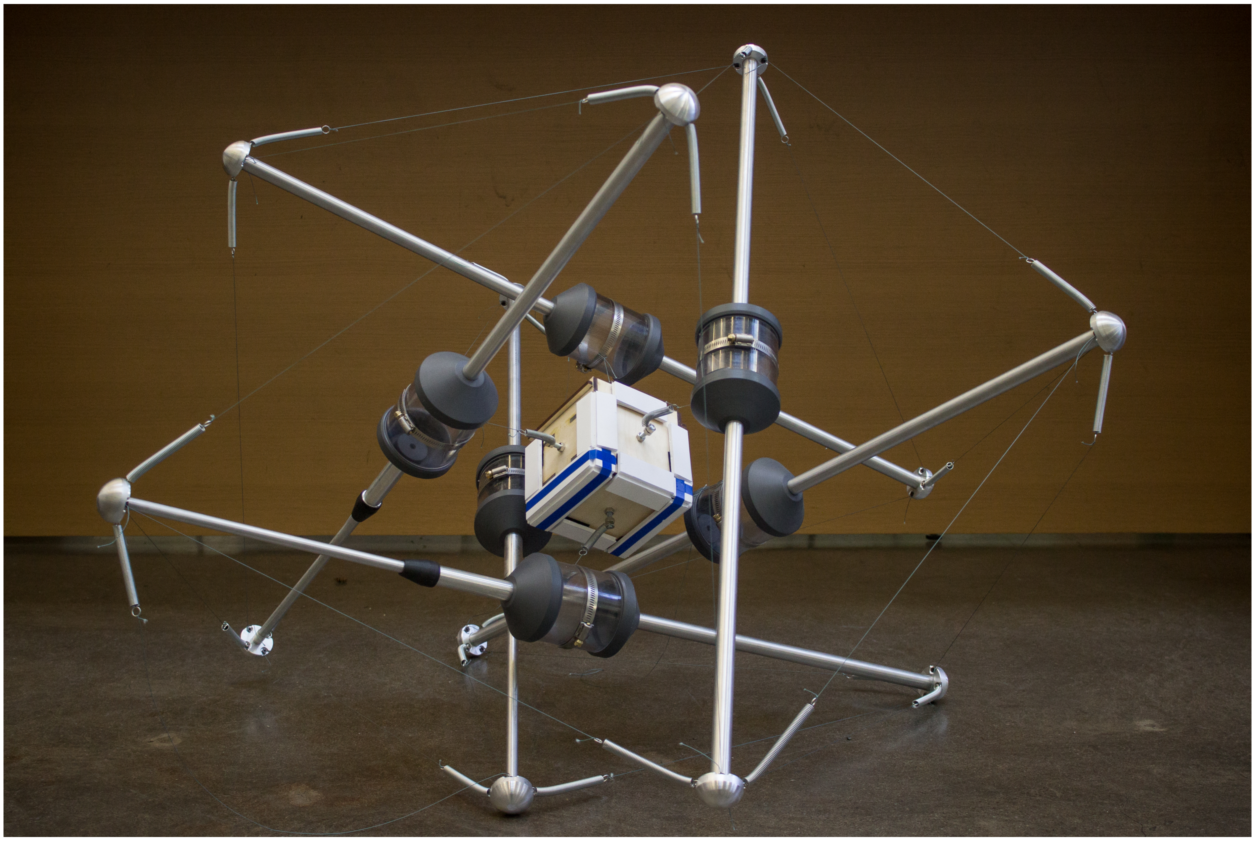

Figure 6.4: TT-4$_{\text{IMPACT}}$ a replica of the TT-4 robot to better study the shock experience by the rods and payload.

Without knowing which triangle is the contact surface, the robot can have trouble initiating its first step. This is especially crucial during an autonomous mission. For example, when the robot is deployed on the Moon, it would be difficult to place it on a particular triangle plane. If the robot were to roll down a crater during the mission, it would be difficult to predict which plane was supporting the structure. These examples further emphasize the importance of knowing what surface of the robot is in contact with the ground.

One solution for this problem is to use contact sensors. Contact sensors are attached to the end of the rods and can be used to sense either the force or pressure that is exerted on them. A set of piezoresistive force sensors had been implemented on the end of the rods of TT-2 robot to sense the ground reaction force in order to determine the contact surface. The piezoresistive contact sensor prototypes were sufficient as a proof of concept. There were a few problems with these contact sensors, however. First, these sensors would not function well with point force, so either a smooth and level surface or an elastic surface has to be used as the contact between the ground and the sensor. The piezoresistive force sensors were potted with a silicone compound on one end of a piston rod inside of a 3D printed enclosure. The other end of the piston rod was be in contact with the ground as the robot was rolling. The ground reaction force was transferred from one end of the piston rod to the piezoresistive force sensors through the silicone potting compound. The volume of potting compound used in each sensor varied which resulted in variation of initial force reading due to the residual stress from the compound on each sensor. The variation in initial force reading due to the residual stress made the process of integrating these sensors difficult because individual calibration was required for each sensor before use. Since there at 12 rod-ends on each six-bar tensegrity robot, this calibration process was time intensive during the assembly process.

Pushbutton switches offer an alternative solution to piezoresistive force sensors. Pushbutton switches provide binary inputs to the robot. The pushbuttons would inform the robot if it is in contact with surfaces as long as the force of contact exceeds the threshold force required to activate the electrical contact. Figure 6.5 shows the pushbutton sensor prototype created for tensegrity robots. Shown in this figure is a 3D printed enclosure that contains a pushbutton switch inside. There are two parts to this enclosure, there is a holder base for mounting the pushbutton switch, and there is a rod that slides through to activate the button if it is pushed.

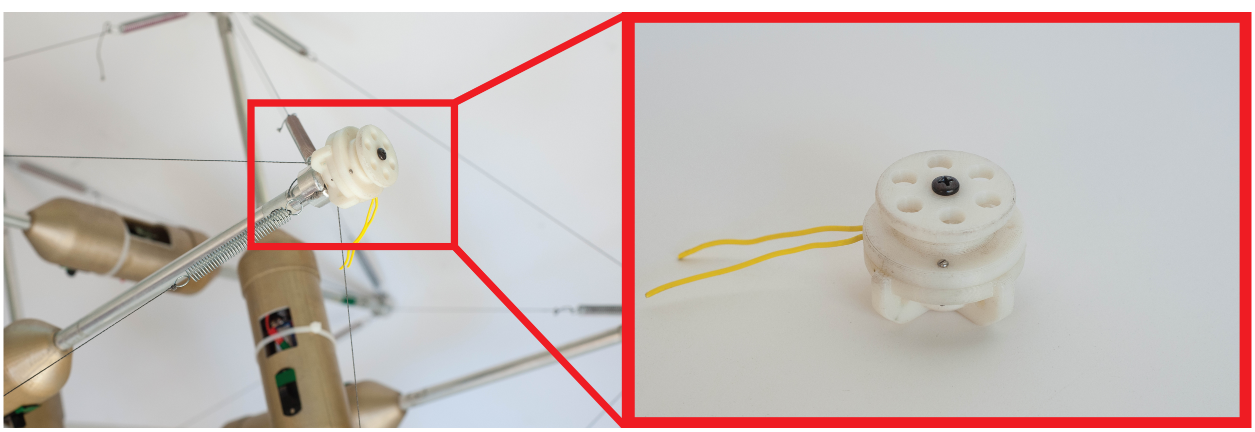

Figure 6.5: A pushbutton contact sensor installed on the end of a rod of a six-bar tensegrity robot.

The preliminary experiment with these sensors was successful. The sensors activated an LED light if they detected contact. The sensors were able to correctly display the points of contact during walking. However, sometimes the sensors would deactivate pre-maturely during shape shifting due to the direction of motion on the end of the rods. As the rods are moving on the ground, certain changes in direction can cause the rod that is in contact with the pushbutton to experience a pull force and deactivate the switch. The solution to this problem is still being investigated.

Elastic Strain Sensors for State Estimation

In addition to the soft tensegrity structure, the use of soft sensors as an integral part of the compliant elements was explored. Figure 6.6 shows an example of a six-bar tensegrity structure. This tensegrity structure uses integrated liquid metal-embedded hyperelastic strain sensors as the 24 tensile components instead of typical springs or bungee cords. These sensors were manufactured by researchers at the Faboratory lab at Purdue University, with whom our lab collaborated with. The Faboratory lab sent manufactured sensors to us for integration and testing.

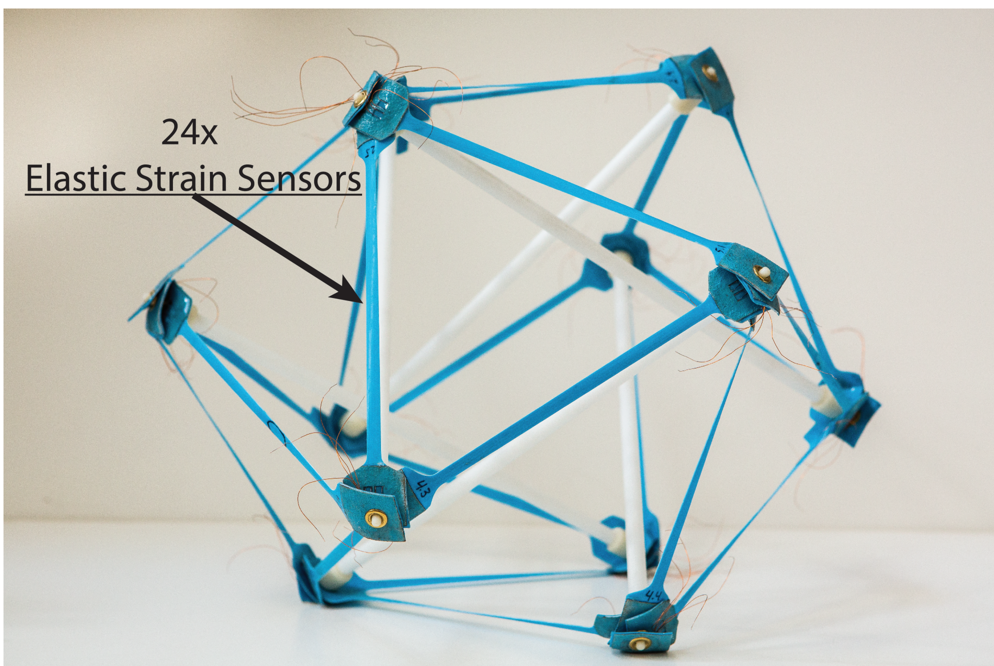

Figure 6.6: six-bar tensegrity structure with 24 liquid metal-embedded hyperelastic strain sensors as the tensile elements.

The strain sensors in this tensegrity are primarily composed of a silicone elastomer with embedded microchannels filled with a conductive liquid metal (eutectic gallium indium alloy (eGaIn), Sigma-Aldrich) Figure 6.7(A). Eutectic gallium indium alloys (eGaIn) consist of 75 percent Gallium and 25 percent Indium by weight and have a melting temperature of 15.5 °C [63]. To better see the microchannels, a hyperelastic strain sensor was placed over a fluorescent light shown in Figure 6.7(B).

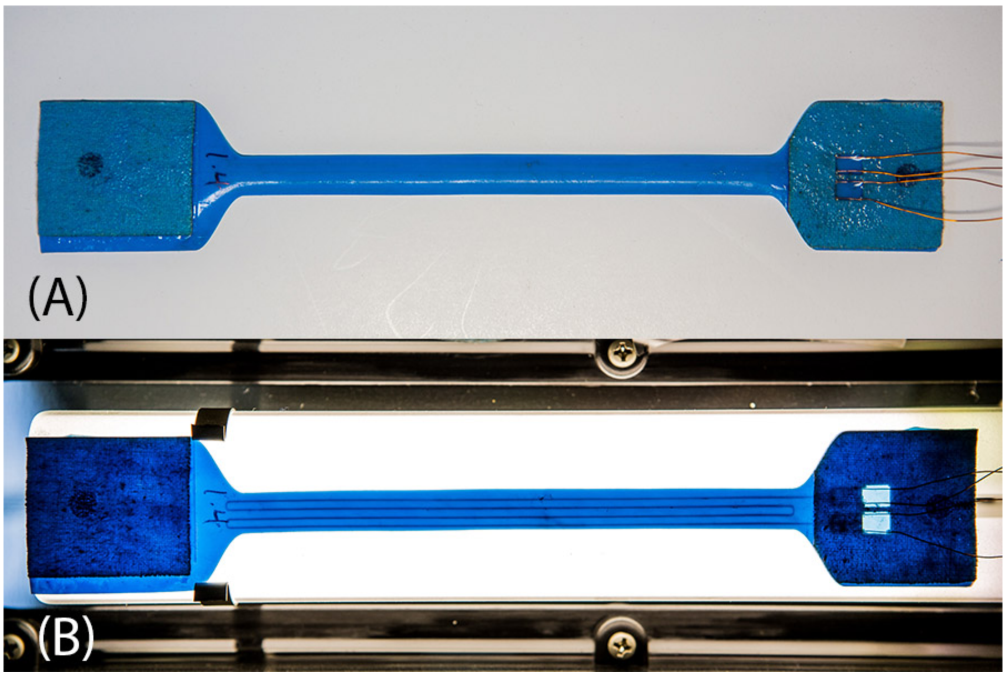

Figure 6.7: (A) The liquid metal-embedded hyperelastic strain sensor used on the six-bar tensegrity structure. (B) The embedded eGaIn microchannels shown through fluorescent light.

As the sensor is elongated, the resistance of the eGaIn channel will increase due to the decreased microchannel cross-sectional area and the increased microchannel length [64]. The primary functions of this hyperelastic sensor tensegrity are model validation, feedback control, and structure analysis under payload. Feedback from the sensors can be used for experimental validation of existing models of tensegrity structures and dynamics, such as for the NASA Tensegrity Robotics Toolkit [50]. In addition, the readings from the sensors can provide distance changed between the ends of the bars, which can be used as a state estimator for UC Berkeley's rapidly prototyped tensegrity robot to perform feedback control [13]. The state estimation of tensegrity robots is still a challenging topic [34]. Furthermore, this physical model allows us to observe and record the force distribution and structure deformation with different payload conditions. Currently, we are exploring the possibility of integrating shape memory alloys into the hyperelastic sensors, which can provide the benefits of both actuation and sensing in a compact module. Preliminary tests indicate that this combination has the potential to generate enough force and displacement to achieve punctuated rolling motion for the six-bar tensegrity structure.

To further understand the potential and validate the performance of these sensors, a simple test platform was constructed shown in Figure 6.8. A total of 10 sensors were tested with 1 cm increment stretches up to total of 6 cm extension. The process was repeated 10 times at each increment. The collected data is plotted shown in Figure 6.9. As can be seen in Figure 6.9, the sensors have a linear relationship between extension length and resistance, which means through calibration the user can estimate the extension length based on the resistance from the sensor. However, the plot also shows how data from the different sensors were offset from each other. This is a concern because it means each sensor requires individual calibration in order to know the resting resistance and the relationship between resistance and extension length.

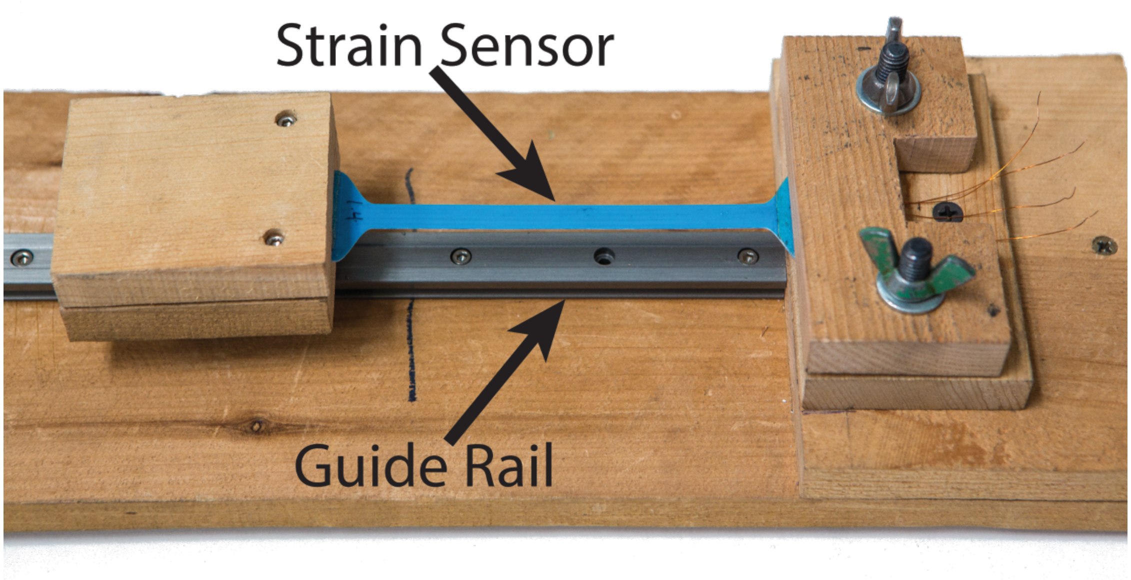

Figure 6.8: A testing platform to perform quick validation of the strain sensors.

In addition to needing to calibrate each sensor individually, of the 10 sensors randomly selected for testing, only five of them functioned for data collection. In conclusion, these

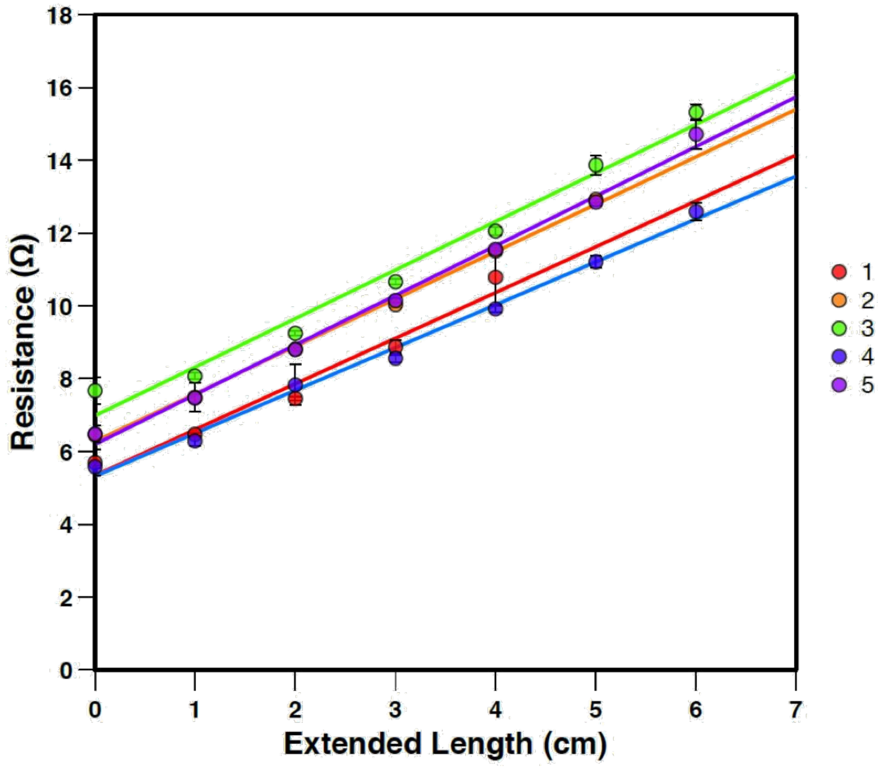

Figure 6.9: A plot of all the data collected during the strain sensor extension experiment.

sensors can be difficult to integrate with the tensegrity robot for feedback sensing. Due to its current developmental state, the sensors were not able to satisfy the requirements for providing consistent feedback for the tensegrity robots. But they are promising sensors for future work once the technology is more developed.

Inertial Measurement Unit for Structure Orientation and Dynamic Properties

The TT-2 robot had a three-axis accelerometer placed at the center of the robot, and the accelerometer was carefully aligned to the robot's geometry. There are eight quadrants in a three-axis accelerometer, and there are eight "closed" triangle in a six-bar tensegrity. The accelerometer was aligned so that each closed triangle was positioned in one of the eight quadrants. This allows the robot to determine its current contact surface. For example, if the tensegrity robot is resting on a particular surface and the accelerometer reading from the gravity vector is positive in the x-axis, positive in the y-axis, and positive in the z-axis, then the robot would be able to determine that its current contact surface is triangle number one.

To further improve contact surface detection, Inertial Measurement Unit (IMU) sensors were used as a potentially more reliable technique. The Bosch BNO055 nine-DOF IMU chip was chosen to test this concept. This particular chip was chosen because the sensor has built in filtering, active calibration and sensor fusion algorithms; these features allow for a separation of gravity from the accelerometer readings. This gives more accurate gravity vector readings while the robot is moving. A mount was created to attach the BNO055 sensors to the TT-3 robot shown in Figure 6.10. A Bosch BNO055 nine-DOF IMU sensor was attached to each rod of the six-bar tensegrity robot shown in Figure 6.11.

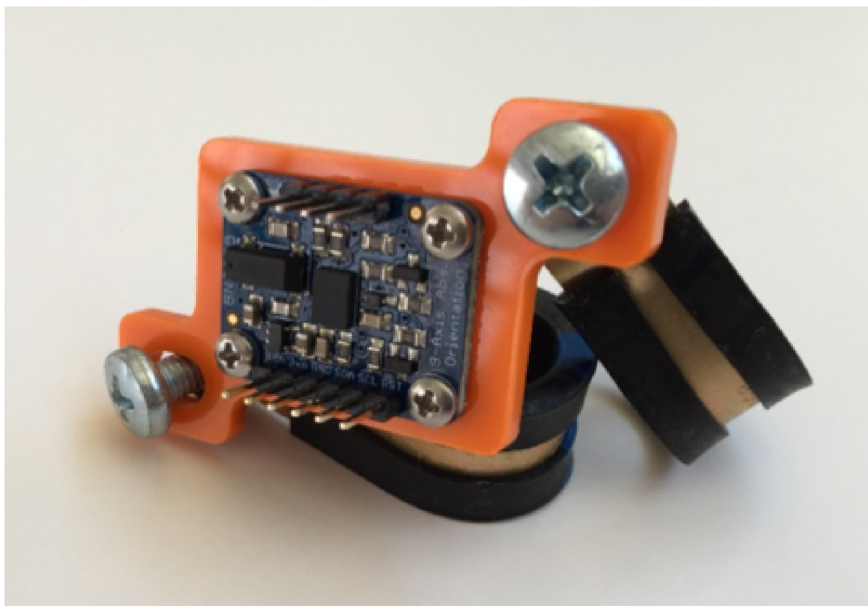

Figure 6.10: Bosch BNO055 nine-DOF IMU sensor on a custom mount for attaching to the TT-3 robot [65].

One of the methods that was successfully implemented was use of the magnitude of the gravity vectors from the six sensors. Sensor data were collected for each triangle of the tensegrity. This data recorded the magnitude of the Cartesian components of the gravity vector for each face. With an empirical threshold value, the magnitude vector could determine which triangle was the contact surface. This method was able to give consistently correct readings during testing.

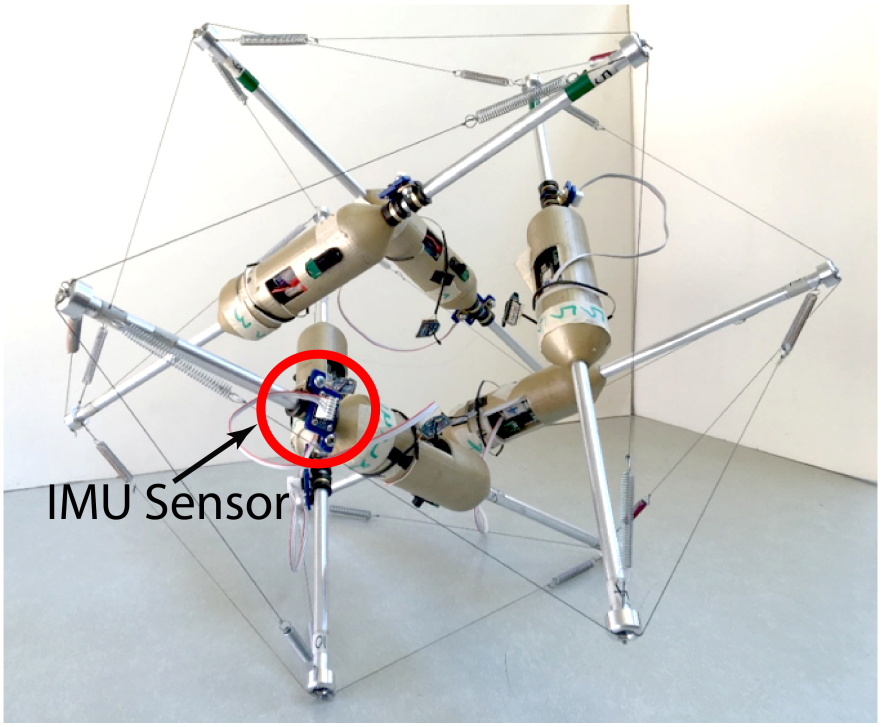

Figure 6.11: The TT-3 robot attached with Bosch BNO055 nine-DOF IMU sensors on its rods [65].

6.2.4 Use of the Modular Elastic Lattice for Rapid Prototyping of 12-Bar Tensegrity Structures

In addition to the BEST Lab's research in six-bar tensegrity robotics, the investigation of 12-bar tensegrity structures as a new platform for tensegrity robots has been initiated. The BEST lab's previous work in hardware development of spherical tensegrity robots has been focusing on six-bar structures. The 12-bar structure is the next-largest symmetric structure, and the anticipation of its greater size and increased number of actuation routes will offer benefits in terms of actuation efficiency, impact characteristics, and payload-to-deadweight mass ratio.

There are several symmetric 12-bar tensegrity structures. Our lab is conducting a design study of three 12-bar tensegrity structures to select one that will best serve the design objectives of the robot. These structures are named cube, octahedron, and rhombicuboctahedron. The cube and octahedron are so named for the shapes from which the rods of the structures evolve [66]. The rhombicuboctahedron is named for the shape of its exterior lattice.

The rubber lattice prototyping method has allowed us to rapidly build these three tensegrity structures. Following the same methodology as was used for the six-bar tensegrity structure, the 12-bar structures' lattices were created by observing geometric patterns and designing modular pieces. The lattice pieces were connected to create lattice shells. The next step was to attached bars to the interior of each lattice shell to erect the tensegrity structure. The structural prototype of the cube, octahedron, and rhombicuboctahedron are shown in Figure 6.12 as examples.

Furthermore, the plan is to use these rapid prototypes to empirically evaluate each structure using the metrics of actuation efficiency, impact orientation sensitivity, and payload-to-deadweight mass ratio. It would be then possible to evaluate the actuation efficiency by actuating the system and measuring the power required to achieve locomotion. In addition, it is recommended that the evaluation of the impact orientation sensitivity be conducted by drop tests and observations of the impact deformation characteristics. Lastly, it is recommended that the evaluation of the payload-to-deadweight mass ratio be performed by attaching weights to the center of the structure and recording its effects on locomotion and impact behavior.

This research has enabled proof-of-concept for a light weight secondary probe for Lunar missions that can perform punctuated rolling while carrying a 1 kg scientific payload. Implementation of these recommendation promises to enable the spherical tensegrity robot to move to a higher technology readiness level and move more steps forward in achieving mission feasibility.

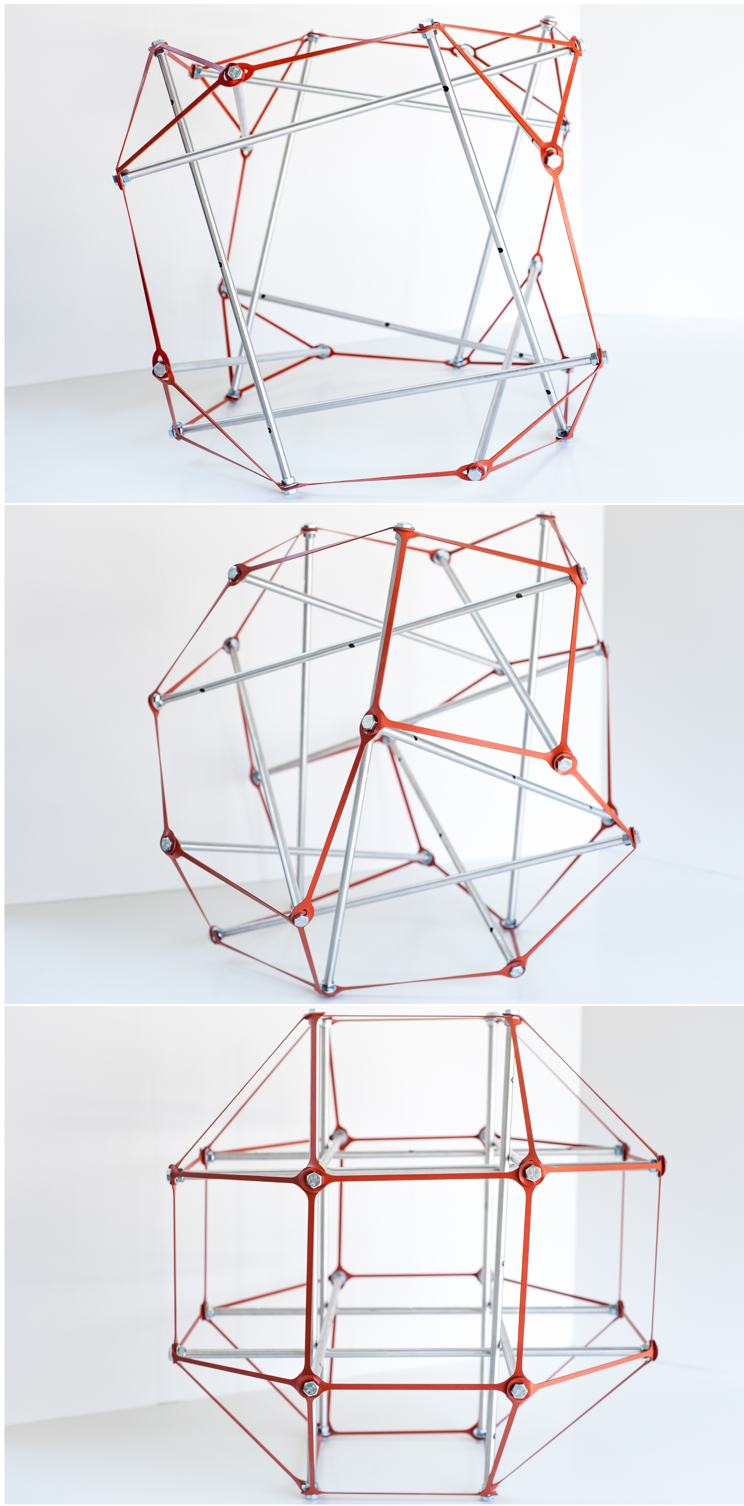

Figure 6.12: Top to bottom: Cube, Octahedron, and Rhombicuboctahedron 12-bar tensegrity structure prototyped using lattice platform.

Bibliography

[1] "Mars Science Laboratory Mission Timeline.." http://mars.nasa.gov/msl/mission/timeline/.

[2] A. K. Agogino, , and A. M. Agogino, "Precision hopping/rolling robotic surface probe based on tensegrity structures," *NASA Early Stage Innovation (ESI) Annual Report*, 2015.

[3] " Kenneth Snelson, Art and Ideas." http://kennethsnelson.net/KennethSnelson_Art_And_Ideas.pdf.

[4] "SuperBall Bot Tensegrity Planetary Lander." https://ti.arc.nasa.gov/tech/asr/intelligent-robotics/tensegrity/superballbot/.

[5] A. P. Sabelhaus, A. K. Akella, Z. A. Ahmad, and V. SunSpiral, "Model-Predictive Control of a Flexible Spine Robot." in *American Control Conference (ACC)*, 2017.

[6] L.-h. Chen, K. Kim, E. Tang, K. Li, R. House, E. Jung, A. M. Agogino, A. Agogino, and V. SunSpiral, "Soft Spherical Tensegrity Robot Design Using Rod-Centered Actuation and Control," in *ASME International Design Engineering Technical Conference (IDETC) Mechanisms and Robotics Conference*, (Charlotte, NC), American Society of Mechanical Engineers, 2016.

[7] L.-h. Chen, K. Kim, E. Tang, K. Li, R. House, E. Jung, E. Zhu, K. Fountain, A. M. Agogino, A. Agogino, and V. SunSpiral, "Soft Spherical Tensegrity Robot Design Using Rod-Centered Actuation and Control." in *ASME Mechanisms and Robotics Journal*, (Charlotte, NC), American Society of Mechanical Engineers, 2017.

[8] K. Kim, A. K. Agogino, A. Toghyan, D. Moon, L. Taneja, and A. M. Agogino, "Robust learning of tensegrity robot control for locomotion through form-finding," in

2015 IEEE/RSJ International Conference on Intelligent Robots and Systems (IROS), pp. 5824–5831, IEEE, 2015.

[9] B. Mirletz, I.-W. Park, T. E. Flemons, A. K. Agogino, R. D. Quinn, and V. Sun-Spiral, "Design and Control of Modular Spine-Like Tensegrity Structures," in *The 6th World Conference of the International Association for Structural Control and Monitoring (6WCSCM)*, 2014.

[10] L.-h. Chen, O. Romero, E. L. Zhu, M. C. Daly, B. Cera, S. R. Malekshahi, C. U. Spangenberg, G. Emmendorfer, E. Tang, Y. W. Chau, A. K. Agogino, and A. M. Agogino, "Modular , Elastic Lattice Platform for Rapid Prototyping of Spherical Tensegrity Robots." in *IEEE International Conference on Robotics and Automation (ICRA)*, 2017.

[11] B. Fuller, "Tensegrity," *Portfolio and Art News Annual*, vol. 4, pp. 112–127, 1961.

[12] R. E. Skelton, R. Adhikari, J.-P. Pinaud, W. Chan, and J. Helton, "An introduction to the mechanics of tensegrity structures," in *Decision and Control, 2001. Proceedings of the 40th IEEE Conference on*, vol. 5, pp. 4254–4259, IEEE, 2001.

[13] K. Kim, A. K. Agogino, D. Moon, L. Taneja, A. Toghyan, B. Dehghani, V. SunSpiral, and A. M. Agogino, "Rapid prototyping design and control of tensegrity soft robot for locomotion," in *2014 IEEE International Conference on Robotics and Biomimetics (ROBIO 2014)*, pp. 7–14, IEEE, 2014.

[14] A. P. Sabelhaus, J. Bruce, K. Caluwaerts, P. Manovi, R. F. Firoozi, S. Dobi, A. M. Agogino, and V. SunSpiral, "System Design and Locomotion of SUPERball, an Untethered Tensegrity Robot," in *2015 IEEE International Conference on Robotics and Automation (ICRA)*, pp. 2867–2873, IEEE, 2015.

[15] R. T. Skelton and C. Sultan, "Controllable tensegrity: A new class of smart structures," in *Smart Structures and Materials' 97*, pp. 166–177, International Society for Optics and Photonics, 1997.

[16] R. Skelton, "Dynamics and control of tensegrity systems," in *IUTAM Symposium on Vibration Control of Nonlinear Mechanisms and Structures*, pp. 309–318, Springer, 2005.

[17] R. E. Skelton and M. C. de Oliveira, *Tensegrity Systems*, Springer, 2009.

[18] A. D. Steltzner, P. D. Burkhart, A. Chen, K. A. Comeaux, D. M. Kipp, L. V. Lorenzoni, G. F. Mendeck, R. W. Powell, T. P. Rivellini, A. M. S. Martin, S. W. Sell, R. Prakash, and D. W. Way, "Entry , Descent , and Landing System Overview," in *IEEE Aerospace Conference*, 2010.

[19] R. B. Fuller, "Tensile-Integrity Structures.," in *United States Patent 3 063 521*, 1962.

[20] D. G. Emmerich, "Construction de réseaux autotendants," in *France Patent 1 377 290*, 1964.

[21] K. Snelson, "Continuous tension, discontinuous compression structures," in *United States Patent 3 169 611*, 1965.

[22] C. R. Calladine, "Buckminster Fuller's Tensegrity structures and Clerk Maxwell's rules for the construction of stiff frames," *International Journal of Solids and Structures*, vol. 14, pp. 161–172, 1978.

[23] C. Sultan, M. Corless, and R. E. Skelton, "Linear dynamics of tensegrity structures," *Engineering Structures*, vol. 24, no. 6, pp. 671–685, 2002.

[24] R. Motro, *Tensegrity: Structural systems for the future*. Butterworth-Heinemann, 2003.

[25] L. Zhang, B. Maurin, and R. Motro, "Form-Finding of Nonregular Tensegrity Systems," *Journal of Structural Engineering*, vol. 132, no. 9, p. 1435, 2006.

[26] N. Bel Hadj Ali, L. Rhode-Barbarigos, A. A. Pascual Albi, and I. F. C. Smith, "Design optimization and dynamic analysis of a tensegrity-based footbridge," *Engineering Structures*, vol. 32, no. 11, pp. 3650–3659, 2010.

[27] "Tensegrity." `http://www.tensegriteit.nl/e-architecture.html`.

[28] G. Tibert, "Deployable Tensegrity Structures for Space Applications," in *Ph.D. Dissertation*, Royal Institute of Technology Department of Mechanics, 2002.

[29] F. Fu, "Structural behavior and design methods of Tensegrity domes," *Journal of Constructional Steel Research*, vol. 61, no. 1, pp. 23–25, 2005.

[30] A. P. Sabelhaus, J. Bruce, K. Caluwaerts, Y. Chen, D. Lu, Y. Liu, A. K. Agogino, V. SunSpiral, and A. M. Agogino, "Hardware design and testing of SUPERball, a modular tensegrity robot," in *Proceedings of The 6th World Conference of the International Association for Structural Control and Monitoring (6WCSCM)*, (Barcelona, Spain), 2014.

[31] J. Bruce, A. P. Sabelhaus, Y. Chen, D. Lu, K. Morse, S. Milam, K. Caluwaerts, A. M. Agogino, and V. SunSpiral, "SUPERball: Exploring Tensegrities for Planetary Probes," in *12th International Symposium on Artificial Intelligence, Robotics and Automation in Space (i-SAIRAS)*, 2014.

[32] A. K. Agogino, V. SunSpiral, and D. Atkinson, "Super Ball Bot – structures for planetary landing and exploration," *NASA Innovative Advanced Concepts (NIAC) Program, Final Report*, 2013.

[33] A. Iscen, K. Caluwaerts, J. Bruce, A. K. Agogino, V. SunSpiral, and K. Tumer, "Learning Tensegrity Locomotion Using Open-Loop Control Signals and Coevolutionary Algorithms," *Artificial Life*, vol. 21, pp. 119–140, 2015.

[34] X. Geng, M. Zhang, J. Bruce, K. Caluwaerts, M. Vespignani, V. SunSpiral, P. Abbeel, and S. Levine, "Deep Reinforcement Learning for Tensegrity Robot Locomotion," in *2016 IEEE International Conference on Robotics and Automation (ICRA)*, 2017.

[35] K. Caluwaerts, J. Bruce, J. M. Friesen, and V. SunSpiral, "State estimation for tensegrity robots," in *2016 IEEE International Conference on Robotics and Automation (ICRA)*, pp. 1860–1865, IEEE, 2016.

[36] K. Caluwaerts, J. Despraz, A. Iscen, A. P. Sabelhaus, J. Bruce, B. Schrauwen, and V. SunSpiral, "Design and control of compliant tensegrity robots through simulation and hardware validation," *Journal of The Royal Society Interface*, vol. 11, pp. 20140520–20140520, 2014.

[37] K. Caluwaerts, J. Despraz, A. Işçen, A. P. Sabelhaus, J. Bruce, B. Schrauwen, and V. SunSpiral, "Design and control of compliant tensegrity robots through simulation and hardware validation," *Journal of The Royal Society Interface*, vol. 11, no. 98, 2014.

[38] J. Bruce, K. Caluwaerts, A. Iscen, A. P. Sabelhaus, and V. SunSpiral, "Design and Evolution of a Modular Tensegrity Robot Platform," in *2014 IEEE International Conference on Robotics and Automation (ICRA)*, pp. 3483–3489, IEEE, 2014.

[39] V. SunSpiral, G. Gorospe, J. Bruce, A. Iscen, G. Korbel, S. Milam, A. K. Agogino, and D. Atkinson, "Tensegrity Based Probes for Planetary Exploration: Entry, Descent and Landing (EDL) and Surface Mobility Analysis.," in *10th International Planetary Probe Workshop (IPPW)*, 2013.

[40] A. K. Agogino, V. SunSpiral, and D. Atkinson, "{Super Ball Bot} - Structures for Planetary Landing and Exploration," *NASA Innovative Advanced Concepts (NIAC) Program, Final Report*, 2013.

[41] J. Friesen, A. Pogue, T. Bewley, M. de Oliveira, R. Skelton, and V. SunSpiral, "DuCTT: A tensegrity robot for exploring duct systems," in *IEEE International Conference on Robotics and Automation (ICRA) Conference*, pp. 4222–4228, 2014.

[42] J. M. Friesen, P. Glick, M. Fanton, P. Manovi, A. Xydes, T. Bewley, and V. Sunspiral, "The second generation prototype of a Duct Climbing Tensegrity robot, DuCTTv2," in *2016 IEEE International Conference on Robotics and Automation (ICRA)*, pp. 2123–2128, IEEE, 2016.

[43] B. R. Tietz, R. W. Carnahan, R. J. Bachmann, R. D. Quinn, and V. SunSpiral, "Tetraspine: Robust terrain handling on a tensegrity robot using central pattern generators," in *2013 IEEE/ASME International Conference on Advanced Intelligent Mechatronics*, pp. 261–267, IEEE, 2013.

[44] L. Rhode-barbarigos, *An active deployable tensegrity structure*. PhD thesis, Ecole Polytechnique Fédérale de Lausanne, 2012.

[45] C. Paul, F. J. Valero-Cuevas, and H. Lipson, "Design and control of tensegrity robots for locomotion," *Robotics, IEEE Transactions on*, vol. 22, no. 5, pp. 944–957, 2006.

[46] C. Paul, J. W. Roberts, H. Lipson, and F. J. Valero Cuevas, "Gait production in a tensegrity based robot," *ICAR 05 Proceedings 12th International Conference on Advanced Robotics 2005*, pp. 216–222, 2005.

[47] C. Paul, H. Lipson, and F. J. V. Cuevas, "Evolutionary form-finding of tensegrity structures," in *Proceedings of the 2005 conference on Genetic and evolutionary computation*, GECCO '05, (New York, NY, USA), pp. 3–10, 2005.

[48] A. P. Sabelhaus, H. Ji, P. Hylton, Y. Madaan, C. Yang, A. M. Agogino, J. Friesen, and V. SunSpiral, "Mechanism Design and Simulation of the ULTRA Spine: A Tensegrity Robot," in *ASME International Design Engineering Technical Conference (IDETC) Volume 5A: 39th Mechanisms and Robotics Conference*, ASME, 2015.

[49] A. P. Sabelhaus, L. Janse van Vuuren, A. Joshi, Z. A. Ahmad, A. K. Agogino, V. SunSpiral, and A. M. Agogino, "Ground Reaction Forces Under a Quadruped Robot with

a Flexible Actuated Spine." in *2016 IEEE International Conference on Robotics and Automation (ICRA)*, 2017.

[50] "NASA Tensegrity Robotics Toolkit." `https://ti.arc.nasa.gov/tech/asr/intelligent-robotics/tensegrity/NTRT/`.

[51] "298:1 Micro Metal Gearmotor HPCB 12V with Extended Motor Shaft." `https://www.pololu.com/product/3056`. Accessed: 2016-09-07.

[52] "Pro Micro and Fio V3 Hookup Guide." `https://learn.sparkfun.com/tutorials/pro-micro--fio-v3-hookup-guide`. Accessed: 2016-09-06.

[53] M. Shibata, F. Saijyo, and S. Hirai, "Crawling by body deformation of tensegrity structure robots," in *ICRA*, ICRA'09, (Piscataway, NJ, USA), pp. 3617–3622, IEEE Press, 2009.

[54] C. Paul, F. Valero-Cuevas, and H. Lipson, "Design and control of tensegrity robots for locomotion," *IEEE Transactions on Robotics*, vol. 22, pp. 944–957, 2006.

[55] D. S. Mckay, J. L. Carter, W. W. Boles, C. C. Allen, and J. H. Allton, "JSC-1: A New Lunar Soil Simulant," *In Lunar and Planetary Inst., Twenty-Fourth Lunar and Planetary Science Conference*, pp. 963–964, 1993.

[56] "True Fakes: Scientists Make Simulated Moondust.." `https://science.nasa.gov/science-news/science-at-nasa/2006/28dec_truefake/`.

[57] C. Ray, S. Reis, S. Sen, and J. O'Dell, "Jsc-1a lunar soil simulant: Characterization, glass formation, and selected glass properties," *Journal of Non-Crystalline Solids*, vol. 356, no. 44-ĂŞ49, pp. 2369 – 2374, 2010. 12th International Conference on the Physics of Non-Crystalline Solids (PNCS 12).

[58] E. Hill, M. J. Mellin, B. Deane, Y. Liu, and L. A. Taylor, "Apollo sample 70051 and high- and low-ti lunar soil simulants mls-1a and jsc-1a: Implications for future lunar exploration," *Journal of Geophysical Research: Planets (1991-2012)*, vol. 112, 2007.

[59] R. Gustafson, B. White, and M. Gustafson, "Development of a high fidelity lunar soil simulant," in *AIP Conference Proceedings*, vol. 969, pp. 213–220, 2008.

[60] Y. Zheng, S. Wang, Z. Ouyang, Y. Zou, J. Liu, C. Li, X. Li, and J. Feng, "Cas-1 lunar soil simulant," *Advances in Space Research*, vol. 43, no. 3, pp. 448 – 454, 2009.

[61] S. Sen, C. Ray, and R. Reddy, "Processing of lunar soil simulant for space exploration applications," *Materials Science and Engineering*, vol. 413-414, pp. 592–597, 2005.

[62] Y. Zheng, "Spherical Tensegrity Soft Robots for NASA Missions: Design of the Next Generation Tensegrity Robot," Master of Engineering Report, University of California at Berkeley, 2016.

[63] M. D. Dickey, R. C. Chiechi, R. J. Larsen, E. A. Weiss, D. A. Weitz, and G. M. Whitesides, "Eutectic gallium-indium (EGaIn): A liquid metal alloy for the formation of stable structures in microchannels at room temperature," *Advanced Functional Materials*, vol. 18, no. 7, pp. 1097–1104, 2008.

[64] M. Yuen, A. Cherian, J. C. Case, J. Seipel, and R. K. Kramer, "Conformable actuation and sensing with robotic fabric," *IEEE International Conference on Intelligent Robots and Systems*, pp. 580–586, 2014.

[65] J. L. Ware, "Spherical Tensegrity Soft Robots for NASA Missions: IMU Integration for Orientation Detection and System Drop Response," Master of Engineering Report, University of California at Berkeley, 2016.

[66] "XOZZOX Design Consult - the art and engineering of tensegrity structures.." `http://www.xozzox.com/index.html/`.